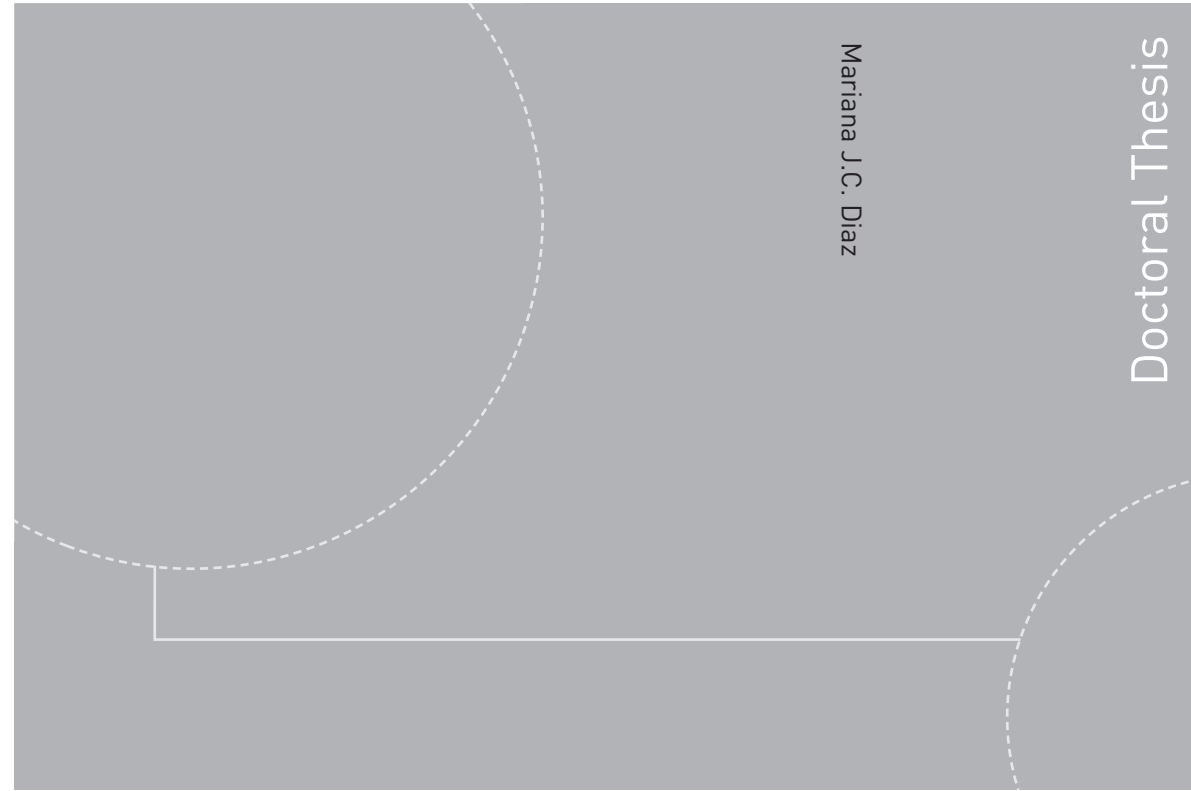


ISBN 978-82-326-1556-8 (printed version)
ISBN 978-82-326-1557-5 (electronic version)
ISSN 1503-8181



Doctoral theses at NTNU, 2016:109

Mariana J.C. Diaz

Two-Phase Slug Flow Experiments with Viscous Liquids

 **NTNU**
Norwegian University of
Science and Technology

Doctoral theses at NTNU, 2016:109

 NTNU

NTNU
Norwegian University of
Science and Technology
Faculty of Engineering
Science and Technology
Department of Energy and Process Engineering

 **NTNU**
Norwegian University of
Science and Technology

Mariana J.C. Diaz

Two-Phase Slug Flow Experiments with Viscous Liquids

Thesis for the degree of Philosophiae Doctor

Trondheim, May 2016

Norwegian University of Science and Technology
Faculty of Engineering Science and Technology
Department of Petroleum Engineering and Applied Geophysics



Norwegian University of
Science and Technology

NTNU

Norwegian University of Science and Technology
Faculty of Engineering Science and Technology
Department of Petroleum Engineering and Applied Geophysics

Thesis for the degree of Philosophiae Doctor

© Mariana J.C. Diaz

ISBN 978-82-326-1556-8 (printed version)
ISBN 978-82-326-1557-5 (electronic version)
ISSN 1503-8181



Doctoral theses at NTNU, 2016:109
Printed by Skipnes Kommunikasjon as

Two-Phase Slug Flow Experiments with Viscous Liquids

Mariana J.C. Díaz Arias

Supervisor: Prof. Ole Jørgen Nydal

Co-supervisor: Prof. Zhilin Yang

Abstract

The challenges behind the multiphase transport of oil and gas mixtures are increasing as the oil and gas industry is moving towards production from non-conventional reservoirs and in remote locations. Transport of high viscosity fluids in long multiphase pipelines is a particular challenge. Previous experiments have shown that gas-liquid slug flow is a frequent two-phase flow pattern at high liquid viscosities. The slug flow regime is an unstable flow, which may lead to operational problems, as the slug lengths and velocities can become very large. Most of the available experimental data and flow models are based on low viscosity fluids, and therefore, the computational models have some uncertainty regarding the viscous effects.

With this in mind, the main objective of this thesis is to extend the knowledge of the two-phase flow transport of slug flow with viscous liquids by experimental work, data analysis of available information and evaluation of certain flow concepts within slug flow models, such as bubble propagation, wake effect, severe slugging stability, and flow regime transition.

All the experiments were carried out at the Multiphase Flow Laboratory of the Norwegian University of Science and Technology and the experimental data were used to evaluate the performance of existing models. Dedicated set-ups and measurement methods were designed for each of the studied phenomena. Instrumentation has included an array of video cameras with image analysis, as well as external and internal impedance ring probes.

Flow stability was evaluated for gas-liquid severe slugging in a lazy wave shaped riser with different liquid viscosities. The experimental results show flow stability at lower gas velocities as the liquid viscosity is increased.

The history effect of the flow in an upstream pipe connected to a downwards inclined pipe was studied. The results confirm the existence of a metastable region in the flow regime map where both stratified and slug flow can be stable flow regimes depending on the flow pattern at the inlet. This effect is stronger for liquids that are more viscous. It is demonstrated that slug tracking models in principle can capture this phenomenon.

The bubble propagation velocities for horizontal flows at Reynolds numbers for laminar flow and for transition to turbulent flow have been measured. An empirical correlation

for estimation of the bubble front velocity in the full range from laminar to turbulent flow is suggested, based on the experimental results.

The wake effect between two consecutive bubbles in laminar horizontal flow has been measured. In comparison with the turbulent case, an earlier interaction of the bubbles was observed in terms of the slug length between them.

A new multi-beam gamma densitometer was also designed and fabricated to measure three phase fractions along the cross-sectional area of acrylic pipes. The new gamma densitometer is subject to additional testing.

Further works might address to extend the metastable region study to include stronger pipe inclinations and much longer pipes, in order to verify the sustainability of the slugs generated on this region. Moreover, additional sensitivity studies can be made with dynamic slug tracking models, regarding the effects of the bubble velocity relations and the wake effect on the simulations of the slug flow evolution in a pipes.

Acknowledgements

I would like to give thanks to all the persons that have been part of this thesis by directly collaboration or by supporting me in many different ways. My infinite gratitude to our God, for the talents received and for giving me the strength to finish this important chapter of my professional life.

I am grateful and hugely indebted to my main supervisor Ole Jørgen Nydal. He gave me the amazing opportunity of become part of his research group, where I have been able to grow personally and professionally and to have one of the best experience of my life. Many thanks Ole Jørgen (Professor!) for all your support, guidance and for being so kind and always to show interest in my research. I also appreciate the road trips, the fishing time and the usual dinners: salmon, potatoes and ice creams with oranges.

I would like to express my gratitude to the Research Council of Norway and Statoil for economically support this research project. In addition, I wish to give thanks to mi co-supervisor Zhilin Yang for his advises and the workshops organized for the Multiphase Flow group meeting.

I also would like to gratefully acknowledge to the amazing team of the Energy and Process Engineering Department, especially to Martin Bustadmo, Stein Kristian Skånøy, Halvor Haukvik, Per Bjørnaas and Anita Yttersian. Without them it would have been a lot more difficult to finish this work.

I am deeply grateful to my colleague and friend Andrea Shmueli not just for her support, guidance, technical discussions, and thesis editor, but also for the refreshing coffee-breaks, shopping time, trips and her friendship that were essential to keep me going.

Of course, I am always grateful to my family because they are my unconditional support, their love and encouragement has been a vital ingredient to my success. And finally, but not least, thank you Joaco for your help in every aspect of my research, in the lab, when the PC did not want to work, reading my papers, but above all, for always be there when I needed you... Gracias al infinito!

CONTENTS

Chapter 1	Introduction.....	1
1.1	Motivation.....	1
1.2	Objectives	2
1.3	Research method.....	2
1.4	Contribution	2
1.5	Thesis structure	4
Chapter 2	Gas-Liquid Slug Flows in Pipelines	7
2.1	Flow patterns and flow pattern maps	7
2.2	Stratified and slug flow.....	9
2.3	Slug flow modeling.....	10
Chapter 3	Experimental Procedures and Facilities.....	17
3.1	Experimental facilities	17
3.2	Test sections.....	21
3.3	Experimental measurements and data processing.....	28
3.4	Design of two-energy multibeam gamma densitometer	38
Chapter 4	Conclusions	45
References	49
Appendix A	51
Paper I:	Experiments on Severe Slugging in a S-Riser System with Viscous Liquids	63
Paper II:	Severe Slugging with Viscous Liquids experiments and simulations.	77
Paper III:	Inlet Effects on Flow Regimes in Downwards Inclined Pipes.	91
Paper IV:	Bubble Translational Velocity in Horizontal Slug Flow with Medium Liquid Viscosity.....	109
Paper V:	Inlet Effects on Gas-Liquid Flow Regimes in Downwards Inclined Pipes.....	133
Paper VI:	Wake Effect on the Slug Bubble Velocity: Experiments in Laminar Flow	153

List of Figures

Fig. 1-1 Research method diagram.....	3
Fig. 2-1 Flow pattern for gas-liquid flow in horizontal pipes.	8
Fig. 2-2 Flow pattern for gas-liquid flow in vertical pipes.....	8
Fig. 2-3 Flow regime map presented by Mandhane et al. (1974).....	9
Fig. 3-1. Sketch of the facility	18
Fig. 3-2 Newtonian analysis	20
Fig. 3-3 Liquid solutions with 2% QP40, 5% QP09L after some months.	21
Fig. 3-4 Geometry of the pipeline and S-riser system.....	21
Fig. 3-5 Sketch of the experimental set-up.....	23
Fig. 3-6. Bubble injection system.....	23
Fig. 3-7 Picture of the test section	25
Fig. 3-8. Sketch drift velocity set-up	26
Fig. 3-9 Sketch of the test section for oil-air experiments with upward inlet	27
Fig. 3-10. Sketch of the test section for water-air experiments with upward inlet.....	27
Fig. 3-11 Conductance probes	29
Fig. 3-12 Calibration curve of conductance probe.	29
Fig. 3-13 Capacitance sensor and electronic card	30
Fig. 3-14 Calibration curve of capacitance probe.....	31
Fig. 3-15 Slug discrimination criteria.....	32
Fig. 3-16 Visualization system	33

Fig. 3-17 Bubble identification with image processing technique	33
Fig. 3-18 Bubbles movements a) Horizontal profile of all frames, b) Position and time coordinate for front and tail of each bubble	34
Fig. 3-19 Hold-up time trace for single bubble	35
Fig. 3-20 Comparison of measurement methods: image processing vs capacitance rings	35
Fig. 3-21 Screw pump calibration for liquid flow mass. (Oil 90cP; 850kg/m ³).....	37
Fig. 3-22 Viscosity vs. temperature for oil 65cP	37
Fig. 3-23 Mixture viscosity relation when mixing oil at 10cP and oil 65cP	38
Fig. 3-24 Scheme of the gamma densitometer	39
Fig. 3-25 Main parts of the gamma densitometer.....	39
Fig. 3-26 Source holder 3D representation.....	42
Fig. 3-27 a) Amplifier-detector assembly and b) 3D Representation detector holder. .	42
Fig. 3-28 Mobile base for supporting the assembly	43
Fig. 3-29 Safety mechanism sketch. a) transversal cut after Shmueli (2015), b) lateral view, c) isometric view.....	44

List of Tables

Table 3-1 Viscosity of tested fluids.....	19
Table 3-2 Experimental matrix of severe slugging experiments.....	22
Table 3-3 Measuring section position	24
Table 3-4 Experimental matrix of single bubble experiments	25
Table 3-5 Experimental matrix of two bubble experiments.....	25
Table 3-6 Experimental matrix of bubble front velocity in slug flow experiments	25
Table 3-7 Experimental matrix of history effect experiments.....	28
Table 3-8 Flow meter characteristics	36
Table 3-9 Comparison between sources.....	40
Table 3-10 Source properties.....	40
Table 3-11 Shielding thickness calculation.....	41

Nomenclature

ABBREVIATIONS

STD	Standard deviation
meanP _{MAX}	Mean value of maximum pressure
meanP _{MIN}	Mean value of minimum pressure
SDP	Standard Deviation of Inlet Pressure
F _{slugs}	Slugs frequency
SI	Terrain slugging I
SII	Terrain slugging II
Exp	Experiment
N _{slug}	Number of slugs
RGB	Red, green, blue

SYMBOLS

σ	Surface tension
θ	Pipe inclination
ϵ_D	Stratified flow gas fraction
ϵ_s	Gas fraction in the slug
τ_w	Shear stress
ϵ_s	Gas fraction in the slug buddy region
ϵ_D	Gas fraction in stratified/ bubble/film region of a slug unit
ρ	Density
Ψ	Volume error
λ	Darcy friction factor
ϕ, θ	Angle

α	Gas fraction
ν	The liquid kinematic viscosity
μ	Dynamic viscosity

LATIN LETTERS

A	Pipe transversal area
Ar	Archimedes number
C_o	Taylor bubble distribution coefficient
C_o^l, C_{o1}	C_o for laminar flow
C_o^t, C_{o2}	C_o for turbulent flow
C_o^{tr}	C_o in transitional region
$C_{\infty,h}$	Froude number of the drift velocity for horizontal pipe
$C_{\infty,v}$	Froude number of the drift velocity for vertical pipe
D,d,ID	Pipe internal diameter
E_o	Eötvös number
f	Friction factor
Fq	Frequency
Fr	Froude number
Fr_{crit}	Critical Froude number
g	Gravitational acceleration
HI	Liquid fraction (liquid hold-up)
h_1	Liquid level
ID	Regime identification
L	Section length
M	Mass
n	Coefficient of the power law for the velocity profile in turbulent flow

N_f	Dimensionless number
N_μ	Inverse of the square root of Ar
P, p	Pressure
R	Inner pipe radius
Re	Reynolds number
Re_{tr}	Reynolds number limit for transition from laminar to turbulent flow
Re_{turb}	Reynold number limit for turbulent flow
Re_{vl}	Reynolds number calculated from the mean relative velocity
S	Pipe perimeter
T	Period
T	Temperature
\bar{U}	Mean flow velocity
u	Phase velocity
U_b, U_B	Bubble propagation velocity
$U_{b,i}^{trail}$	Bubble front velocity of a trailing bubble
U_c	Maximum velocity of the liquid profile
U_f, U_f	Velocity of the bubble front
U_g	Actual Gas velocity
U_g	Gas velocity in stratified flow prior to the transition to slug flow
U_{GD}	Gas velocity in stratified/ bubble/film region of a slug unit
U_{GS}	Average gas velocity in the liquid slug
U_∞	Bubble front velocity of a bubble behind a very long slug
U_L	Actual liquid velocity
U_{L_critic}	Critical velocity
U_m	Mixture velocity

U_o	Bubble drift velocity
DU	Relative velocity
USG, U_{sg} , U_{sg}	Air superficial velocity
USL, U_{sl} , U_{sl}	Liquid superficial velocity
U_t	Velocity of the bubble tail
Ut	Slug tail propagation velocity
V	Section volume
v	Bubble velocity ratio
V_L	Liquid mean relative velocity
w	Weighted average

SUBSCRIPTS

max	Maximum
min	Minimum
o	Oil
W	Wall
w	Water
k	Phase
g	Gas phase
l	Liquid phase
n	Time step increment
s	Slug region
b	Bubble region
i	Interphase

Chapter 1

Introduction

1.1 Motivation

The transportation of high viscosity oil is a major challenge in the flow assurance areas, especially for offshore fields. Flow assurance is a general term for the transport phenomena in multiphase oil and gas pipelines.

Handling multiphase flow in offshore pipeline-riser systems represents an important task for the oil production industry, and so, many simulators have been developed in order to predict the physics of the flow. Research efforts aim at improving the reliability and accuracy of system design tools. These are also the basis for evaluation of operational processes looking for reducing costs and environmental risks.

Most of the multiphase flow model developments until now have been on the basis of low viscosity fluids. However, some experimental results have shown that the multiphase flow behavior for high viscosity fluids is significantly different from that of low viscosity liquids (Akhiyarov et al. (2010)). Since the current computational models have some uncertainty regarding the viscous effects, and the experimental databases are more limited for high viscous fluids, the industry is requiring improvements on some particular aspects of multiphase flow with viscous liquids, in order to increase the confidence of those models for high viscosity systems.

One of the major complications of the multiphase flow is the gas-liquid slug flow regime, due to its unstable behavior and to the numerous operational problems that it can generate. Moreover, experimental works have shown that for high viscosity liquid and gas flow, the slug flow is the most predominant flow pattern (Gokcal et al. (2008)). Therefore, improvement of slug flow models is the goal of many researchers.

1.2 Objectives

The primary objective of this work is to extend the knowledge of the two-phase flow transport of slug flow with viscous liquids by experimental work, data analysis of available information and evaluation of certain flow concepts within slug flow models, such as bubble propagation, wake effect, severe slugging stability, and flow regime transition.

1.3 Research method

The research work is mainly experimental. Different experiments were designed to support directly specific sub-models in slug flow, such as the bubble propagation velocity, the wake effect, and flow regime transition models.

The diagram presented in Fig. 1-1 summarizes the task and scope of the present research project. The major activities include the academic training, the experimental work and the comparison with existing numerical models. The experimental stage started with the laboratory preparation, which included the design of different test sections, construction or improvements of instrumentation, construction or updating of the system, fluid selection, updating acquisition system among other activities.

1.4 Contribution

During the period of this PhD several activities and task were accomplished, in terms of both the research work and the multiphase laboratory improvements:

- An independent measurement system based on multiple cameras and image-processing was implemented. The implementation included the camera selection, installation, and programming of the acquisition code in LabVIEW, as well as the setting up the proper illumination and anti-reflecting casing.
- New capacitance sensors were built. The acquisitions system was updated and electronics for the capacitance probes were established.
- Updating and implementing general procedures for the starting-up and shutting-down of the main experimental facilities.
- Developing an exploratory study of aqueous solution mixtures to obtain a high viscosity, but retaining the Newtonian behavior.

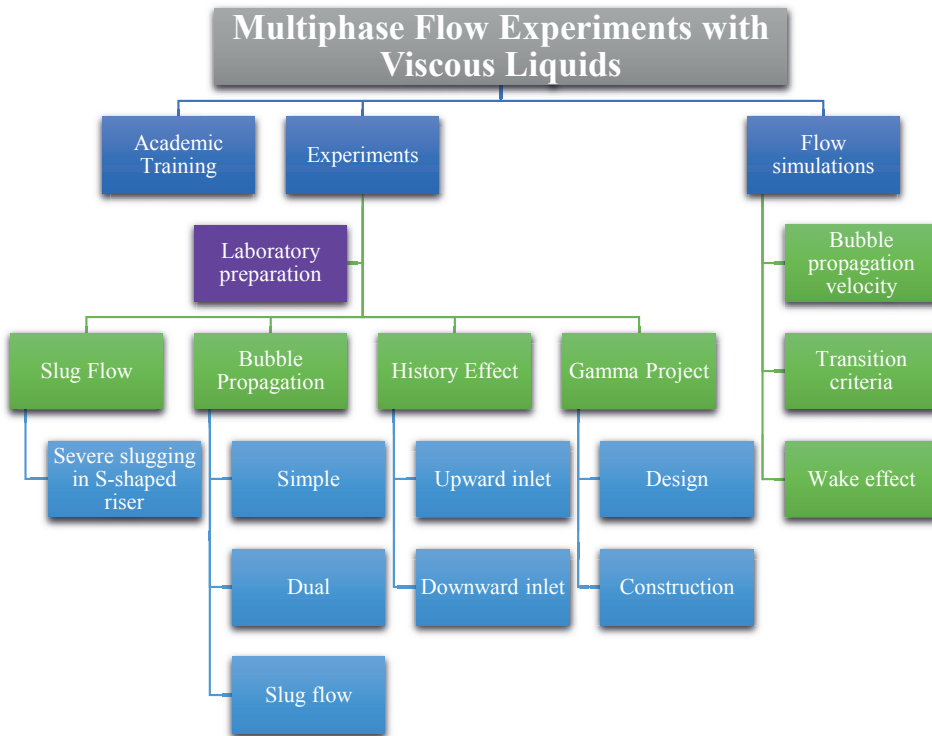


Fig. 1-1 Research method diagram.

- Design and construction of dedicated test sections for different purpose: single bubble experiments, wake-effect, history effect, slug generation, and drift velocity.
- Design and construction of a multi-been gamma densitometer in collaboration with other researchers.
- Collecting experimental data with medium viscosity liquids in terms of slug statistical characteristics such as slug frequency, slug length distribution, holdup, pressures (in severe slugging), bubble velocity propagations along the pipe, and bubble interaction phenomenon.
- Performing numerical simulations in dynamic multiphase flow simulators of severe slug flow in S-riser for two-phase flow with both low and medium liquid viscosity.
- Performing numerical simulations in dynamic multiphase flow simulators of inlet dependent flow systems.

- Documentation of the work in the form of publications: three presented in technical conference and three to be submitted to scientific journals.

1.5 Thesis structure

The present thesis is based on a collection of papers. However, complementary chapters have been included to extend the theoretical background, explain the experimental techniques and procedures, and to summarize the conclusions and recommendations for further work. Thus, Chapter 2 gives a brief general review of the most relevant concepts that cover the scope of the thesis. Literature reviews, however, have been included in each particular paper. Chapter 3 describes in detail the experimental procedures as well as the instrumentation and data processing methods, which might be useful as basis for similar experiments in the future. Chapter 4 contains the conclusions of the work, and recommendations for further studies.

1.5.1 Paper list

Paper 1: Experimental Investigation of Severe Slugging in a S-Riser System. *Submitted and presented at the International Conference of Multiphase Flow 2013.*

Paper 2: Severe Slugging with Viscous Liquids Experiments and Simulations. *Submitted and presented at the Multiphase Technology Conference (BHR group) 2014.*

Paper 3: Inlet Effects on Flow Regimes in Downwards Inclined Pipes. *Presented at the Offshore Technology Conference Brazil 2015.*

Paper 4: Bubble Translational Velocity in Horizontal Slug Flow with Medium Liquid Viscosity. *To be submitted to the International Journal of Multiphase flow.*

Paper 5: Inlet Effects on Gas-Liquid Flow Regimes in Downwards Inclined Pipes. *Draft paper to be submitted to the Society of Petroleum Engineers Journal.*

Paper 6: Wake Effect on the Slug Bubble Velocity: Experiments in Laminar Flow. *Draft paper to be submitted to the International Journal of Multiphase flow.*

Papers 1 and 2 study the severe slugging phenomenon in S-shaped risers by the comparing systems of low viscosity with systems of higher viscosity (65cP and 90 cP). The research focused on the severe slugging behavior for different operating conditions, which allowed documentation of the flow stability, transition boundaries, inlet hold-up and pressure of the severe slugging cycle. Paper 1 includes experimental data for water-air system and oil

(90cP)- air system and compare the results with simulations carried out with a dynamic slug flow model (SLUGGIT) developed at the NTNU to evaluate the performance of the model at viscosity higher than water. Paper 2 includes experimental data for extended operating conditions for both water-air and medium viscous liquid (65cP)-air system; the results were compared against simulations with a commercial dynamic multiphase flow program (OLGA 7.3) in terms of amplitudes of pressure oscillations in the base of the riser and slug frequencies.

Papers 3 and 5 study the history effect phenomenon, and the region in the flow regime map where both stratified and slug flow can be stable flow regimes. The slug formation and evolution along the pipeline is studied for air-water flow in terms of the slug frequency, liquid hold-up and decay or growth of slugs. The experimental results were compared against a commercial simulator (OLGA 7.3) regarding the flow patterns predicted by a standard slug model and a slug-tracking model. Paper 5 continues the analysis of the transition boundary, but focuses on comparing systems with different liquid viscosity and against common transition models.

Paper 4 covers the bubble propagation velocity in laminar to transitional flow in horizontal pipes. The work presents experimental data on the propagation velocity of a single air bubble in co-current liquid flow within Reynolds numbers of 250 and 5100. The outcomes were compared with existing correlations and experimental results in continuous slug flow. An averaging procedure is proposed for the bubble propagation velocity in the transitional region from laminar to turbulent flow.

Paper 6 studies the wake effect phenomenon for two-phase flow within the laminar region in horizontal pipes. The experiments were based on the observation of the interaction of two consecutive bubbles, and the measurement of the front propagation velocity. Thus, the work presents experimental results in terms of the bubble velocity as function of the separation distance (slug lengths) between bubbles and compares the experimental data against wake effect relations available in the literature.

Chapter 2

Gas-Liquid Slug Flows in Pipelines

Multiphase flow is the term often used to define the simultaneous occurrence of multiple phases in the same flow stream. This type of flow plays an important role in the operational process of different industries including nuclear, oil & gas, food and drink, and many others. In the oil & gas industry, the wells may produce oil, gas, and often water simultaneously, and this mixture should be transported from the wellhead to the treatment facility. The multiphase flow assurance is therefore a major task in the oil production system.

Depending on the number of phases involved in the process, it is referred as a two-phase flow (liquid-liquid or gas-liquid system) or as a three-phase flow (normally liquid-liquid-gas systems). When one denotes a liquid-liquid system as a two-phase flow, it is because the two liquid are immiscible, as for the case of oil and water.

The following section comprises an overview of relevant concepts for the development of the scope of this research work. A detailed literature review, however, will be presented in each of the papers dedicated to each topic within this investigation.

2.1 Flow patterns and flow pattern maps

In two-phase flow pipelines, the flow takes many configurations as the phases distribute themselves on the pipe cross-sectional area in different patterns, depending on the operating conditions: flow rate, fluid properties, pipe geometry and pipe inclination. The two-phase flow characteristics such as flow velocity, pressure drop, and hold-up (liquid fraction) distribution, will then depend on the flow regime in the pipe. One of the challenges in two-phase flow computations is the accurate prediction of these flow patterns and the transition boundaries between them. The flow patterns, also called flow regimes, are often classified by visual observation of the flow behavior in the pipe section,

and characteristic maps are built in terms of the flow rates or in terms of different dimensionless numbers. Fig. 2-1 and Fig. 2-2 show the most common flow pattern definitions found in the literature, for both horizontal and vertical pipes respectively.

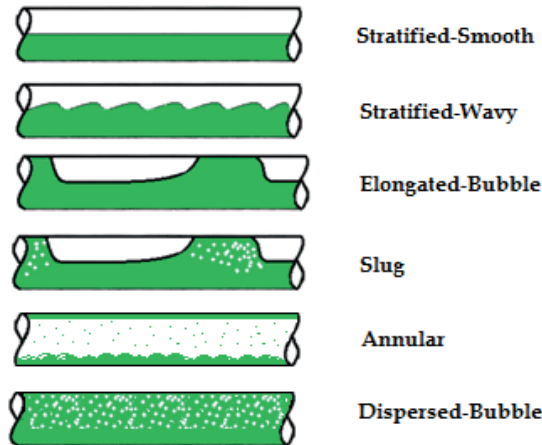


Fig. 2-1 Flow pattern for gas-liquid flow in horizontal pipes.
Adapted from Shoham (2006)

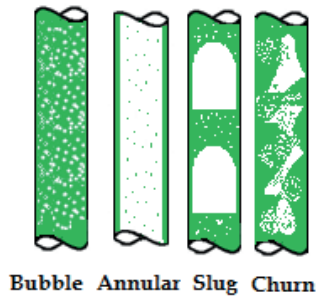


Fig. 2-2 Flow pattern for gas-liquid flow in vertical pipes.
Adapted from Shoham (2006)

Several authors have proposed flow regime maps from experimental work for different flow conditions, (Baker (1954), Mandhane, (1974), Govier and Aziz, (1972) cited by Shoham (2006)). Nevertheless, each map is particular for the experimental data under which they were created (geometry, fluids, pressure, etc.), and they might not represent to other data sets. An example of a horizontal flow regime map is presented in Fig. 2-3 Mandhane et al. (1974) in terms of superficial velocities.

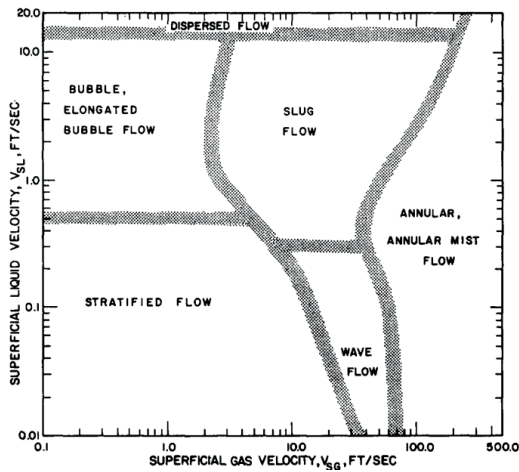


Fig. 2-3 Flow regime map presented by Mandhane et al. (1974).

The present thesis focuses on the transition mechanism from stratified to intermittent flow. Hence, annular, churn and bubble flow will not be included in this overview.

2.2 Stratified and slug flow

Stratified flow is present mainly in horizontal and moderately inclined pipelines. It occurs at relatively low gas and liquid flow rate as it is shown in the flow map of Fig. 2-3. The phases are separated by gravity, where the liquid phase flows on the bottom of the pipe and the gas phase on the top, over the liquid layer.

The intermittent flow can be found over the whole range of pipe inclinations. It is characterized by alternating flow of liquid slugs (covering completely the cross-sectional area of the pipe) and elongated bubbles of gas. As the liquid slug propagates forward in the pipe, the slug scoops liquid at the front and sheds it at the tail. Intermittent flow may be subdivided into elongated bubble or slug flow, but both configurations share the same flow mechanism. They just differ in the gas entrainment into the liquid slug; thus in the elongated bubble flow the liquid body is free of gas (Shoham (2006)).

The slug formation mechanism can change between gravity dominated and friction dominated flow. For instance, hydrodynamic instabilities in a stratified flow may produce enough perturbation in the gas-liquid interphase that leads to the growth of large waves and slugs. On the other hand, hilly terrain pipeline can also induce slug formation when the liquid accumulates in the lowers points. An extreme case of this type of slug flow is well known as severe slugging, in particular for pipeline-riser systems.

2.3 Slug flow modeling

Multiphase flow transport modeling aims to predict the flow behavior and local condition of the flow in pipeline systems: fluid and wall temperature, system pressure, phase velocities and liquid fractions. Depending on the choice of the scale of the flow problem is possible to develop models under steady-state conditions or to consider the dynamic behavior of the flow (fluctuation in phase fraction, pressure, and velocities).

Slug flow is a dynamic flow by nature. Nevertheless, for hydrodynamic slug flow in a straight section and at constant inlet flow conditions, the scale of the flow problem is such that it does not cause severe problems for the transport system. Severe slugging and terrain slugging, on the contrary, imply large-scale dynamics, which may represent operational challenges. The dynamics is now large fluctuation in space (generation of long liquid slug) and with time scales in the order of transport times in the system.

A flow model is based on a set of conservation equations: momentum, mass, and energy, together with closure relations to describe the flow dynamics. In 1D models, the variables are functions only of time and the coordinate along the pipe. Therefore, the flow properties are considered as the average value over the cross-sectional area of the pipe. The choice of the model formulations can depend on the phases distribution in the pipe; a “two-fluid model” solves a set of momentum equations for each region of the multiphase flow while a “mixture model” solves a single momentum equation for the mixture. Consequently, two computational approaches are possible: one changes the model scheme between two-fluid model or mixture model according to the flow-regime defined in each section of the pipe, and at each time step. The second option solves the same model scheme always (two fluids or mixture), and only adjust the closure models according to the local flow pattern (Nydal (2012)).

In terms of the grid scale, one may resolve all the scales of the problem (slugs and roll waves), or only resolve the large-scale dynamics and consider average values for the small scales. In order to consider all scales, the model should be able to predict the evolution of each slug and wave in time and space. Three strategies are possible: front capturing with a fixed grid, slug tracking with a moving grid, or a mixture of these two. If the interest is to average the small scales and only capture the large scale dynamics, then a “unit cell model” may apply for averaged slug flow. The numerical grid and time scale should then be larger than the slug flow scale.

Slug unit cell model

The model considers slug flow as a sequence of characteristic slug-bubble units. Conservation equations are typically written in a moving frame, which gives a steady formulation for the units. Fully developed flow is also assumed in both bubble and slug region within the unit cell (Fabre (1994)). The sub models in each region are often based on the two-fluid model for the bubble region, and the mixture model for the liquid slug section. In addition to the closure relations required for each sub model, expressions for the bubble front velocity, the void fraction in the slug region, and a length scale (slug length or slug frequency) are required. The unit cell model can also be implemented into dynamic simulator schemes, both two-fluids models and mixture models (Nydal (2012)).

Slug capturing

The slug capturing schemes use a very fine computational grid to capture automatically the initiation of the slugs and follow their evolution along the pipe. This method uses one single model framework for all flow conditions and the flow regime changes result directly from the solution of the equations, without the need for flow regime transition models. The only empirical correlation required is for the calculation of the shear forces for the liquid-wall, gas-wall and interfacial region (Issa and Kempf (2003)). The penalty of this model is that the solving of the equations on a fine grid requires large computational resources and long simulation times. Accurate numerical schemes are also required to capture the sharp fronts. Moreover, to specify the friction closure relations to be valid for all phases distributions, from separate to mixed flows, is also a challenge to be considered.

Slug tracking

The scheme applies a moving grid that follows each slug and tracks their evolution along the pipe. The conservation equations are now formulated on a moving grid, which eliminates numerical diffusion of the fronts. Border specific closures can also be implemented directly (e.g. bubble propagation velocity and mixing relations) (Nydal (2012)) as well as particular models for each sub-domain. For instance, a two-fluid model may be applied at the bubble region, while solving an integral momentum equation for the whole slug length. The method also allows direct implementation of the wake effect due to bubble-bubble interactions.

Slug tracking solvers require fewer numerical sections than the capturing scheme, and thus less computational times. A challenge in slug tracking schemes is the sub grid slug

initiation models and the management of the dynamic grid, which includes control volumes that can disappear or be created as slugs can grow and decay.

Hybrid scheme

As the name suggests, the scheme is a combination of front capturing and slug tracking model. The slug tracking domains are divided into a compressible region on the bubble unit and an incompressible one for the liquid slug, and at the same time, each region can have a sub-grid. If a fine grid is used in the bubble region (stratified flow region) then this region will have a model similar to the capturing scheme. A hybrid scheme then gives the positive parts of each model: self-generation of slugs from the capturing scheme, and slug tracking thereafter (Nydal (2012)).

2.3.1 Stratified to slug flow transition

The common method to identify the transition from stable to non-stable flow is through a stability analysis of the two-fluid model. This analysis predicts whether an infinitesimal disturbance on the interphase will lead to a stable interphase or to an unstable flow with wave growth (Shoham (2006)). The analysis can be done neglecting the fluid viscosity, Inviscid Kelvin-Helmholtz (IKH), or considering the liquid viscosity (VKH) (Lin and Hanratty (1986)).

Based on a phenomenological cell approach, Taitel and Dukler (1976) suggested a criterion for the transition boundary of stable to non-stable flow for horizontal and slightly inclined pipelines:

$$U_g \geq \left(1 - \frac{h_l}{d}\right) \left[\frac{(\rho_l - \rho_g) g \cos(\theta) A_g}{\rho_g S_i} \right]^{0.5} \quad (2-1)$$

U_g	Gas velocity	g	Gravity acceleration
h_l	Liquid level	θ	Pipe inclination from the horizontal
d	Pipe inner diameter	A_g	Area occupied by gas
ρ_l	Liquid density	S_i	Interphase length
ρ_g	Gas density		

Here, if the gas velocity is greater than the right hand side of the equation, then the Bernoulli destabilizing force from the gas overcomes the liquid gravity force leading to an unstable interphase. Otherwise, the flow is stable with smooth stratified flow along the pipe section. Lin and Hanratty (1986) suggested that the previous criterion of Taitel and Dukler (1976) might be incorrect for more viscous liquid than water, since the

model considers the effect of the liquid inertia by only including the term h_1/d regardless the fluid viscosity.

Bendiksen and Espedal (1992) performed a similar stability analysis than Lin and Hanratty (1986) including the viscous and inertial effects, and suggested a simplified version of the transition criterion based on the VKH theory:

$$(C_R - U_1)^2 + \frac{\rho_g}{\rho_1} \frac{1-\varepsilon}{\varepsilon} (C_R - U_g)^2 = \frac{\rho_1 - \rho_g g A_1 \sin(\theta)}{\rho_1 \frac{dA_1}{dh}} \quad (2-2)$$

U_g	Gas velocity	g	Gravity acceleration
U_1	Liquid velocity	θ	Pipe inclination from the horizontal
C_R	Wave velocity	ε	Void fraction
ρ_1	Liquid density	A_1	Area occupied by liquid
ρ_g	Gas density	h	Liquid level

It is important to realize that non-stable flow does not necessarily imply slug flow. Thus, the stability analysis for stratified flow only predicts the gas and liquid rate at which waves start to grow on the interphase. Consequently, it is necessary to define stability criteria for slugs to exist. With this intention, Bendiksen and Espedal (1992) proposed a slug stability criterion where the slug front must travel at equal or higher velocity than the slug tail for sustaining slug flow. This criterion does not determine the onset of slugging but gives a necessary condition for stable slug flow:

$$U_b < U_{GD} \frac{\varepsilon_D - \varepsilon_S \frac{U_{GS}}{U_{GD}}}{\varepsilon_D - \varepsilon_S} \quad (2-3)$$

U_b	Bubble front velocity
U_{GD}	Gas velocity in stratified flow prior to the transition to slug flow
ε_D	Volumetric gas fraction in stratified flow
ε_S	Volumetric gas fraction in the slug
U_{GS}	Average gas velocity in the liquid slug

2.3.2 OLGA model

The OLGA development started at the Institute for Energy Technology (IFE) in 1980, since then, the model has been improved and complemented with correlations and experimental data from the large-scale flow loop at SINTEF and the medium scale loop at IFE. The following summary is based mainly from the OLGA 7.3 user manual (Schlumberger (2013)).

OLGA is a dynamic multiphase flow simulator. It presents a transient flow behavior model to predict the flow characteristics over time, in terms of flow rates, fluid compositions, temperature and solid deposition. The model also includes a steady-state pre-processor that gives initial values for the transient simulations.

The three fluid model of OLGA includes the state equation and a total of seven conservation equations. Three for mass (each phase: oil, water, and gas), three momentum equations (one for each liquid continuous phase and one for the gas with the liquid droplets), and one for mixture energy (assuming thermal equilibrium among the phases). The fluid properties are supplied in the form of table, while boundaries and initial conditions can be specified by the user.

In general, the OLGA model resolves the same set of equations for all regimes and only changes the closure model according to the flow regime generated. The transition model is based on the minimum slip principle, which is similar to the slug existence condition (Eq. 2-3). It distinguishes four flow regimes: distributed flow (bubble and slug flow) and separate flow (stratified and annular flow).

Two models are available: the standard Olga model and the slug-tracking model. The former is based on the slug unit model with average properties over the cross-sectional area, which does not give details on the individual slugs. The second model is based on a sub grid slug tracking method, which follows individual slugs and supplies detailed information of the slug unit characteristics. The slugging onset is determined by the differences in the gas fraction. Therefore, it requires as an input the maximum void fraction allowed in the liquid slug body (SLUGVOID), and the minimum void fraction in the bubble region (BUBBLEVOID). When a given section presents void fraction less than the SLUGVOID, a slug might be initiated depending on the phase fractions in the neighboring sections. That is, a slug tail is generated if the void fraction exceeds the BUBBLEVOID within two upstream section, whereas, a slug front is initiated if this occurs within two downstream sections. Initially, the new slugs are as short as possible to avoid discontinuities, but if the flow conditions are favorable, the hydrodynamic slugs

will propagate through the pipe growing and decaying according to the local flow conditions. Before initiating the slug in a section, the model verifies a minimum distance from nearby slugs, and the minimum time elapsed (Δt) since a slug was generated or passed through the section. The minimum distance (L_{\min}) is calculated in terms of the slug initiation frequency (F_i) and the bubble nose velocity (U_b) (Eq.2-4). While Δt is calculated in terms of DELAYCONSTANT (DC), the pipe diameter (D), and average liquid velocity (U_L) according:

$$L_{\min} = \frac{F_i}{U_b} \quad (2-4)$$

$$\Delta t = DC \frac{D}{U_L} \quad (2-5)$$

2.3.3 Sluggit model

Sluggit is a dynamic slug-tracking simulator developed at the Norwegian University of Science and Technology. The model has been developed over the past years with the contribution of different researchers of the multiphase flow group at the Department of Energy and Process Engineering. The following summary is taken mainly from Kjeldby (2013).

Sluggit applies the hybrid concept (tracking and capturing scheme) in an object-oriented program with a computational grid organized in terms of borders, section and unit objects. In slug flow, a section can be a slug or a bubble, and a unit is a sequence of sections of the same type. The borders separate consecutive sections, and those can be moving or stationary. The section contains flow parameters such as pressure, temperature, and phase fraction while the borders store the phase velocities.

The object-oriented scheme allows formulating different models for the different computational objects. Thus, for the three-phase flow model presented by Kjeldby (2013), a two-fluid model is solved in the separate flow regions (bubble region), while an integral momentum balance applies to the slug objects. Moreover, from the grid formulation point of view, the object-oriented concept also allows combining coarse and fine grids, depending upon the variables to compute. In this regards, Sluggit can initiate slugs either by a capturing scheme with a fine grid where the slugs evolve automatically from the two fluids model or by supplying a sub grid slug inhibition model on a coarse grid. Subsequently and independently of the slug formation method, the grid is adjusted dynamically as slug or wave objects move along the pipe. Stratified sections that become

smaller than a minimum grid length merges with a neighboring section, and similarly, if they exceeded a maximum grid length they split into two identical sections (De Leebeek and Nydal (2010)).

The capturing slug transition model is based on the section liquid fraction. Thus, a slug is initiated if the liquid fraction in a stratified region exceeds a maximum value, and it is killed or converted into a wave if the section reaches a minimum hold-up criterion.

Chapter 3

Experimental Procedures and Facilities

The experiments were carried out at the Multiphase Flow Laboratory at the Norwegian University of Science and Technology. The laboratory facilities include several test loops for different purposes: risers, horizontal and inclined pipe sections, flexible pipes and mini loops. The facilities are quite flexible, and it is possible to create or modify the test sections to adapt them to a range of phenomena. The test sections are developed to demonstrate the physics behind the multiphase flow phenomenon and it is possible to generate valuable information and experimental results for validation and testing of numerical models.

3.1 Experimental facilities

The infrastructure consists of all the fixed elements that allows supplying the fluids and controlling the operating conditions. These elements include the pumping system, single-phase pipelines, control valves, flow meters, separators and tanks, mixing section, and miscellaneous components. The working fluids: oil, water, and air are at ambient conditions around 21° and atmospheric pressure. The mixing section is designed to operate with any combination of the three phases up to three-phase flow. Fig. 3-1 presents a sketch of the facility, showing the principal single phase flow lines and equipment.

The pumps, control valves, and instruments are connected to the main control system, which is remotely controlled by means of a dedicated program written in LabVIEW. The control system allows controlling the pumps (starting up, shutting down and frequency variation), opening/closing valves, and visualization and logging of the instruments data. The liquid flow rate is controlled by adjusting the valves and the pumps frequency.

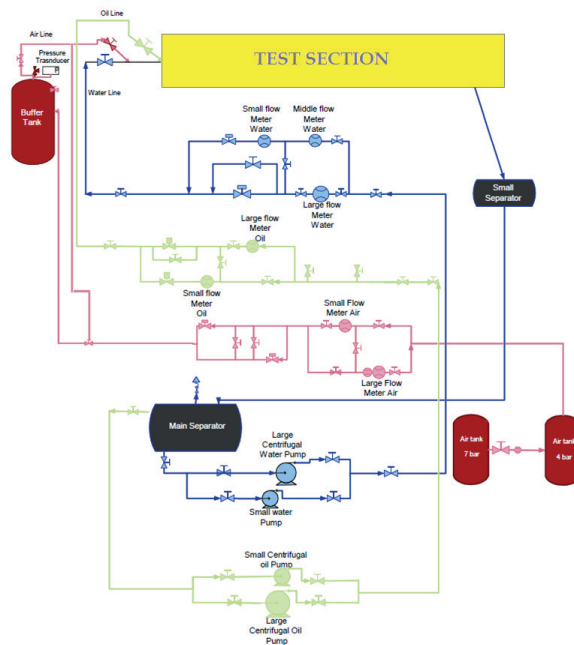


Fig. 3-1. Sketch of the facility

3.1.1 Fluids selection

The central line of the university supplies the air at 7 bar, which is delivered into the single phase line at 4 bar by a pressure reduction valve. The water is tap water with an artificial green color (fluorescein sodium $C_{20}H_{10}Na_2O_5$) to improve the visualization of the phase when working in two or three phase flow systems. The oil is mineral oil that can be replaced according to the experiment requirements. Both oil and water are stored in the main tank where they separate by gravity.

The liquid phase for the experiments in this investigation required viscosity range from 20cP to 100cP. There were already available mineral oil of different viscosities, and by mixing different oils, it was possible to reach the desired viscosity. Nevertheless, the instrumentation available to measure liquid fraction was not compatible with oil. Hence, the alternatives were either changing the fluid or changing the instrumentation. The following is a brief description of an exploratory study to change the viscosity of water.

In order to work with different liquid viscosities based on aqueous solutions, glycerin or thickening agents were tested to regulate the desired viscosity. The chosen fluid should meet certain characteristics: Newtonian behavior, good electric conductivity, stability over time, and fast liquid-air separation times. Newtonian flow and a good electric

conductivity was the priority in order to be able to measure liquid fraction with the available instrumentation. The maximum desired liquid viscosity was 100cP and the product concentration to achieve this viscosity was also a parameter to consider for the final selection.

The viscosity and Newtonian behavior analysis was measured with a rheometer (model ARES –G2), while the conductivity property was tested directly on a small bench with the conductance rings used in the test sections.

Different mixtures were tested and compared against the performance of the mineral oil to find the appropriate fluid. Table 3-1 presents the characteristics of the solutions tested and Fig. 3-2 shows the comparison of rheology of the fluids.

Table 3-1 Viscosity of tested fluids

Product ID	Volume Concentration	Viscosity [Pa·s]
Cellulose QP-09-L	5%	0.10
Cellulose QP-09-L	8%	0.44
Cellulose QP-09-L	6%	0.26
Cellulose QP-40	2%	0.11
Methyl Cellulose	2%	0.02
Hydroxyethyl Cellulose	4%	0.38
Hydroxyethyl Cellulose	2%	0.07
Hydroxyethyl Cellulose	1.5%	0.04
Hydroxyethyl Cellulose	1%	0.01
Nexbase 3080	100%	0.09
Glycerin	98%	0.98
Glycerin	30%	0.02
Glycerin	70%	0.04
Glycerin	90%	0.29
Glycerin	95%	0.30

Hydroxyethyl and Methyl presented the highest deviation from the Newtonian behavior and, therefore, they were discarded. The polymers QP09L and QP40 show a better linear behavior than the previous components, but they still deviate from the Newtonian behavior as the concentration of product in the solution increases. Solutions at 2% QP40 and 5% QP09L reach the desired maximum viscosity, and they still have a Newtonian behavior. The Glycerin is Newtonian, but the required concentration to reach the desired viscosity is too high, more than 70% of the mixture.

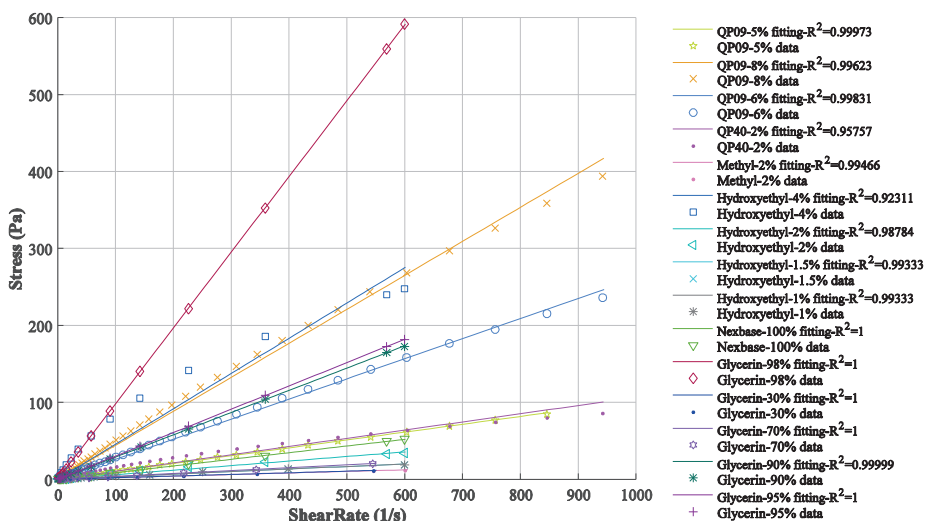


Fig. 3-2 Newtonian analysis

In a second step of this exploratory study, the response of the conductance rings was tested with samples of liquid solution of 2% QP40, 5% QP09L and 70% Glycerin. After this test, the Glycerin was discarded when the instrument did not detect liquid fractions lower than 25%. On the other hand, the instrument registered a good and consistent signal for both polymeric solutions.

The liquid solution of 2% QP40, 5% QP09L seemed to be a good alternative. However, the major concern was the stability of the solution over time. According to the manufacturer, the solution remains stable over a short period, suggesting that it should be added a long-term biocide to prevent any bacterial or fungal growth from occurring. At this point of the exploratory study, the idea to change the fluids was given up, because it required further tests including the additives, and a careful evaluation of the solution stability over time. It was decided to work with the available mineral oil and develop new instrumentation to measure the oil fraction. However, QP40 and QP09L might have the potential for this application, but further studies are required on the long-term stability with added biocide, and on how this new component may change the fluid rheology. The mineral oil used during the experiments differs for each setup, and therefore a proper description is given in their corresponding section

Fig. 3-3 shows the sample of 2% QP40, 5% QP09L after several months stored. The QP09L presented more evident change with a dark substance that might be bacteria. The QP40, apparently, conserved better its properties and did not show bacterial growth.



Fig. 3-3 Liquid solutions with 2% QP40, 5% QP09L after some months.

3.2 Test sections

The test section is referred as all the process and equipment located between the mixing section point and the first separator indicated in Fig. 3-1.

3.2.1 Set-up for severe slugging experiments

The objective of the experiments was to study the effect of the liquid viscosity on the severe slugging behavior (occurrence and characteristics). The test loop consists of a pipeline and S-shaped riser system of 14 m length and around of 6.4 m of total height, including a first riser of 4 m height and a second riser of 3.7 m height as shows Fig. 3-4. The line has 50 mm of internal diameter and it is constructed of acrylic for better visualization. The first section of the line has a downwards slope toward the first riser base, to promote the terrain slugging generation. At the inlet of the flow loop, the air single phase line is connected to a buffer tank to simulate a large pipe upstream with an equivalent volume of 0.255m^3 .

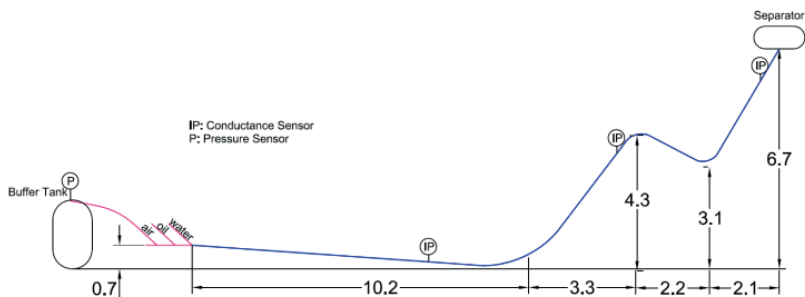


Fig. 3-4 Geometry of the pipeline and S-riser system

Experimental procedure: For a constant velocity of liquid, several air velocities were logged in order to build the flow regime map for both oil-air and water-air systems. The simple slug type classification reported by Nydal et al. (2001) was applied. The inlet pressure was monitored using the pressure transducer located at the top of the buffer tank. The identification of the type of terrain slugging I, II or stable slug was done by simple observation of the flow behavior in the test section and by analyzing the time series of the inlet pressure.

Table 3-2 summarizes the experimental test matrix of the flow development for different liquid viscosities. The outcomes were presented in terms of the maximum and minimum inlet pressure, cycle periods, and stability flow maps regarding the gas and liquid flow velocities.

Table 3-2 Experimental matrix of severe slugging experiments

	N° Experimental Points	Phase	Viscosity (cP)	Density (kg/m ³)	Superficial Mixing Velocity Range (m/s)
CASE 1	19	oil	90	850	0.2-0.4
		air	0.02	1.2	1.0-5.6
CASE 2	116	water	1	998	0.1-0.8
		air	0.02	1	1.2-7.8
CASE 3	74	oil	60	831	0.1-0.9
		air	0.02	1.2	1.0-5.6

3.2.2 Set-up for bubble propagation velocity experiments

The objective of these experiments was to study the propagation velocity of the air bubbles in the slug flow regime for viscous liquids. The test section was used for two different studies: front propagation velocity of a solitary bubble in continuous liquid flow, and wake effect on the interaction of two consecutive bubbles in continuous liquid flow. Focus was on laminar flow, to complement other existing data on turbulent flows.

3.2.2.1 Single and double bubble experiments

The test section consists of a horizontal pipe of 60mm inner diameter and 50m total length, including three straight segments of 16m and two U-bends of radius 1.42m and 0.92m respectively. Fig. 3-5 illustrates a sketch of the facility.

The air injection system consists of a fast-acting magnetic valve (Bosch Rexroth Series 560, 15/30 ms opening/closing time), a reduction valve and a pressure gauge (1000kPa of range, and accuracy ± 50 kPa). A dedicated program in LabVIEW allows remotely control of the valve by setting the opening time, the number of injections and the time

interval between consecutive injections. After some trial and error, it was found that a T-shaped pipe configuration showed the best performance among the different configurations tested. The injection point was fixed at 110 pipe diameters downstream of the liquid inlet. Fig. 3-6 presents the magnetic valve and the pressure controller installed in the T-shape configuration respect the main pipeline.

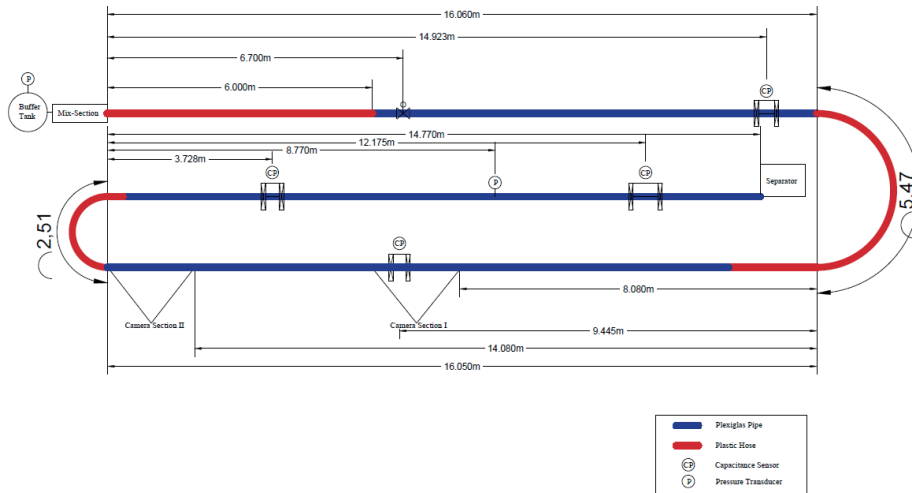


Fig. 3-5 Sketch of the experimental set-up

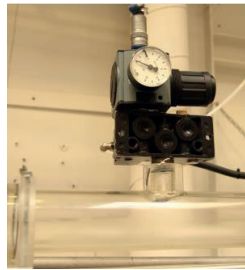


Fig. 3-6. Bubble injection system

The single-bubble experiments were carried out for different liquid viscosities. The desired viscosities were obtained by mixing two mineral oils of around 0.090 Pa.s, (850kg/m^3) and 0.01Pa.s (843kg/m^3), according to a volume ratio found experimentally (see section 3.3.4). The blend viscosity and density were measured using a rheometer and a Coriolis meter respectively.

The front propagation velocity was measured by detecting the air-liquid interphase of the bubble tip and measuring the time interval to move between two consecutive points. The selected method to detect the bubble interphase depended upon the instrumentation available. At the time of the first experimental campaign, there were not available sensors to detect the oil phase in the pipe. Therefore, while waiting to build the capacitance sensors and their corresponding electronic cards, an optical method was used instead, based on several synchronized cameras.

With the visualization technique, the measuring section was located at section I or II as shown in Fig. 3-5. With the capacitance method, four rings probes were positioned along the section, as indicates Fig. 3-5. Table 3-3 gives the location of each measuring section relative to the injection point.

Table 3-3 Measuring section position

Measuring section ID	Distance from the injection point (D)
Camera section I	383
Camera section II	483
Probes 1	137
Probes 2	400
Probes 3	617
Probes 4	767

Experimental procedure:

A constant liquid flow rate was set by adjusting the valve and the pump frequency. The liquid level along the test section should cover the entire cross-sectional area of the pipe. To achieve this condition in a horizontal pipe, a small loop was included before the outlet of the section to prevent air from entering the pipe (see Fig. 3 7). The liquid was circulated several minutes until the pressure at the outlet of the section was stable and there were not air bubbles in the pipe. Once the liquid stream reached the stable condition, an air bubble or a pair of air bubbles were injected into the section. The effect of the injection of air in the liquid was monitored through the pressure transducer at the outlet, and the experimental point was logged once the pressure was stable again. If the bubble arrived before the pressure was stabilized at the measuring section, the experimental point was discarded. Table 3-4 and Table 3-5 summarize the experimental matrix of the single bubble experiments and two bubbles experiments respectively.

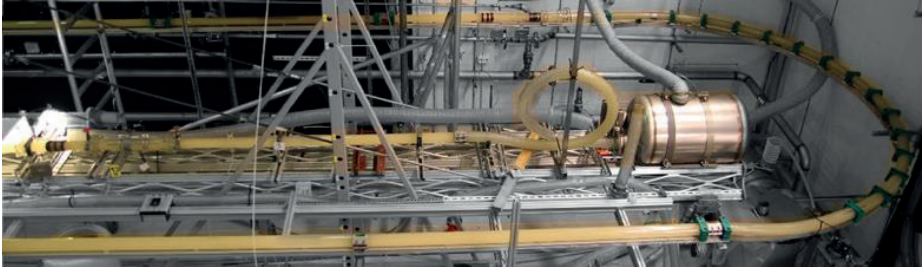


Fig. 3-7 Picture of the test section

Table 3-4 Experimental matrix of single bubble experiments

Case	N° Experimental Points	Phase	Viscosity (cP)	Density (kg/m ³)	Superficial Liquid Velocity Range (m/s)
CASE 1	118	Oil	10	843	0.42-1.26
CASE 2	48		20	846	0.50-1.20
CASE 3	127		26	846	0.35-1.24
CASE 4	22		65	831	0.28-0.90

Table 3-5 Experimental matrix of two bubble experiments

Case	N° Experimental Points	Phase	Viscosity (cP)	Density (kg/m ³)	Superficial Liquid Velocity Range (m/s)
CASE 1	402	Oil	65	831	0.35-0.89

3.2.2.2 *Slug flow experiments*

These experiments were carried out in order to compare the front velocity measured from the single bubble experiments and the front velocity in continuous slug flow. For these experiments, the liquid and air flow rates were set in a way that the mixture superficial velocity were equal to the superficial liquid velocity established on the single bubble experiments. The bubble front interphase was captured by the capacitance rings located along the pipeline as show Fig. 3-5.

Table 3-6 Experimental matrix of bubble front velocity in slug flow experiments

Case	N° Experimental Points	Phase	Viscosity (cP)	Density (kg/m ³)	Superficial Mixing Velocity Range (m/s)
CASE 1	52	Oil	10	843	0.42-1.21
CASE 2	20		26	846	0.52-1.18
CASE 3	14		65	831	0.78-1.31

3.2.3 Set-up for drift velocity experiments

The experiments aimed to measure the drift velocity with viscous liquids. The set-up consisted of a horizontal pipe of 60mm inner diameter and 2m long; one extreme sealed and the other one connected to a ball valve. Three capacitance probes were installed on the pipe as shows Fig. 3-8. A video camera was also installed to record the displacement of the gas-liquid interphase between capacitance probes 2 and 3.

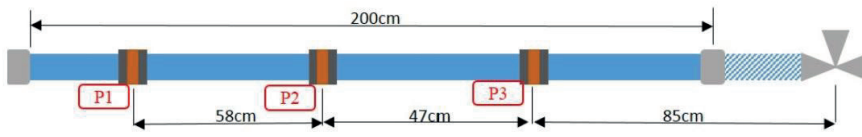


Fig. 3-8. Sketch drift velocity set-up

Experimental procedure: Prior to the experiments, the pipe was filled with the working fluid through a three-way valve. Then, the valve was opened suddenly, allowing air to enter the section while the liquid drains out of the pipe. The drift velocity was the measurement of the air cavity propagation along the pipe by cross-correlating the capacitance signals. The reported velocity corresponds to the last probe, close to the sealed end. The experiments were carried out for Nexbase (65cP and 831 kg/m³) in stagnant flow and atmospheric conditions.

3.2.4 Set-up for history effect experiments

The experiments were addressed to study the existence of a region in a flow regime map for downward flow, where both stratified and slug flow can be stable flow regimes. The study comprised the statistical analysis of the slug flow formation and their development along the section when changing the flow pattern at the inlet. The term of “history effect” is used to define the influence of the flow pattern of the upstream section on the downstream flow.

The test loop consisted of two straight sections of acrylic pipe with 60mm of internal diameter. The first section corresponds to the inlet section, which is a 3m pipe connected to the main flow section by a flexible hose at the pivot point as show Fig. 3-9 and Fig. 3-10. This pivot point allows rotating the inlet section any angle from 26° to -90° to the horizontal. For the present experiments, angles of 14.6 degrees downward and

25 degrees upward were used. The second section corresponds to a 16m long and 3.2° downward pipe, which was connected to the inlet section and to an atmospheric separator at the outlet.

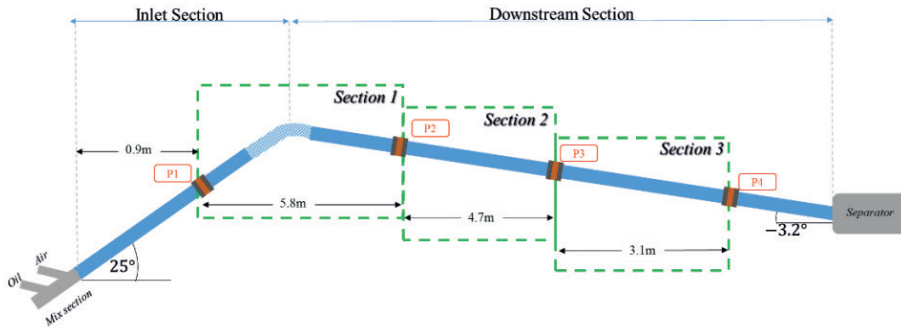


Fig. 3-9 Sketch of the test section for oil-air experiments with upward inlet

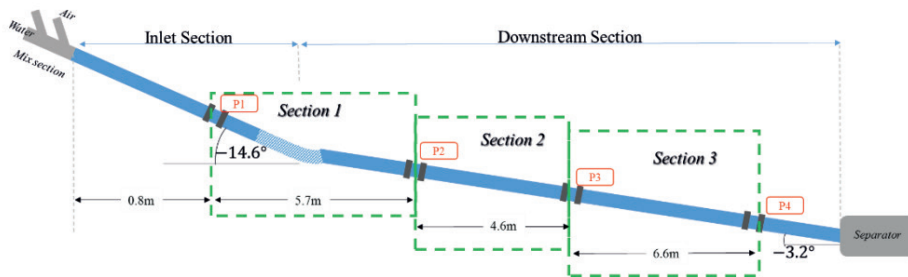


Fig. 3-10. Sketch of the test section for water-air experiments with upward inlet

Experimental procedure: A flow map was built according to the experimental matrix presented in Table 3-7. For each geometry studied, (upward and downward inlet) two fluids were used: air-water and air-oil, in order to evaluate the liquid viscosity effect on the slug formation and evolution. The slug characteristics were tracked along the pipe by means of hold-up sensors located at four fixed positions. For the air-oil experiments, capacitance rings located according to Fig. 3-9 were used. While for air-water experiments, conductance rings were used as shows Fig. 3-10.

Table 3-7 Experimental matrix of history effect experiments

Case	N° Experimental Points	Phase	Viscosity (cP)	Density (kg/m ³)	Superficial Mixture Velocity Range (m/s)
CASE 1 Upward Inlet	41	Water	1	998	0.21-1.8
		Air	0.02	1.2	0.29-2.47
CASE 2 Downward Inlet	39	Water	1	998	0.21-1.84
		Air	0.02	1.2	0.29-2.47
CASE 3 Upward Inlet	41	Oil	65	831	0.37-0.87
		Air	0.02	1.2	0.40-3.28
CASE 4 Downward Inlet	41	Oil	65	831	0.37-0.87
		Air	0.02	1.2	0.40-3.37

3.3 Experimental measurements and data processing

The following outlines the measuring methods and instrumentation employed to measure the relevant variables of each experiment explained in the previous section. For each variable, the instrumentation used is described, as well as their operating range, calibration procedure and the methodology to process the raw data.

The liquid hold-up sensors (capacitance or conductance rings), pressure transducer, and flow meter are connected to the main control system, which allows monitoring and logging the data. Flow rate measures are acquired at a sample rate of 10 to 20 Hz, while the signals from the hold-up and pressure transducers are acquired at 230 to 2000 Hz, depending on the acquisition system available. The camera system was connected to a separate acquisition arrangement that was not synchronized with the main control program.

3.3.1 Liquid Hold-up

The liquid fraction (hold-up) was measured by mean of a non-intrusive impedance method. Two types of impedance probes were used depending on the working fluid. Thus, external capacitance rings were installed to detect oil phase fraction and internal conductance ring to work with the water phase.

3.3.1.1 Conductance Probes

The conductance probes consist of a pair of parallel electrode rings of the same diameter as the inner diameter of the pipe. The method is based on one phase having much better electric conductivity than the other one. Hence, the minimum value of the instrument is

set based on the poorest conductivity medium (in this case air), and any change in the signal is due to the phase with good electric conductivity (in this case the water). The signal (voltage) received from the instruments is proportional to the volumetric fraction of the phases, for separated flows and for rings far apart. Fig. 3-11 shows two pairs of conductance rings.

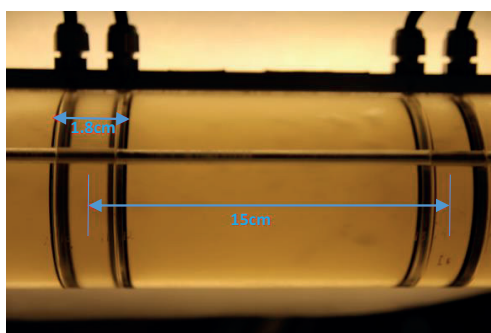


Fig. 3-11 Conductance probes

Each conductance probe should be calibrated separately. The signal depends on the rings geometry and the electronics for each sensor. The calibration consisted of filling the pipe with a known volume and read the voltage given by the instrument. An example of the curve calibration for a close pair of rings, is shown in Fig. 3-12.

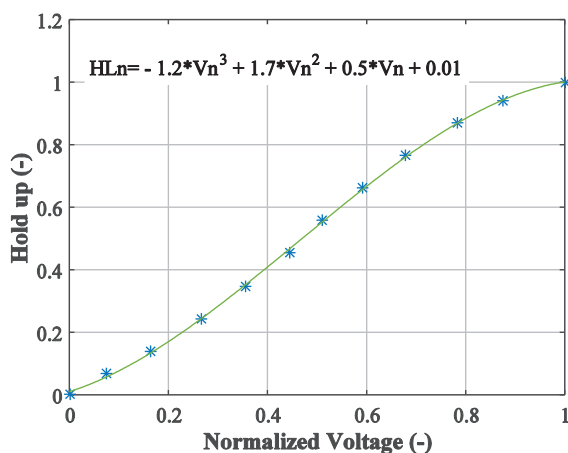


Fig. 3-12 Calibration curve of conductance probe.

3.3.1.2 Capacitance Probes

The capacitance probes measure the differences in the dielectric constant of the different phases in the flow. This type of instrument has been used previously to measure slug flow successfully (Johansen (2006), Gokcal (2008)). The instruments were designed to measure liquid fraction in oil-air two-phase flow.

The capacitance sensors were built at the multiphase laboratory of the NTNU, and SINTEF laboratory supplied the acquisition electronics. The sensor consists of a copper or aluminum foil wrapped around the external wall of the acrylic pipe. The inner strips on the foil, act as the electrodes while the outer acts as the active guard. The sensor is covered with an outer shield (normally a copper foil) to avoid external interference. Fig. 3-13 shows the final mounting of the capacitance sensor on the pipe together with the electronic card.

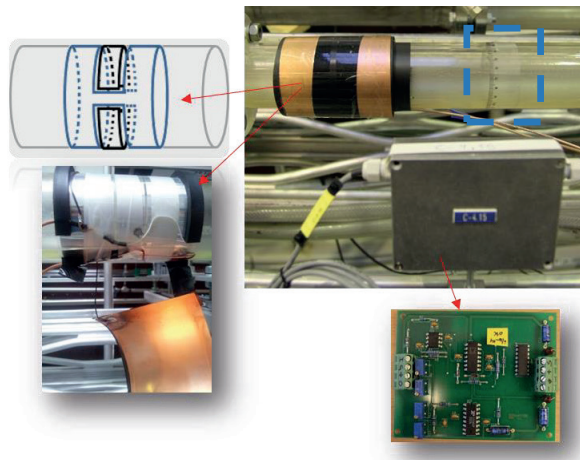


Fig. 3-13 Capacitance sensor and electronic card

The instrumentation was calibrated daily in order to register the reference point for empty pipe and full liquid pipe. Each capacitance ring was calibrated in situ, which means that it was not possible to control the liquid volume in the pipe, and the calibration were performed for co-current flow in stratified regime. The local liquid fraction at the measurement point was determined by measuring the liquid level with a scale strip wrapped around the external wall of the pipe as show Fig. 3-13. An example of the calibration curve for one capacitance ring is presented in Fig. 3-14.

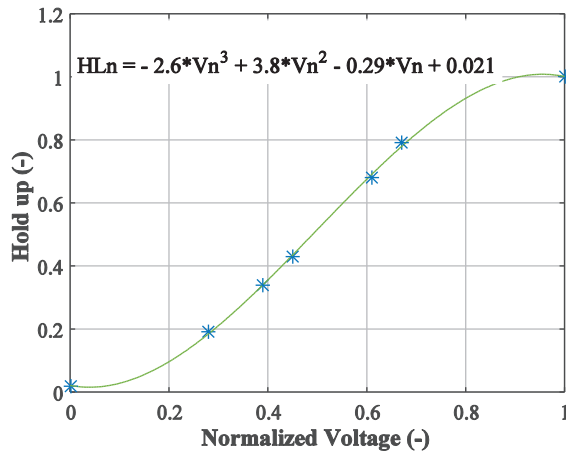


Fig. 3-14 Calibration curve of capacitance probe

These type of sensors are highly sensitive to environmental conditions, consequently changes in the fluid temperature, the quality of the liquid, and even in the room temperature might change the reference values and lead to higher error in the hold-up measurement after some hours of running experiments.

3.3.1.3 Signal processing

The hold-up time series (HI) were post-processed using a dedicated code written in Matlab2014®, which reads the raw data, filters de signal, and extracts the slug characteristics such as slug frequency, front velocity, and hold-up mean value or amplitude. An upper and lower limit was set to discriminate slugs from waves. Thus peaks in the signal that cross both limits are considered slugs, otherwise waves. Fig. 3-15 shows an example of the hold-up time series interpretation. Here the liquid hold-up of the slug body was calculated as the mean value of the top peaks (HLmax), while the hold-up in the film region corresponds to the average of the bottom peaks (HLmin); the signal amplitude was the difference between these two values. The slug frequency was calculated as the inverse of the period. The extracted hold-up values will have systematic uncertainties due to the analysis procedure. The hold-up results, however, are mainly used for flow development studies and for bubble propagation velocities by comparing the results from the different probes.

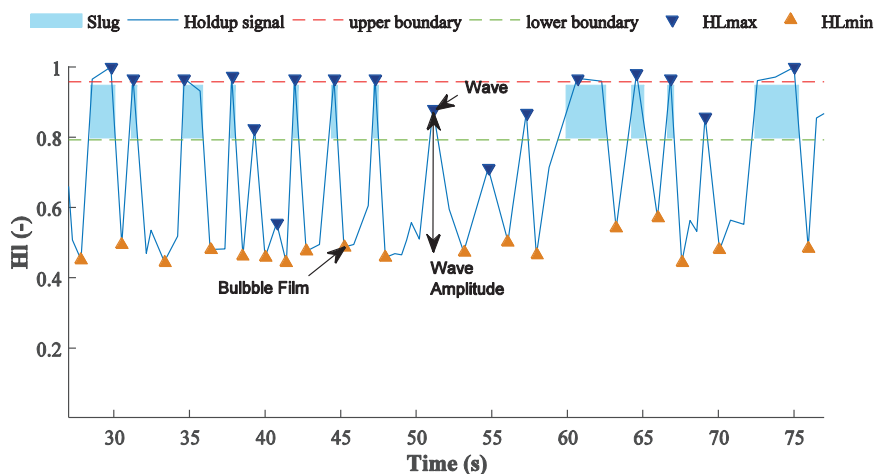


Fig. 3-15 Slug discrimination criteria

3.3.2 Front velocity

The front velocity propagation was calculated following two different non-intrusive methods. The first one was through an image processing technique, and the other one was by comparing the hold-up time series of two sensors. The use of one or another technique depended upon the availability of the instrumentation at the time of the experimental campaign.

3.3.2.1 Image analysis

The bubble displacement was measured by mean of videos recording. The videos were acquired with five synchronized cameras at 120 fps. The visualization system is shown in Fig. 3-16, and this included up to five GigE cameras model Basler acA640-120fps, a computer Intel® core™ i7 and a GigE Vision frame grabber of National Instrument model PCIe-8233. The video synchronization was done by means of a dedicated program written in LabView 2012®, which allowed starting/stopping the video recording simultaneously in all the cameras, and stamping the capturing time on each frame with a precision of 0.008s.

Special care was taken regarding the surrounding illumination in order to keep a uniform color distribution in the image and to avoid reflection from external lights that might disturb the image. The idea was to have a relatively static image in the videos, so the only mobile “object” was the bubble traveling inside the pipe. In this way, it was possible to track the bubble motion and get a close view of the interaction between consecutive bubbles.

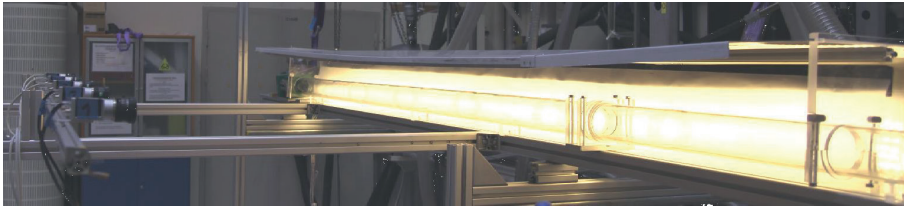


Fig. 3-16 Visualization system

The image processing was done with a dedicated code written in Matlab2014®. The script loads the videos, extracts each frame, reads the time stamped and the RGB value of the pixels in a straight line given as an input, and afterwards, it generates a matrix with the time and the pixel information. The RGB value of a particular pixel in the image changes from low intensity (dark color) to high intensity (light color) according to the motion of the bubble through that specific point. Fig. 3-17 shows an example of the signal of the bubble movement produced after the image processing.

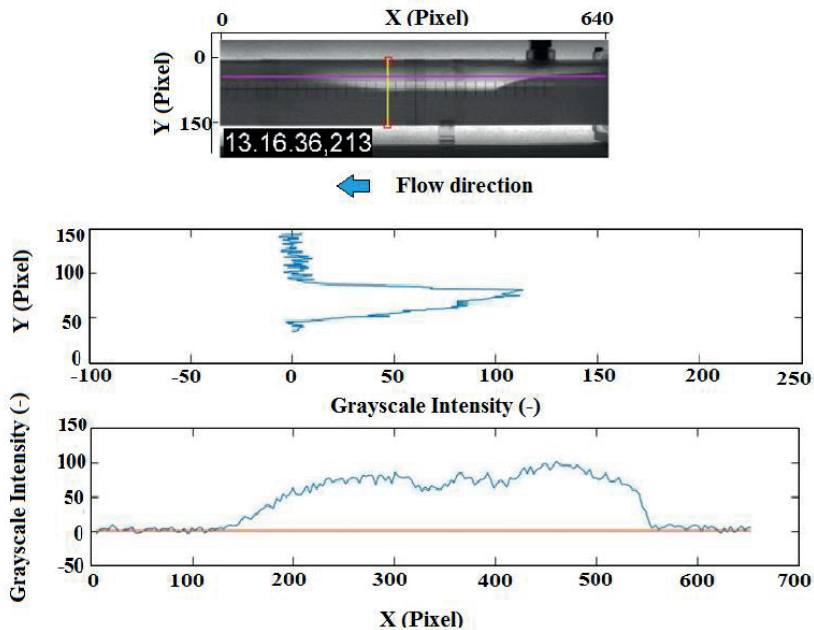
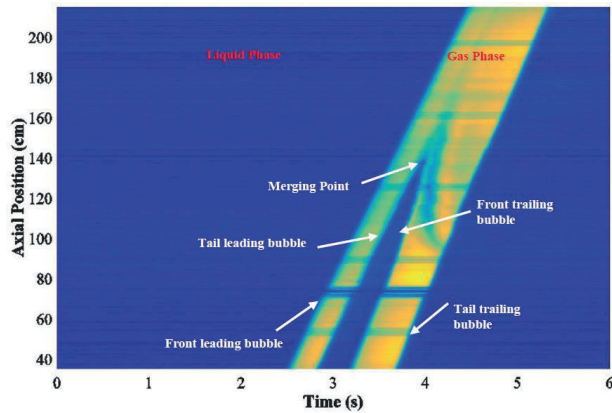
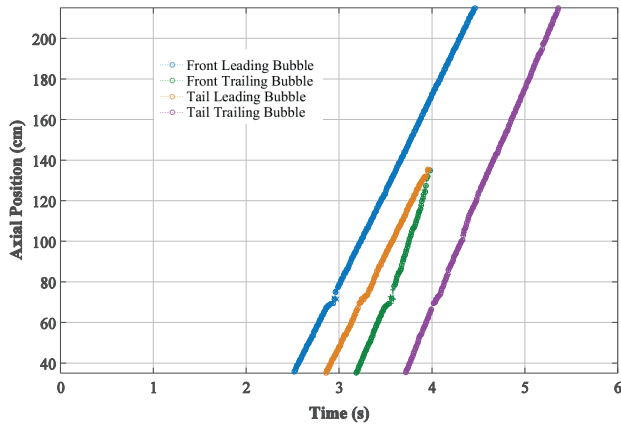


Fig. 3-17 Bubble identification with image processing technique

The output of the image processing is converted to coordinates of time and axial position after a careful process of calibration, where it is taken into consideration the image deformation (due to the camera lens), the image superposition of consecutive cameras and the relation between pixels and metric distance. After the calibration process, it is then possible to track the bubble over a horizontal profile and pinpoint the front and tail of the bubbles simultaneously. Hence, the velocity in the bubble borders can be calculated with the linear fitting over the time and space coordinates. Fig. 3-18 shows an example of the bubble movement in time and space.



a)



b)

Fig. 3-18 Bubbles movements a) Horizontal profile of all frames, b) Position and time coordinate for front and tail of each bubble

3.3.2.2 Correlation of hold-up time series

For the slug flow case, the bubble velocity was calculated by applying a cross-correlation function to the hold-up time series of each couple of rings. In the case of a single bubble, the reported velocity was the average of nine horizontal lines along the bubble nose as shows Fig. 3-19

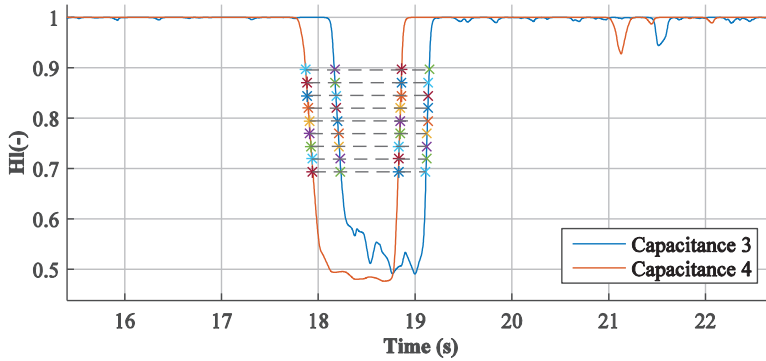


Fig. 3-19 Hold-up time trace for single bubble

Fig. 3-20 shows the comparison between the two measuring methods applied for the bubble propagation velocity measurements. The comparison results suggest a quit well performance of the image processing technique, which presents a deviation within the 10% respect the measurements with the capacitance probes.

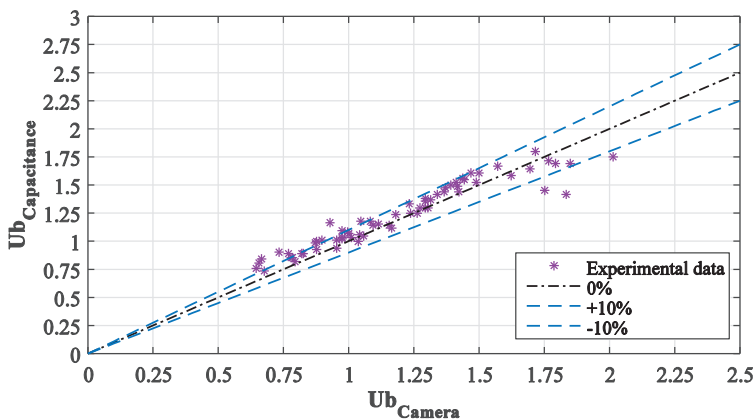


Fig. 3-20 Comparison of measurement methods: image processing vs capacitance rings

3.3.3 Superficial phase velocity

The calibration of each liquid flow meter was verified at the beginning of the first experimental campaign. The calibration setup consisted of a weight scale, a chronometer, and a video camera. The flow coming from the horizontal flow loop was diverted toward the weight scale while the video camera recorded the weight change of the scale. Thus, from the video, it was possible to determine the mass flow rate and compare it against the flow meters reading. Table 3-8 summarizes the characteristics of the different flow meters including the operating range and accuracy.

Table 3-8 Flow meter characteristics

Flow Meter	Model	Type	Range	Accuracy
Oil flow meter	Micro Motion T150	Coriolis	0-36 000 kg/h	±0.15% of rate
	Micro Motion F025	Coriolis	109-1088.4 kg/h	±0.15% of rate
Air flow meter	Micro Motion CMF025	Coriolis	Up to 2180 kg/h	±0.05% of rate
	Siemens Sitrans Fc	Coriolis	0-4000 kg/h	±0.15% of rate
Water flow meter	COPA XM	electromagnetic	3-60m ³ /h	±0.01 to 0.5% of rate
	Promag	electromagnetic	0.19-31.8 m ³ /h	±0.01 to 0.5% of rate

The phase superficial velocity was calculated from the mass flow rate or volumetric flow rate measured in the single-phase lines, using the inner diameter of the test section and the flow properties at the atmospheric conditions.

Severe slugging experiments performed with oil over 80cP were a particular case because the liquid flow rate was out of the range of the flow meters. In this case, it was used a screw pump to assure a stable and constant flow rate. The calibration of the pump frequency with the supplied mass flow rate is shown in Fig. 3-21.

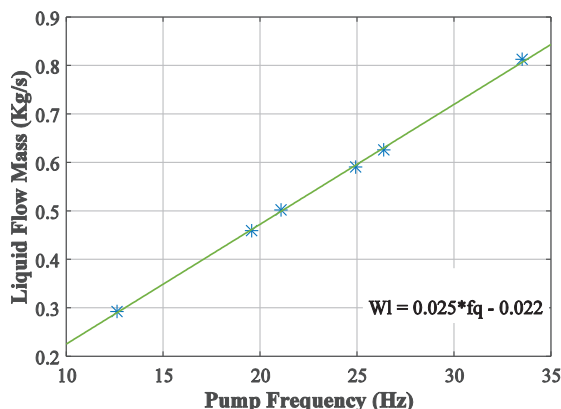


Fig. 3-21 Screw pump calibration for liquid flow mass. (Oil 90cP; 850kg/m³)

3.3.4 Liquid viscosity

The liquid viscosities reported were measured by means of a rheometer ARES-G2. The Newtonian behavior of the fluids were analyzed by the linear regression of the stress and the shear rate measured at atmospheric conditions (1bar and 21 °C). Fig. 3-22 presents the temperature ramp analysis for the oil 65cP. The oil temperature and density was monitored from the values reported by the Coriolis meter. The temperature variation over 8 hours of continuous work was no higher than 2°C, thus the temperature range was around 21 to 23 °C.

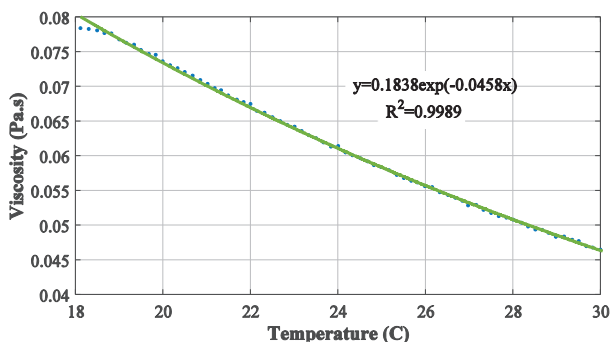


Fig. 3-22 Viscosity vs. temperature for oil 65cP

Fig. 3-23 shows the liquid viscosity of the mixed oil as a function of the volume proportion of the oil mixed: oil 65cP and oil 10cP

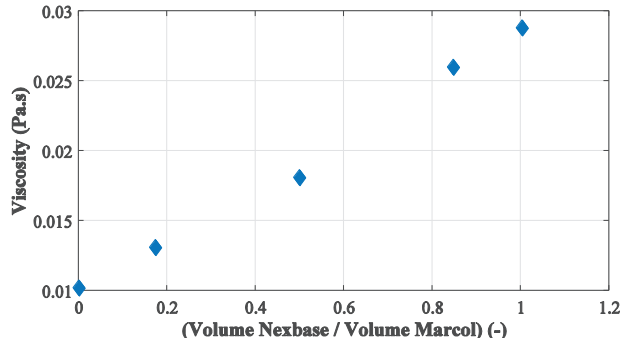


Fig. 3-23 Mixture viscosity relation when mixing oil at 10cP and oil 65cP

3.4 Design of two-energy multibeam gamma densitometer

A gamma densitometry is a widely used non-intrusive technique to measure densities and phase fractions in multiphase flows. It consists in determining the attenuation of a collimated gamma beam through the multiphase mixture, where each phase presents different absorption coefficient (Falcone et al. (2009)). Ideally the beam should cover the whole cross-sectional area of the pipe in order to obtain the average value regardless of the flow configuration. In this project, a new multibeam instrument was designed and built with support from The Multiphase Flow Assurance Centre (FACE). This work is a continuation of Plasencia (2013), and it was done in close cooperation with another PhD student, Andrea Shmueli, and the engineer Halvor Haukvik. The direct contribution of the present PhD work was mainly on the evaluation and selection of the gamma source, calculation of the shielding holder, design and drawings of the different components, following up the manufacture of parts and testing of the safety mechanism and radiation emissions.

The instrument aims to measure the phase fractions all along the cross-sectional area using five gamma beams as is shown in Fig. 3-24. The sources and detectors with their respective preamplifiers were distributed in a compact arrangement to fit pipes with a minimum external diameter of 70mm. The unit is able to rotate around the pipe and traverse linearly along the vertical diameter, to cover different directions of the beams and to allow working with pipes of larger external diameter (up to 90mm).

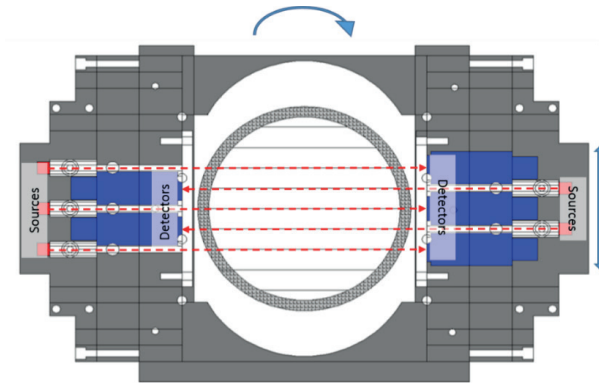


Fig. 3-24 Scheme of the gamma densitometer

The design of the instrument included the selection of the gamma source, sizing both source and detector holder, defining collimators distribution and size, design the safety mechanism, as well as the mobile base where all the parts were assembled together. Fig. 3-25 shows and identifies the main parts of the instrument, and the following section describes each of the main components.

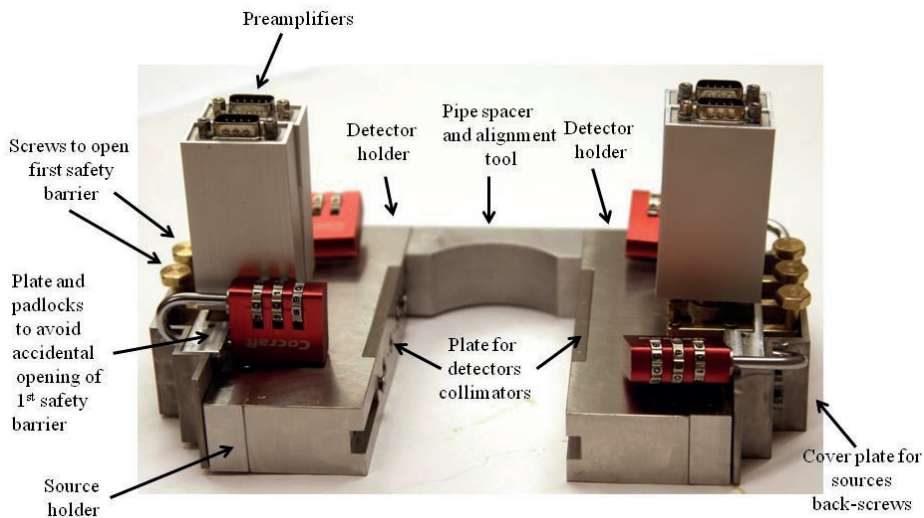


Fig. 3-25 Main parts of the gamma densitometer

The Gamma sources were selected based on the previous work of Plasencia (2013), where the author compared two type of gamma sources: Americium (Am^{241}) and Barium (Ba^{133}). Table 3-9 presents the major pro and cons reported for Plasencia (2013)

when comparing the two type of sources in terms of their technical characteristics, costs and complexity of the source holder.

Table 3-9 Comparison between sources

Ba133	Am241
Energy level peaks around 31 keV and 81 keV for the low and high peaks respectively. The higher energy level offers a better penetration and it is still low enough to get a good discrimination of a liquid-liquid system.	Energy level peaks around 18 keV and 60keV for the low and high peaks respectively. The contrast between the two liquid phases is still good enough.
Estimated life 10.5 years	Long life of the source, estimated life around 432 years
High cost per source	Significant lower cost in comparison with Ba ¹³³
Higher energy level in comparison with Am ²⁴¹ . Ba133 can present energy levels around 400keV	Energy levels about 100keV
Needs a significantly thicker shielding, increasing size and weight of the instrument.	Less shielding material in comparison with the required for the Barium. Allows building a more compact unit.
Lower counting rates	Provides with higher counting rates than Ba ¹³³ in all energy levels, which is high enough to get a higher sampling speed in comparison to Ba ¹³³
No information available	Shmueli (2015) reported a limitation of the Am ²⁴¹ source to measure three phases (oil-water-air) when the water layer was high enough to make the lowest energy peak disappear. She found that the critical water thickness layer for this to happen was about 4mm of water measured from the bottom pipe wall
Source activity available up to 1GBq	Source activity available up to 11GBq

After analyzing the possible performance of each type of source and considering cost and sizing of an instrument of five sources, it was decided to use Am241 of 3.7 GBq (Eckert and Ziegel. Model: AM132330100M) supplied by Gammadata. The source properties are summarized in Table 3-10.

Table 3-10 Source properties

Source	Photon flux (s·sr)⁻¹		Activity (MBq)
	59.5 keV	17.8 keV	
Am-241	6.7·108	107	3700

The source holder was designed according to the Norwegian Law Regulations for handling radiation (2008). According to this standard, the radiation exposure must be less than 0.5 $\mu\text{Sv/h}$ at 5cm from the instrument, less than 7.5 $\mu\text{Sv/h}$ at 1m from the instrument and a dose rate less than 85 $\mu\text{Sv/h/GBq}$ at 1 m from the instrument.

The Lambert's Law expresses the intensity exponential decay:

$$I = I_0 e^{-\mu d} \quad (3-1)$$

Where **I** is the intensity at distance **d** from the source, **I₀** is the initial intensity and **μ** is the linear attenuation coefficient.

Then from Eq. 3-1, it is possible to calculate the thickness required to reduce the exposure rate to at half of its value (HLV) and to a tenth of its value (TVL). Table 3-11 summarizes the calculation of the wall thickness for different materials required to satisfy the safety regulations.

Table 3-11 Shielding thickness calculation

Distance from instrument	Requirement (mSv/h)	Intensity without shielding (mSv/h)	Required Dampening (times)	Shielding material	Thickness (mm)	times-TVL (times)
5 cm	0.5	125.8	251.6	Aluminum	74.5	2.4
				Lead	0.99	
				Iron	5.82	
				Stainless Steel	6.70	
				Tungsten	0.98	
1 m	7.5	314	41.9	Aluminum	50.34	1.6
				Lead	0.68	
				Iron	3.92	
				Stainless Steel	4.57	
				Tungsten	0.66	

Based on the results from Table 3-11 the source holder was made mainly in stainless steel with thin layers of lead surrounding each source and on the back of them, giving extra shielding to the holder. Fig. 3-26 presents a 3D representation of the source holder (for the three sources side), which include the sources (red circles) and the safety mechanism.

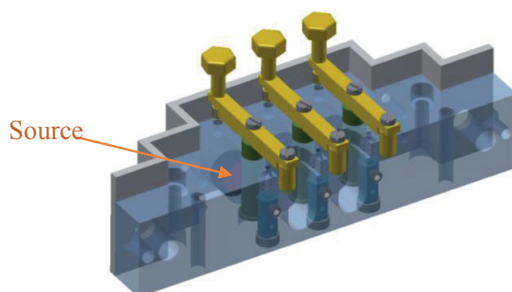


Fig. 3-26 Source holder 3D representation

The **detector-preamplifier units** are located on the opposite side of the multiphase pipe. The device includes the detector that receive the gamma rays from the sources and the preamplifier that collects the produced energy and transmits the signal to be further processed. A dedicated evaluation of the proper equipment was performed by Plasencia (2013) who recommended a spectrum quality detector CdTe ($5 \times 5 \times 2$ mm³) together with a preamplifier PR 16-H supplier by Eurorad.

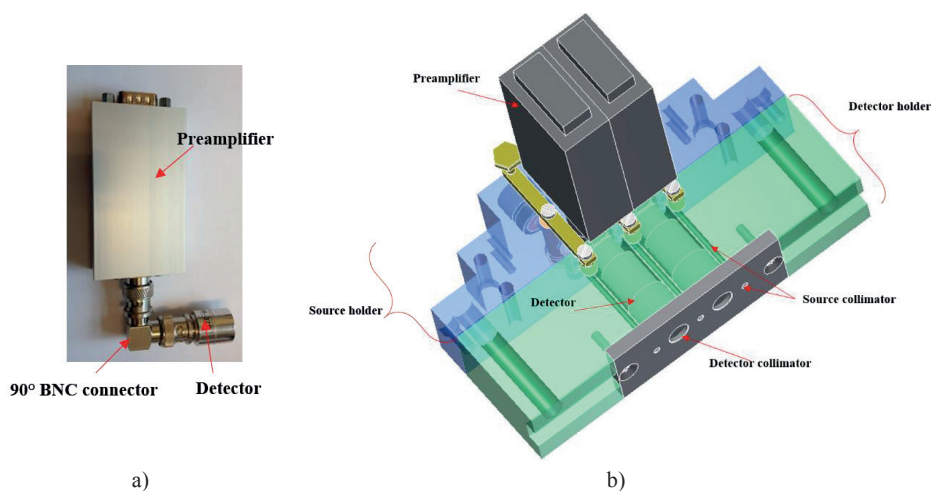


Fig. 3-27 a) Amplifier-detector assembly and b) 3D Representation detector holder.

The unit detector-preamplifier (Fig. 3 27 a) is assembled into the detector holder, which is designed to keep aligned the detector with its corresponding source. This part also includes the collimators of the sources and detectors, which allows defining the direction of the gamma rays from each source and limits the measurement region capturing by each detector, preventing gamma rays from neighboring sources to interfere the signal of a given detector. The source collimators consist in 70 mm long cylindrical channels of

2.2 mm of diameter. While the detector collimators correspond to 5.5 mm long cylindrical channels of 8.5 mm of diameter, drilled in a small plate attached in front of the detectors.

The mobile base: The assembly of source and detector holders of Fig. 3-25 is fixed to a mobile base that can freely rotate around the pipe and to move linearly. Fig. 3-28 presents the assembly base with the rotary and linear mechanism.

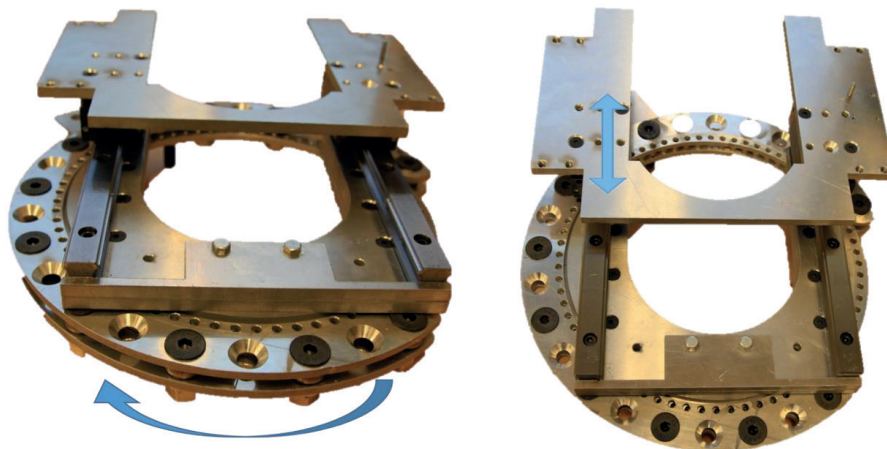


Fig. 3-28 Mobile base for supporting the assembly

The safety mechanism includes two protection stages in order to keep the radioactive sources shielded when the instrument is not used. The first safety barrier is manually closed to “shutdown” when the instrument is not in operation. It consists of tungsten heavy alloy rods located individually in front of each source; in the open positions a transversal hole of 2.2mm is aligned to the collimator allowing the beam to go out. The second barrier prevents the holder to be removed from the base without properly closing the sources holder. It consists of internal rods (also of tungsten) aligned with the first barrier that are normally closed, and they are only open when the source holder is placed on the base plate, which is designed to push the barrier up when the holder is fixed in the right position. A sketch of the source holder safety mechanisms is shown in Fig. 3-29.

The efficiency of the safety mechanisms was tested at IFE. The local reading of the radiation was less than 2 μSv with the two safety mechanisms and less than 10 μSv with one of the safety mechanisms open.

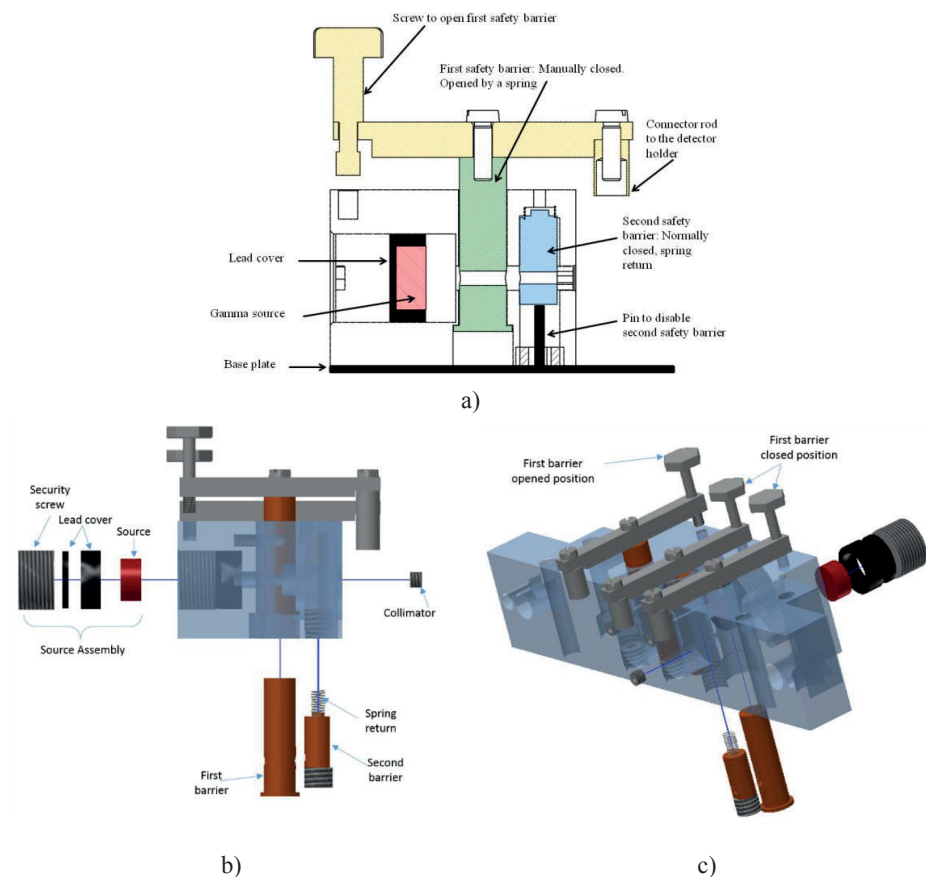


Fig. 3-29 Safety mechanism sketch. a) transversal cut after Shmueli (2015), b) lateral view, c) isometric view

Electronic components: The preamplifiers are connected to the spectroscopy amplifiers and from there to a computer with multichannel analyzer software. A high voltage supplier is required to give the electric field to collect the charge produced by the interaction between the gamma ray and the detector. Hence, the Canberra 3106D power supply was selected for this application as it is specially designed for operation with semiconductor detectors requiring up to 6 kV bias and up to 300 μA of current. One spectroscopy amplifier is required for each detector in the system. For this instrument, a Canberra amplifier model 2022 was selected. The amplified pulses are sent now to a multichannel analyzer. This analyzer comprises a digitizer (Spectrum model M2I.3122-EXP 12 bit) and a PC with analysis software.

Chapter 4

Conclusions

An experimental study has been carried out on particular aspects of gas-liquid slug flow with liquid viscosities in the range 1–90 cPs. The study included severe slugging in S-shaped risers and hydrodynamic slug flow in horizontal and near horizontal pipes. The focus has been on bubble velocity measurements from laminar to turbulent flows and on history effects on the stratified-slug transition boundary. The bubble propagation velocity (with the wake effect) and flow regime transition models are required as closure relations for unit cell slug flow models and for dynamic models. The following conclusions were derived from this work:

Severe slugging

Severe slugging maps in an S-shaped riser were generated for air-liquid flow with three liquid viscosities: 1cP, 65cP and 90cP. Increasing the liquid viscosity reduces the region with unstable flow in the flow regime map. At high liquid flow rates, the transition to slug flow in the upstream pipe occurs earlier at higher viscosities, which stabilizes severe slugging. At lower liquid flow rates, the higher friction component of a more viscous mixture stabilizes the severe slugging. Another observation is that severe slugging type II (partial blockage of the bend) vanishes at higher viscosities and the flow stability map showed only the extreme unstable case (full blockage of the bend) and the stable condition.

OLGA simulations compared reasonably well with the experimental results for the air-water case, but less so for the viscous cases. A hybrid capturing and tracking scheme at NTNU (SLUGGIT) compared quite well with the experiments also for the viscous case.

History effect on flow regime transitions

The history effect of the upstream flow on the downstream flow regime in a downwards inclined pipe was studied for air-oil (65cP) and air-water (1cP) flows. The experiments confirm the existence of metastable region in the flow regime map where both stratified and slug flow can be stable flow regimes depending on the flow patten at the inlet. Intermittent flow as inlet condition induced a larger region with intermittent flow in a flow regime map in comparison with the case with stratified flow at the inlet. The metastable region was larger for the high viscosity case. For the air-water case, the comparisons with stratified stability models from the literature show acceptable results for the stratified-slug transition with stratified flow at the inlet, and the meta-stable region is in reasonable agreement with the slug stability criterion. For the air-oil case, the two criteria give quite close transition boundaries, and the metastable region is underestimated.

Simulations with standard OLGA did not show any difference in the flow map with different inlet condition changes; it predicted the same flow behavior regardless of the inlet flow regime. On the contrary, the OLGA slug-tracking model predicted different flow patten maps according to the initial conditions, in more agreement with the experimental results. However, the history effect of the flow was overestimated, giving either stratified or intermittent flow in the downward pipe for the stratified inlet or intermittent inlet condition respectively, for all flow rates.

Bubble propagation velocity

Two aspects of the bubble propagation velocity were studied: the propagation along the pipe of single bubbles from laminar to turbulent flow and the merging of two bubbles in laminar flow. The merging occurs because the trailing bubble accelerates as the distance between the bubbles decreases (the wake effect). The wake effect, when implemented in slug tracking models, can provide the mechanism for predictions of the statistical slug length distributions along a straight pipe.

For transitional flow, single bubbles tended to move with velocities between the expectations from laminar flow and for turbulent flow. A simple weighted averaging between the two, based on an estimated transitional region in terms of Reynolds numbers, was proposed as a practical relation for bubble velocities in transitional flows.

On the wake effect, the experimental data were compared against correlations available in the literature, mostly for turbulent flows. Most relations overestimate the wake effect, and it appears that the laminar flow case does not deviate significantly from the turbulent

flow case. A stronger wake effect was observed for the limiting cases where the liquid velocity approaches the values of the drift velocity. For these low liquid flow rates in a horizontal pipe the slug front decays to a hydraulic jump, with a free surface extending into the slug and affecting the trailing bubble for quite long slug lengths.

Recommendations for further work

The use of aqueous based solution mixtures for the liquid phase is recommended for further work on multiphase flows with viscous liquids in the Multiphase Flow Laboratory. This way it would be easier to change the viscosity and the liquid fraction instruments based on electric conductance are also applicable. The challenge is to retain the Newtonian behavior of the liquid.

The measurement system based on image processing was useful for capturing the wake effect of two trailing bubbles. The system could be applied for further studies in inclined flows and could possibly also be applied to three phase flows, for cases where the oil-water interface is well defined.

The history effect could also be further mapped with stronger pipe inclinations and, if possible, with much longer pipes. For some cases it was not clear whether a slug flow at the inlet would decay further downstream if the pipe had been much longer.

Further sensitivity studies can be made with dynamic slug tracking models, regarding the effects of the bubble velocity relations and the wake effect on the simulations of the slug flow evolution in a pipe.

References

- AKHIYAROV, D. T., ZHANG, H.-Q. & SARICA, C. 2010. *High-Viscosity Oil-Gas Flow in Vertical Pipe*. Offshore Technology Conference. Houston, Texas, USA.
- AUTHORITY, N. R. P. 2008. *Guidance to Regulation on Radiation Protection and Use of Radiation*". Guidance No 9. Norway, Østerås.
- BENDIKSEN, K. & ESPEDAL, M. 1992. *Onset of Slugging in Horizontal Gas-Liquid Pipe-Flow*. International Journal of Multiphase Flow, 18, 237-247.
- DE LEEBEECK, A. & NYDAL, O. J. 2010. *Simulation of large amplitude waves in a slug tracking scheme compared to roll wave experiments at high pressure*. International Journal of Multiphase Flow, 36, 40-50.
- FABRE, J. 1994. *Advancements in Two-Phase Slug Flow Modeling*. Society of Petroleum Engineers Journal.
- FALCONE, G., HEWITT, G. & ALIMONTI, C. 2009. *Multiphase Flow Metering: Principles and Applications*, Elsevier Science.
- GOKCAL, B. 2008. *An experimental and theoretical investigation of slug flow for high oil viscosity in horizontal pipes*. Doctor of Philosophy The University of Tulsa.
- GOKCAL, B., WANG, Q., ZHANG, H.-Q. & SARICA, C. 2008. *Effects of High Oil Viscosity on Oil/Gas Flow Behavior in Horizontal Pipes*. SPE Projects, Facilities & Construction, 3, 1-11.
- ISSA, R. I. & KEMPF, M. H. W. 2003. *Simulation of slug flow in horizontal and nearly horizontal pipes with the two-fluid model*. International Journal of Multiphase Flow, 29, 69-95.
- JOHANSEN, M. 2006. *An experimental study of the bubble propagation velocity in 3-phase slug flow*. PhD, NTNU.
- KJELDBY, T. K. 2013. *Langragian Three-phase Slug Tracking Methods*. Philosophiae Doctor, Norwegian University of Science and Technology.
- LIN, P. Y. & HANRATTY, T. J. 1986. *Prediction of the Initiation of Slugs with Linear-Stability Theory*. International Journal of Multiphase Flow, 12, 79-98.
- MANDHANE, J. M., GREGORY, G. A. & AZIZ, K. 1974. *A flow pattern map for gas—liquid flow in horizontal pipes*. International Journal of Multiphase Flow, 1, 537-553.
- NYDAL, O. J. 2012. *Dynamic Models in Multiphase Flow*. Energy & Fuels, 26, 4117-4123.

- NYDAL, O. J., AUDIBERT, M. & JOHANSEN, M. 2001. *Experiments and Modeling of Gas-Liquid Flow in S-shaped Riser*. 10th International Conference on Multiphase Production, BHR Group.
- PLASENCIA, J. L. 2013. *Experimental study on two phase oil-water dispersed flow*. Doctoral Thesis, Norwegian University of Science and Technology.
- SCHLUMBERGER 2013. *User Manual OLGA 7.3*, Schlumberger Software.
- SHMUELI, A. 2015. *Experiments on the Droplet Field in Multiphase Pipe Flow*. Doctoral Thesis, Norwegian University of Science and Technology.
- SHOHAM, O. 2006. *Mechanistic Modeling of Gas-liquid Two-phase Flow in Pipes*, Society of Petroleum Engineers.
- TAITEL, Y. & DUKLER, A. E. 1976. *Model for Predicting Flow Regime Transitions in Horizontal and near Horizontal Gas-Liquid Flow*. Aiche Journal, 22, 47-55.

Appendix A

A-1. SEVERE SLUGGING EXPERIMENTS NO PUBLISHED

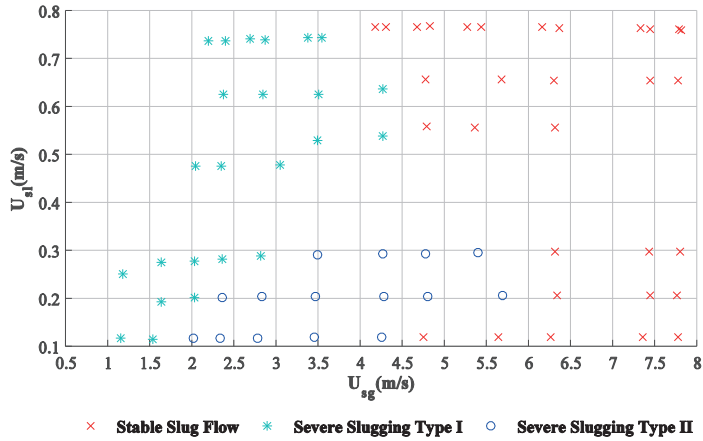


Fig. A- 1 Severe slugging stability map for Water-Air

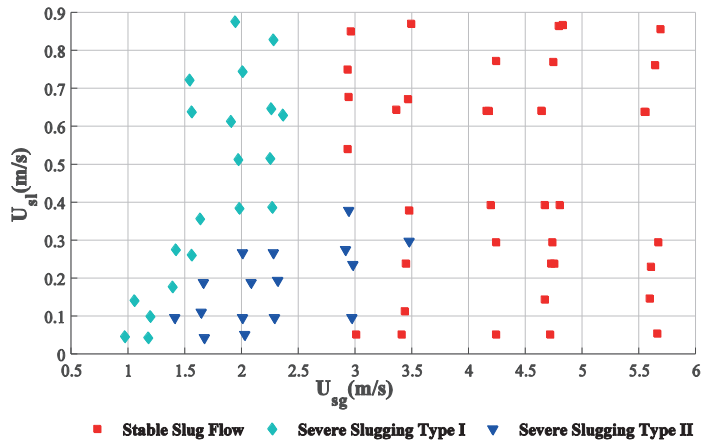


Fig. A- 2 Severe slugging stability map for Oil 65cP-Air

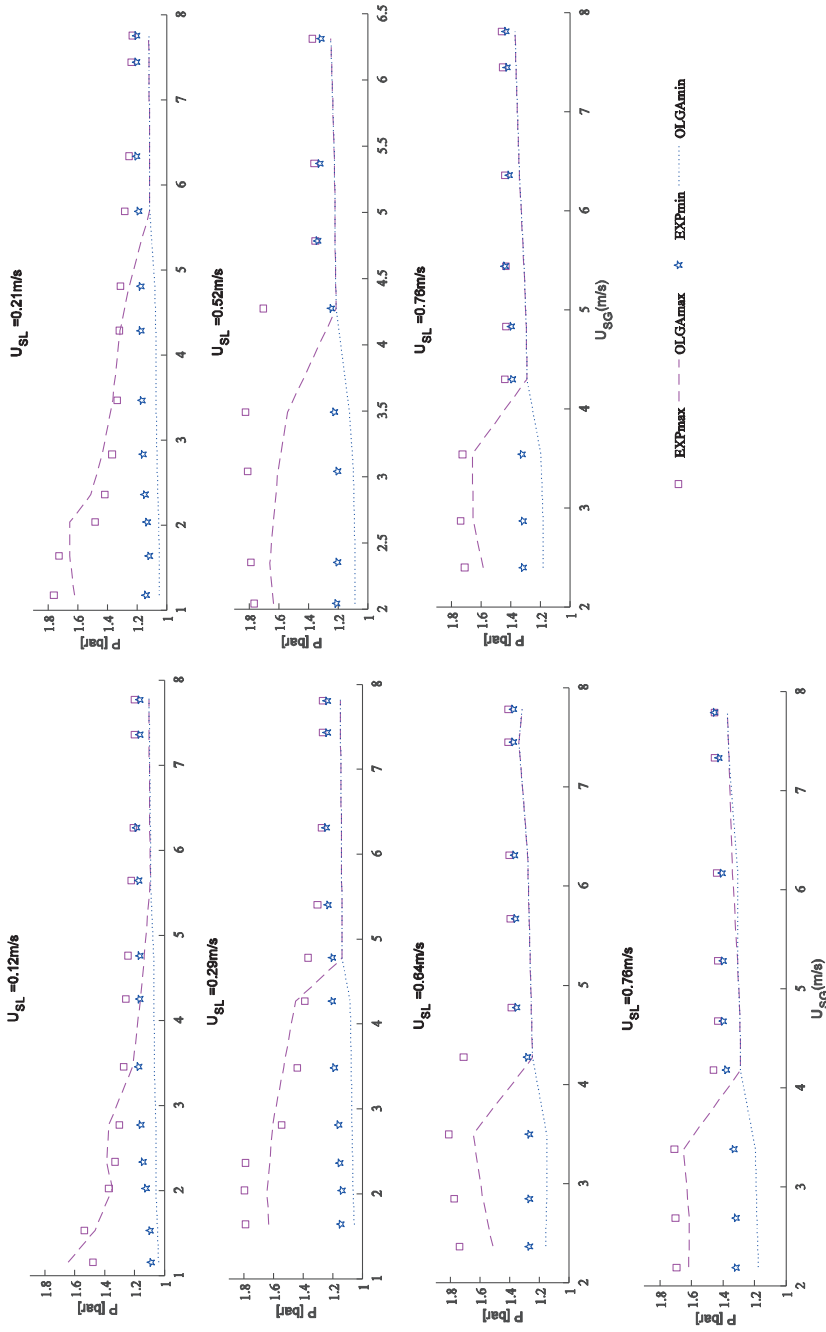


Fig. A-3 Pressure fluctuation for severe slugging experiments with water-air

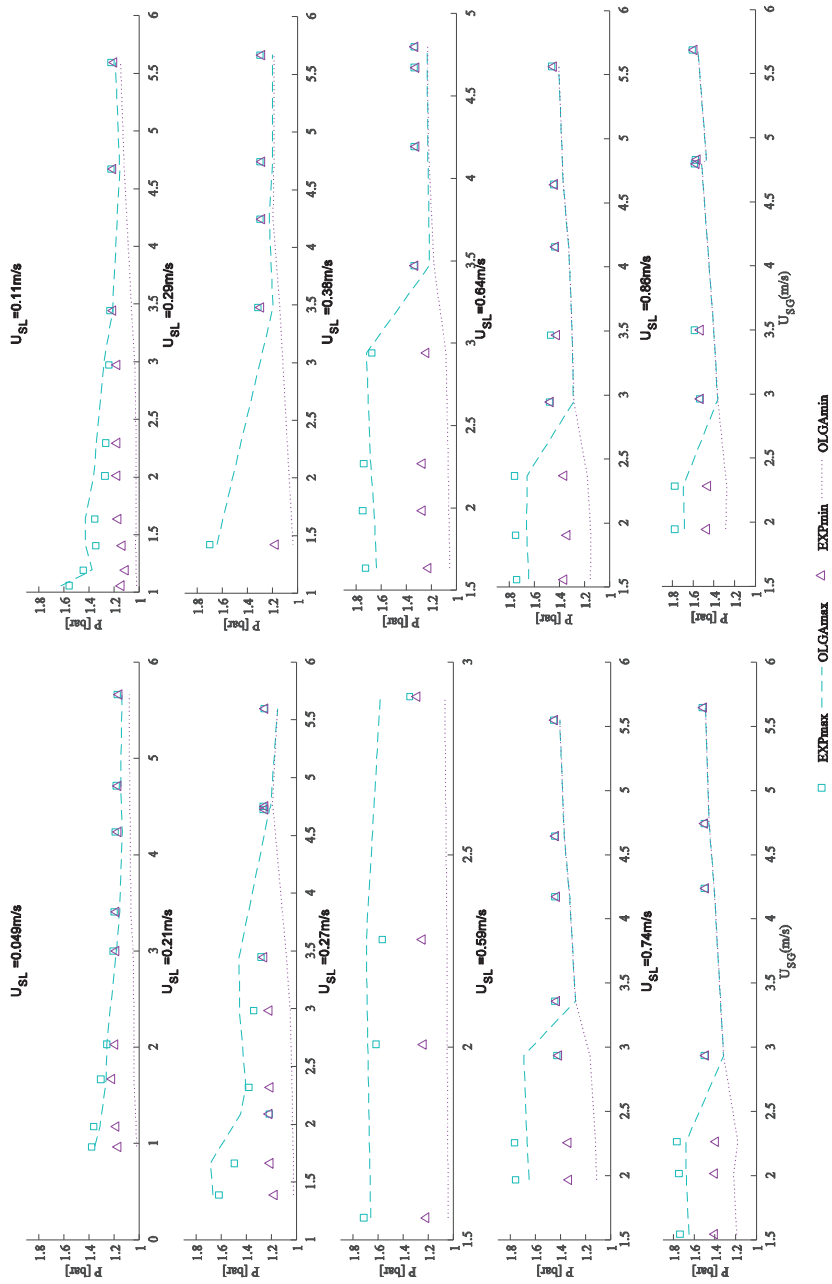


Fig. A-4 Pressure fluctuation for severe slugging experiments with oil-air

A-2. INSTRUMENT SPECIFICATIONS

Capacitance probes:

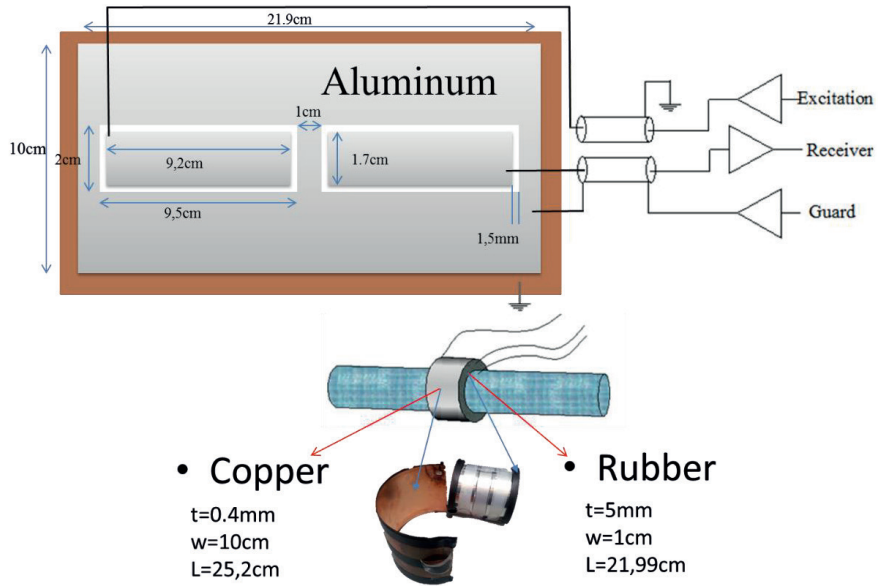


Fig. A- 5 Capacitance probes: sensor ring

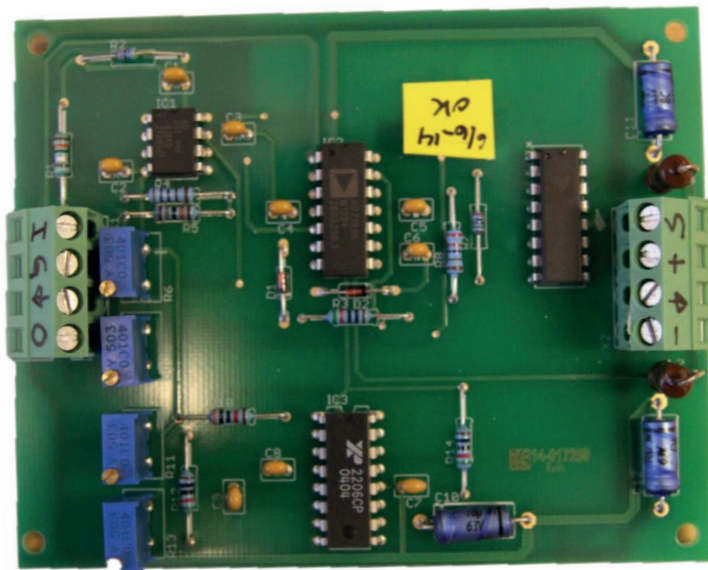


Fig. A- 6 Capacitance probes: electronics

Cameras



acA640-120gm ace Series

SPECIFICATIONS	
Resolution (H x V pixels)	659 px x 494 px
Pixel Size horizontal/vertical	5.6 μm x 5.6 μm
Frame Rate	120 fps
Mono/Color	Mono
Interface	GigE
Video Output Format	Mono 8, Mono 12, Mono 12 Packed, YUV 4:2:2 Packed, YUV 4:2:2 (YUYV) Packed
Pixel Bit Depth	12 bits
Synchronization	external trigger free-run Ethernet connection
Exposure Control	programmable via the camera API external trigger signal
Housing	box
Quantum Efficiency (typical)	61,0 % (at 545 nm)
Dark Noise (typical)	11 e-
Saturation Capacity (typical)	16,6 ke-
Dynamic Range (typical)	63,5 dB
Housing Size (L x W x H) in mm	42.0 x 29.0 x 29.0
Housing Temperature	0 °C - 50 °C
Lens Mount	C-mount CS-mount
Digital Input	1
Digital Output	1
Power Requirements	PoE or 12 VDC
Power Consumption (typical)	2.0 W
Power Consumption PoE	2.3 W
Weight (typical)	90 g
Conformity	CE RoHS GenICam GigE Vision IP30 UL FCC IEEE 802.3af (PoE)
Sensor Vendor	Sony
Sensor Name	ICX618
Shutter	global shutter
Max. Image Circle	1/4 inch
Sensor Type	CCD
Sensor Size (mm)	3.69 mm x 2.77 mm

A-3. CAMERAS ACQUISITION CODE

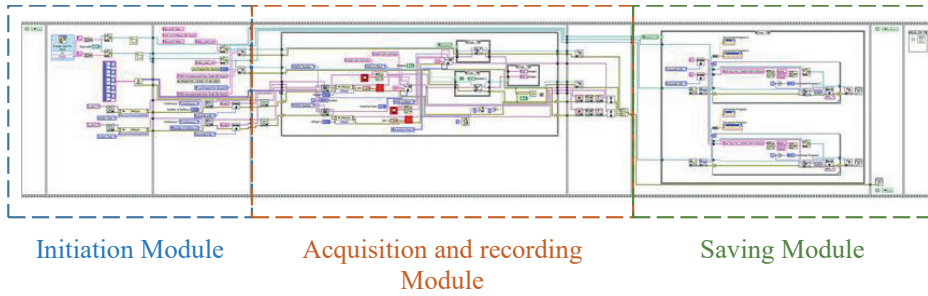


Fig. A- 8 Global view of the LabVIEW code for two cameras synchronized

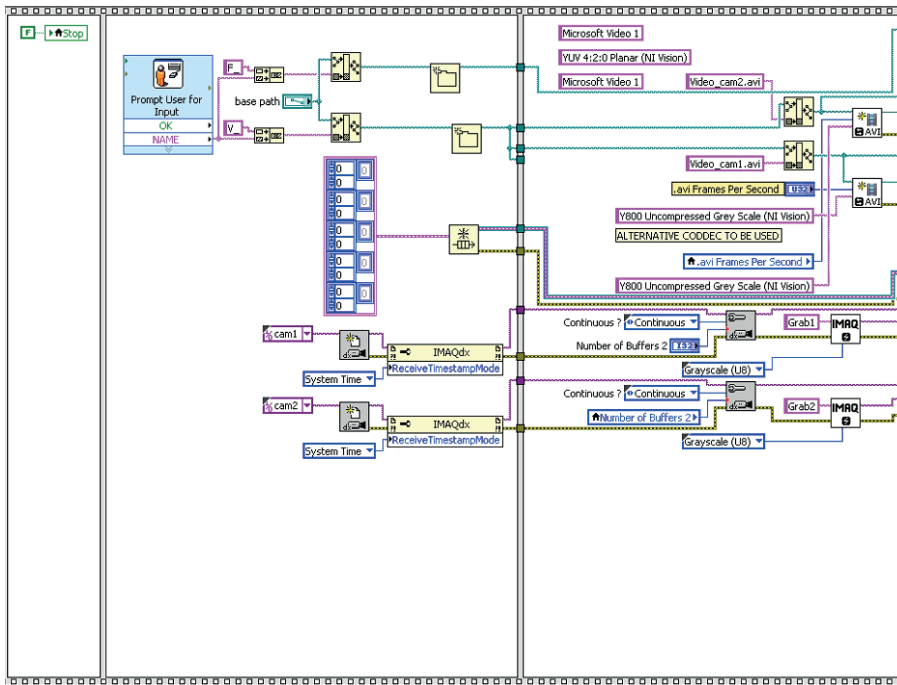


Fig. A- 9 Initiation module view

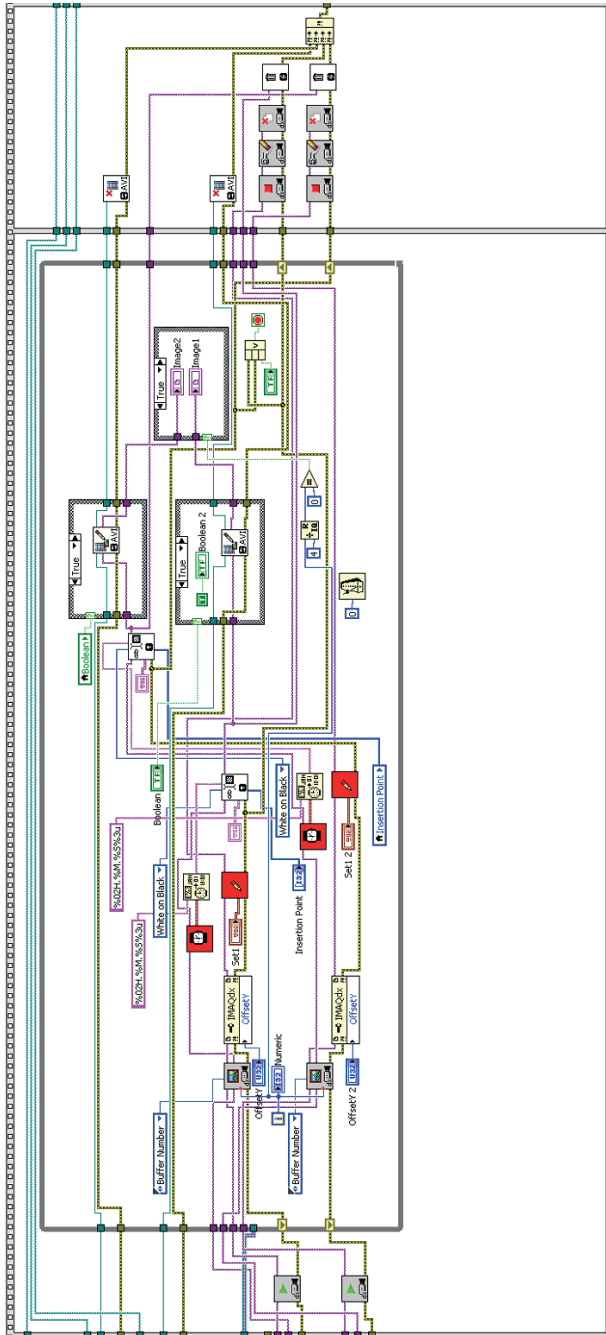


Fig. A-10 Acquisition and recording module

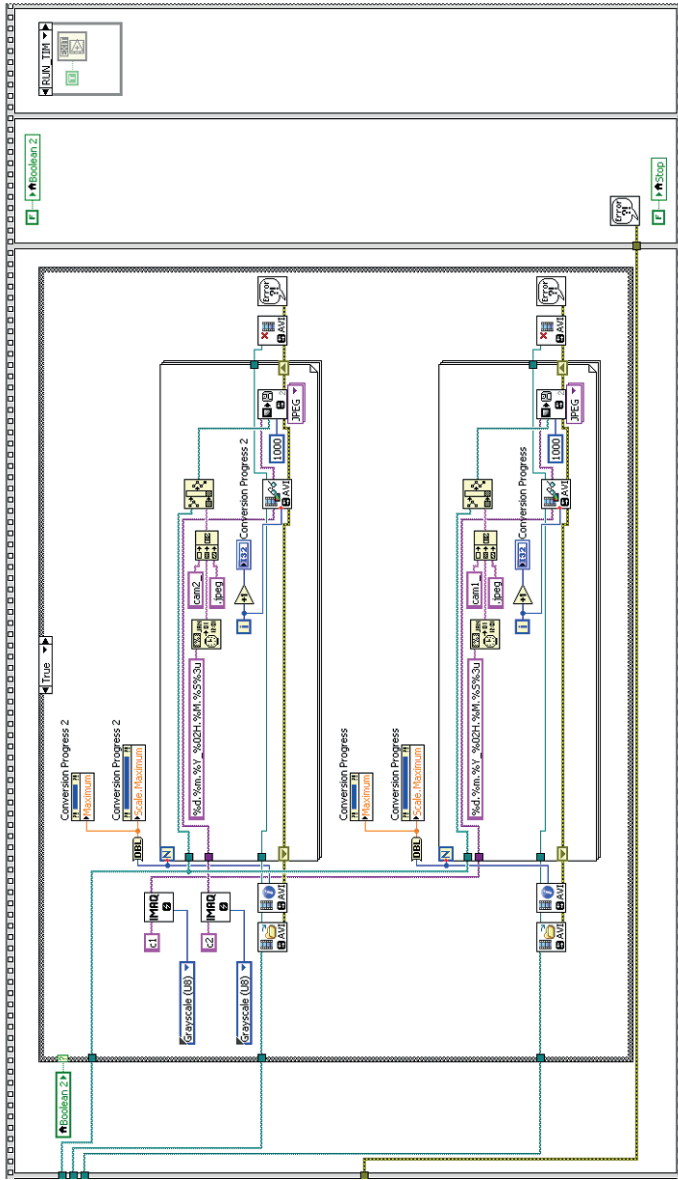


Fig. A-11 Saving module

PAPER I

Experiments on Severe Slugging in a S-Riser System with Viscous Liquids

Is not included due to copyright

PAPER II

Severe Slugging with Viscous Liquids Experiments and Simulations

Is not included due to copyright

PAPER III

Inlet Effects on Flow Regimes in Downwards Inclined Pipes

Is not included due to copyright

PAPER IV

Bubble Translational Velocity in Horizontal Slug Flow
with Medium Liquid Viscosity

Bubble Translational Velocity in Horizontal Slug Flow with Medium Liquid Viscosity

Mariana J.C. Díaz and Ole J. Nydal,
*Department of Energy and Process Engineering
Norwegian University of Science and Technology*

Abstract

The bubble translational velocity is one of the closure relations commonly used in gas-liquid slug flow models. However, the available information regarding viscous effects on this parameter is limited, in particular through the laminar to turbulent flow transition. The present work gives experimental results on the bubble translational velocity in horizontal gas-liquid flows for Reynolds numbers from 250 up to 5100. The experiments were carried out in a 50m long pipe of 60mm inner diameter with air and mineral oils (viscosities 10cp, 20cP, 26cp, and 65cp). The velocity propagation of a single air-bubble traveling in a continuous liquid stream was measured by means of image processing from multiple cameras and from capacitance probes. An empirical relation for the bubble propagation velocity through the transitional region is presented, based on the experimental results.

Keywords: Bubble velocity, slug flow, laminar region, transitional region

Introduction

The accuracy of the multiphase flow models depends on the closure laws implemented in the models. In 1D models, these closure relations are cross-sectional averages which depends on the flow regime. The bubble translational velocity is one of the closure relations commonly used in unit cell models (where slug flow is represented as a characteristic slug and bubble cell) as well as in dynamic slug tracking models.

Nicklin (1962) suggested a relation between the liquid velocity ahead of the bubble nose and the bubble front velocity in vertical flow:

$$U_b = C_o U_m + U_o \dots\dots\dots (1)$$

C_o is the distribution parameter, U_o is the rise velocity in stagnant liquid and U_m is the average liquid velocity ahead of the bubble front. This relation has later been extended and generalized to all pipes inclinations. **Table 1** presents a summary of some correlations found in the literature for different flow conditions and pipe geometries.

Table 1 Correlations in the literature for C_o and U_o (Eq. 1).

Author (Year)	Pipe Geom.	Fluid Properties	(a) C_o	(b) U_o/\sqrt{gD}	Range	Eq.
Nicklin (1962)	Vertical 26mm	Air –Water.	U_c / \bar{U}	0.35		(2)
Collins et al. (1978)	Vertical 51.4mm	Continuous slug flow. Glycerol / Air	$\left[\frac{\log_{10} Re + 0.21}{\log_{10} Re - 0.74} \right]$	0.347	$Fr < 2$	(3)
			$\left[\frac{\log_{10} Re + 0.089}{\log_{10} Re - 0.74} \right]$	$\left(\frac{\bar{U}}{(gD)^{0.5}} \frac{0.083}{\log_{10} Re - 0.74} \right)^{1/3}$ $+ \frac{1}{3} \left(\frac{\bar{U}}{(gD)^{0.5}} \frac{5.84}{\log_{10} Re - 0.74} \right)^{-1/3}$	$Fr > 2$	(4)
			$1.13U_c / \bar{U}$	0.361	Laminar	(5)
Ferre (1979)* ¹	Horiz. 45mm	Continuo slug flow Air-water	1.1	0.45	$Fr < 2$	(6)
			1.3	0	$2 < Fr < 8$	(7)
			1.02	3	$Fr > 8$	(8)
Weber (1981)	Horiz.	Stagnant liquid		$0.54 - 1.76 E_o^{-0.56}$	$E_o > 8.3$	(9)
				0	$E_o \leq 8.3$	(10)
Bendiksen (1984)	Horiz. Inclined 19 / 50mm	Single bubble Air-water	$1.05 + 0.15 \sin^2 \theta$	$0.35 \sin \theta + 0.54 \cos \theta$	$Fr \leq 3.5$	(11)
			1.2	$0.35 \sin \theta$	$Fr > 3.5$	(12)
Bendiksen (1985)	Vertical	Theoretical approach	$2.29 \left[1 - 5 \Sigma (1 - e^{-0.05/\Sigma}) \right]$	$0.486 \sqrt{1 + 5(1 - 1.7\Sigma)\Sigma} \cdot \frac{1 - 0.96e^{-0.066/\Sigma}}{1 - 0.52e^{-0.066/\Sigma}}$	Laminar $\Sigma < 0.1$	(13)
			$\left[\frac{\log_{10} Re + 0.309}{\log_{10} Re - 0.743} \right]$ $\left[1 - \frac{1}{2} \Sigma (3 - \log_{10} Re e^{-0.1/2}) \right]$		Turbulent	(14)
Frechou (1986)* ¹	Vertical 50mm	Continuous slug flow Air-Water / Air-Oil	$\frac{2.27}{1 + (Re/Re_c)^2} + \frac{1.2}{1 + (Re_c/Re)^2}$			(15)
Nuland (1998)	Horiz. 60mm	Continuo slug flow. Glycerin / air	$C_o^l = 2$		Laminar	(16)
			$C_o^{tr} = wC_o^t + (1-w)C_o^l$	0.54	Transition	(17)
			$C_o^t = \frac{(n+1)(2n+1)}{2n^2}$		Turbulent	(18)
Netto et al. (1999)	Horiz. 53mm	Single bubble Water/air	$C_{O1} = 1$	0.48	$Fr < Fr_{crit}$	(19)
			$C_{O2} = 1.2$	0	$Fr > Fr_{crit}$	(20)
Foletti et al. (2011)	Horiz. 22mm	Continuo slug flow	2.14	0	Laminar	(21)
Jeyachandra et al. (2012)	Horiz 50.8mm -152mm	Stagnant liquid		$0.53e^{-13.7N_\mu^{0.46} E_o^{-0.1}}$	High viscosity	(22)

Where $E_o = \rho_l g D^2 / \sigma$, $Fr = U / \sqrt{gD}$, $\Sigma = l / E_o$, $Re = \rho_l U D / \mu$, and $w = (Re - Re_c) / (Re_{urb} - Re_c)$

¹ Taken from FABRE, J. 1994. Advancements in Two-Phase Slug Flow Modeling. *Society of Petroleum Engineers Journal*.

Collins et al. (1978) performed a theoretical study of Taylor bubble motion in laminar and turbulent flow in vertical pipes. They proposed a model based on inviscid liquid theory, assuming irrotational motion around the bubble and that the velocity profile in front of the nose remains unaffected by the nose. Based on the axis-symmetrical motion of the bubble in the pipe, the authors proposed expressions for C_o and U_o as a function of Reynolds (Re) and Froude number (Fr). **Eqs.5a-5b** were developed for laminar flow, in terms of the maximum value of the liquid velocity profile (U_c), while **Eqs.3a-3b-** to **4a-4b** were proposed for the full range of Fr number.

Bendiksen (1984) made experiments in turbulent flows in inclined and horizontal pipes. He found that below a critical Froude number, the gravity effect is predominant, and the bubble motion is determined by the liquid velocity close to the pipe wall. For higher Froude numbers, the liquid stream tends to center the bubble nose, and the liquid velocity close to the pipe axis determines the bubble motion. Based on this criterion the author proposed **Eqs. 11a-11b** and **12a-12b**.

Bendiksen (1985) presented a theoretical study of the motion of long bubbles in vertical pipes. The author deduced expressions for C_o and U_o including the effects of the liquid motion and the surface tension. For laminar flow, he proposed **Eqs. 13a-13b** and improved the correlation presented by Collins et al. (1978) for turbulent flow (**Eq. 14a**). Where Σ represents the inverse of the Eötvös number (E_o).

Frechou (1986) suggested a relation of C_o for vertical flows (**Eq. 15a**), where the flow transition region was reported around $Re_c=1000$ (Fabre, 1994)

Nuland (1998) estimated C_o for turbulent flow directly from the velocity profile as a function of the friction factor as shows **Eq.18a**, where n can be found from the friction factor (f) at the given flow conditions. For laminar flow, he used a constant value of $C_o=2$, while for the transition from laminar to turbulent, he applied the maximum friction factor criterion to determine the transition Reynolds number (Re_{tr}) and proposed **Eq. 17a** to compute an average for C_o in the transitional region.

Netto et al. (1999) carried out a research on the bubble shape in horizontal slug flow. They demonstrated that the bubble front shape is independent of the bubble length, but it is associated with the flow ahead of the nose. They observed, as others, that for low liquid velocities, the bubble nose was mostly at the top of the pipe, while for high velocities, it moved towards the center of the pipe. In both cases, the bubble shape was constant throughout the pipe. They proposed a critical Froude number (**Eq.23**) as a function of the bubble drift velocity.

$$Fr_{crit} = \frac{U_o / \sqrt{gD}}{C_{o2} - C_{o1}} \dots\dots\dots(23)$$

C_{o2} and C_{o1} defined by **Eqs. 19a** and **20a** respectively.

Jeyachandra et al. (2012) measured the drift velocity for air and high viscosity oil flow in pipes. The experiments were carried out with three different internal diameters (50.8mm; 76.2mm and 152.4mm) with oil viscosities range from 0.154 to 0.574 Pa s. As results, the authors proposed a drift velocity correlation using the Froude number, Archimedes number (Ar), and the Eötvös (E_o) number as shows the Eq 22b where N_μ is defined:

$$N_{\mu} = \frac{1}{\sqrt{Ar}} \dots\dots\dots (24)$$

$$Ar = \frac{gD^3\rho_l}{\mu_l^2}(\rho_l - \rho_g) \dots\dots\dots (25)$$

Regarding the drift velocity models (U_o), many researchers show good consensus in their proposals. (Ben-Mansour et al., 2010, van Hout et al., 2002, Fabre, 1994, Fabre and Line, 1992, Jeyachandra et al., 2012, Bendiksen, 1984, Weber, 1981, Zukoski, 1966). Nevertheless, on the distribution parameter (C_o) even though the range of value is limited (between 2.47 and 1), suggestions are more disperse. The researchers assume that C_o is a relation of the liquid velocity just in front of the bubble nose (U(r)) and the mean flow velocity (Ū). Hence, C_o depends on the flow velocity profile and of the position of the bubble nose relative to the centerline of the pipe:

$$C_o = \frac{U(r)}{\bar{U}} \dots\dots\dots (26)$$

U(r) is the liquid velocity at r distance from the pipe centerline. For laminar flow, it is given by:

$$\frac{U(r)}{\bar{U}} = 2\left(1 - \left(\frac{r}{R}\right)^2\right) \dots\dots\dots (27)$$

and for turbulent profile by the power law velocity profile (Munson et al. (2006)), according to the profile shape shown in Fig. 1.

$$\frac{U(r)}{U_c} = \left(1 - \left(\frac{r}{R}\right)\right)^{1/n} \dots\dots\dots (28)$$

$$\frac{U_c}{\bar{U}} = \frac{(n+1)(2n+1)}{2n^2} \dots\dots\dots (29)$$



Fig. 1. Fully developed velocity profile in pipes a) Laminar flow b) Turbulent flow. Adapted from Çengel and Cimbala (2010)

A power fitting of the relation of the exponent n as a function of the Reynold numbers (Appendix A) is proposed by Munson et al. (2006) as an adaptation of the original formulation of Hinze (1975):

$$n = 0.2632 Re^{0.1952} + 4.261 \dots\dots\dots(30)$$

According to this formulation, in fully developed turbulent flow, the distribution parameter C_o may be around 1.2.

Most of the experiments so far have been made with low viscosity fluids, and therefore mainly under turbulent flow condition. The present work covers experiments on the bubble translational velocity with medium viscosity liquids in horizontal flow through the laminar-turbulent transition (Reynolds numbers from 250 up to 5100).

Experimental Setup and Procedure

The experiments were carried out at the Multiphase flow laboratory at the Norwegian University of Science and Technology (NTNU). The experimental setup contains transparent Plexiglas pipes, centrifugal pumps, separator tanks, Coriolis meters, capacitance probes, pressure transducers and medium speed cameras. **Table 2** summarizes the instrumentation range and accuracy.

Table 2 Details on the instrumentations

	Model	Range	Accuracy
Liquid flow meter	Micro Motion T150	0-36 000 kg/h	±0.15% of rate
Air flow meter	Micro Motion CMF025	Up to 2180 kg/h	±0.05% of rate
Cameras	Basler AC A640	120 fps	±0.008s
Density	Micro Motion T150	-	±2.0 kg/m ³
Viscosity	ARES –G2 Rheometer	-	±0.22%

The working fluids were air and mineral oil at atmospheric conditions. In order to cover the full range of Reynolds number from laminar to turbulent flow, different oil viscosities were tested. The desired viscosities were obtained by mixing two mineral oils of around 0.09Pa.s, 850kg/m³ ; and 0.01Pa.s, 843kg/m³ , according to a volume ratio found experimentally. The blend viscosity and density were measured using a rheometer and a Coriolis meter respectively. **Table 3** summarizes the fluid properties used in the experiments.

Table 3 Working fluid properties

Parameter	Oil 1	Oil 2	Oil 3	Oil 4	Air
Viscosity (Pa.s)	0.010	0.020	0.026	0.065	1.8e-5
Density (kg/m ³)	843	846	846	831	1.2
Surface tension (N/m)	0.027	≈0.027	≈0.027	≈0.026	-

Drift velocity experiments: Some experiments on drift velocity were performed in order to confirm the validity of the correlation proposed by Jeyachandra et al. (2012) for the viscosities

range used in this work. The setup consisted of a horizontal pipe of 60mm inner diameter and 2m long; one end sealed and the other one connected to a ball valve. Three capacitance probes were installed on the pipe as shows **Fig. 2a**. A video camera was also installed in order to record the displacement of the gas-liquid interphase between capacitance probes P2 and P3.

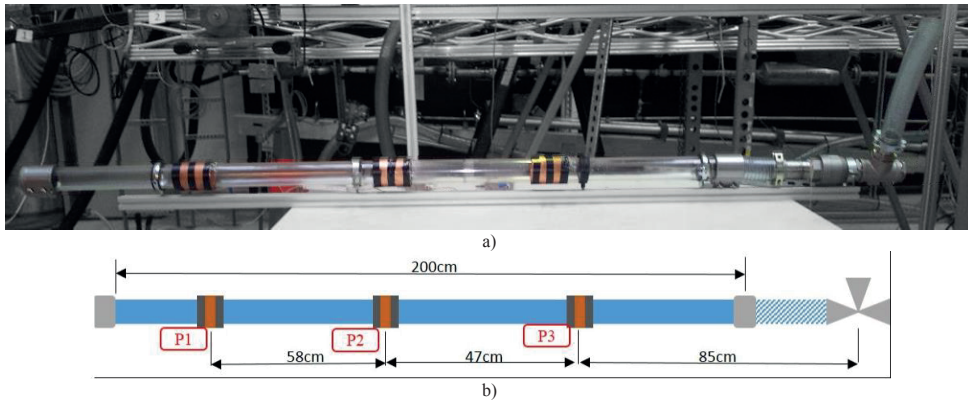


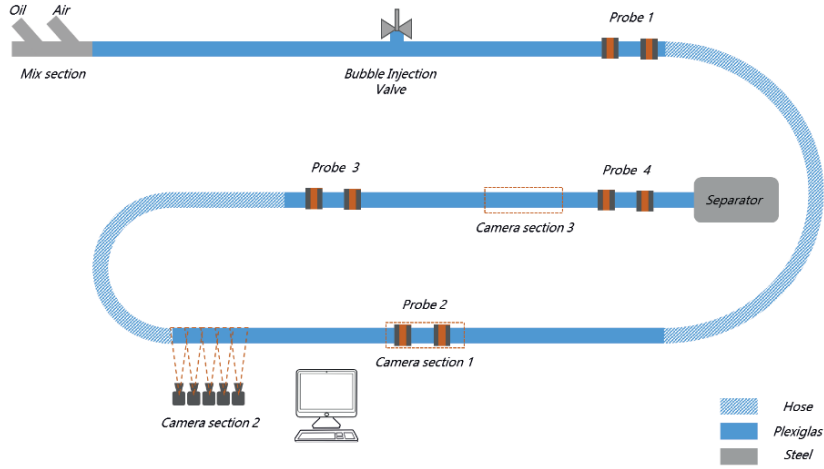
Fig. 2 a) Drift velocity Setup. b) Setup dimensions

Prior to the experiments, the pipe is fully filled with the working fluid through a three-way valve. Then, the valve is suddenly opened allowing air to enter into the section while the liquid drains out of the pipe. The drift velocity is the measurement of the air-cavity propagation along the pipe by cross-correlating the capacitance signals. The use of three capacitance probes permitted to verify the constant shape of the bubble. The velocity reported corresponds to the last probe, close to the sealed end. The working fluids were Oil 4 (0.065Pa.s) and Oil 1 (Marcol 0.010Pa.s) at atmospheric conditions. The experiments with Oil 1 were done by Johansen (2006) at the same laboratory and with a similar setup.

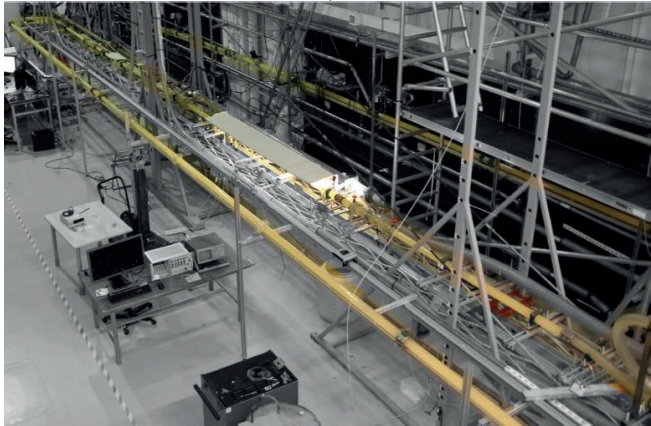
Single bubble experiments in continuous liquid flow were carried out in the flow loop shown in **Fig. 3**. The test section consists of a horizontal pipe of 60mm inner diameter and 50m total length, including three straight segments of 16m and two U-bends of radius 1.42m and 0.92m respectively. The **Fig. 3a** illustrates a sketch of the facility and **Fig. 3b** and **Fig. 3c** show pictures of the actual test section.

The air injection system consists of a fast-acting magnetic valve (Bosch Rexroth Series 560, 15/30 ms opening/closing time Johansen (2006)), a reduction valve and a pressure gauge (1000kPa of range, and accuracy ± 50 kPa). A dedicated program in LabVIEW allowed remote control of the valve by setting the opening time, the number of injections and the time interval between consecutive injections. The bubble volume depends on the air pressure, valve opening time and the liquid velocity in the test section. Consequently, both air pressure and opening time were regulated for different liquid flow rates in order to generate an appropriate bubble. Normally, the air pressure was manually controlled and set between 100 and 150 kPa. After some trial and error, it was found that a T-shaped pipe configuration showed the best performance among the different configurations tested, in terms of the coherent shape of the

bubble obtained. The injection point was fixed at 110 pipe diameters downstream of the liquid inlet (see **Fig. 3a**). Pressure transmitters installed at several locations along the pipe allowed recording of instabilities due to the bubble injection. The bubble velocity measurements were taken once the pressure perturbations had disappeared.



a)



b)



c)

Fig. 3.- a) Layout of the experimental set-up; b) and c) picture of the facility at Multiphase Flow Laboratory

The bubble translational velocity was measured by two ways: calculating the time delay between two logged signals of capacitance probes placed at 4 locations along the pipe, and by

recording videos over 2m of the pipe with synchronized cameras at 120fps, at the camera section 2.

The visualization system includes up to five GigE cameras model Basler acA640-120fps, a computer Intel® core™ i7, a GigE Vision frame grabber of National Instrument model PCIe-8233 and LED light behind a diffuser. By means of a dedicated program written in LabVIEW2012®, it was possible to acquire video simultaneously from the five cameras and stamp the acquisition time on each frame. The cameras were equally spaced along the visualization section in order to cover the longest possible length of the pipe without losing important features of the flow phenomena. **Fig. 4** shows a picture of the visualization section. **Fig. 3a** shows the five measurement points for the both capacitance rings and cameras, and **Table 4** summarizes the distance between probes of capacitance and their position regarding the bubble injection point.



Fig. 4.- Visualization section with five cameras. (Camera section 2)

Table 4 Capacitance dimension (distance between rings $D(x)$) and instrumentation position (x)

Instrument	$Dx(m)$	$X(m)$
Probe 1	0.45	8.2
Probe 2	0.42	24.3
Probe 3	0.43	37.1
Probe 4	0.68	45.6
Camera Section 2 (5 cameras)	2	28.9
Camera Section 3 (4 cameras)	0.88	44

Continuous slug flow experiments. The flow loop used in this set of experiments is similar to the one described in the single bubble experiments. In this case, continuous and stable air-oil flow is fed to the test section through a mixing section as is shown in **Fig. 5**. As in the previous set of experiments, capacitance probes are used to identify the bubble front during the experiments.



Fig. 5 Liquid – air mix section

Data processing: The capacitance probes were not calibrated to measure liquid hold-up but only to detect the change between the slug and the bubble region. The maximum and minimum voltages were recorded daily in order to have updated reference values of the pipe full of oil and the pipe empty. The reference values are then used to normalize the signal between zero and one. A periodic calibration is needed because the capacitance reference value might change during the day due to temperature variations.

For the slug flow case, the bubble velocity was calculated by applying a cross-correlation function to the hold-up time series (HI) of each capacitance probe. In the case of a single bubble, the velocity reported is the average of nine horizontal lines along the bubble nose as is shown in Fig. 6.

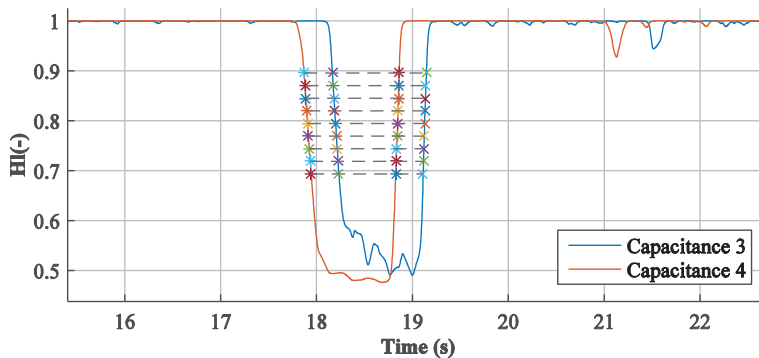


Fig. 6 Liquid fraction (HI) time trace for Probe 2 with OIL1

On the image processing, the acquired videos were post-processed using a dedicated script written in Matlab®. The routine reads the videos and extracts both the light intensity value of each pixel along a given profile line and the capture time of each frame. After reading the whole film, the routine creates numerical matrices containing the time step and the bubble nose position in the axial direction of the pipe. As a result, it is possible to track the propagation of the bubble in time and space. Since the entire bubble unit is recorded simultaneously, by using different cameras, it is possible to have information about the bubble nose and tail at the same time. Consequently, the velocity is easily calculated by a linear fitting of the time and space coordinate. Fig. 7 shows a plot of the bubble in time and space.

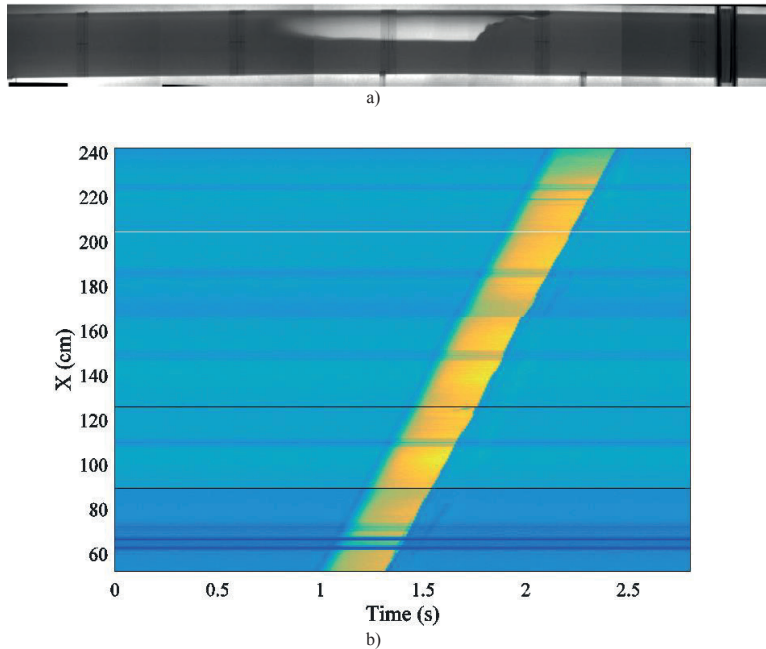
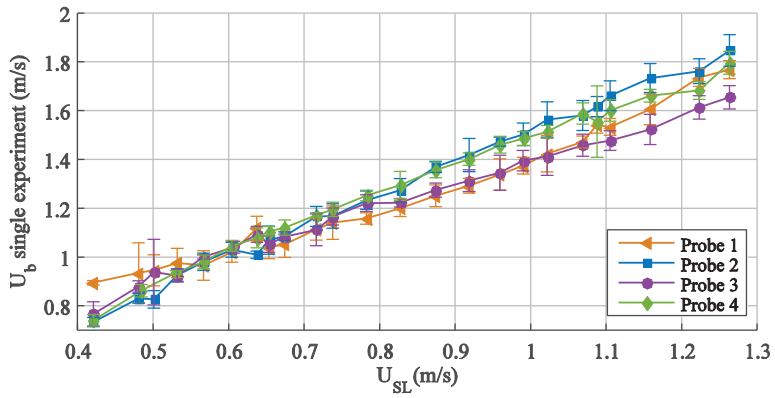


Fig. 7.-a) Bubble recorded by five cameras b) Bubble propagation in time and space (yellow represents high brightness, which corresponds to the air bubble)

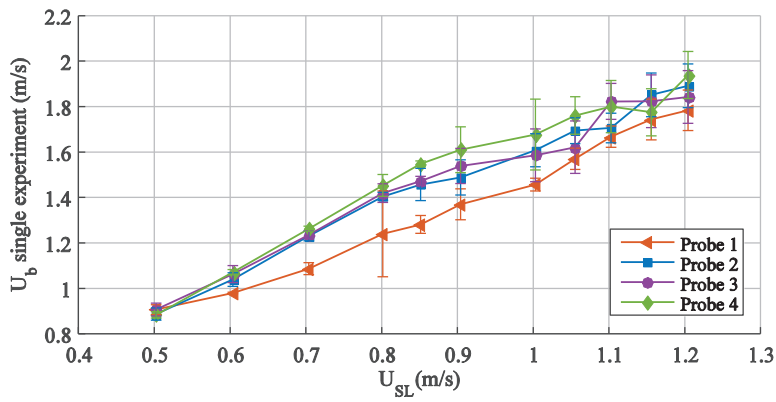
Result and Discussion

Fig. 9 shows the bubble velocity measurement for the single bubble cases. As reference, the transition from laminar to turbulent flow is indicated from single-phase flow in pipes, which occurs at Reynolds numbers from 2000 to 4000 approximately. The first capacitance probe is placed at 15m from the inlet (8.2m from the injection point).

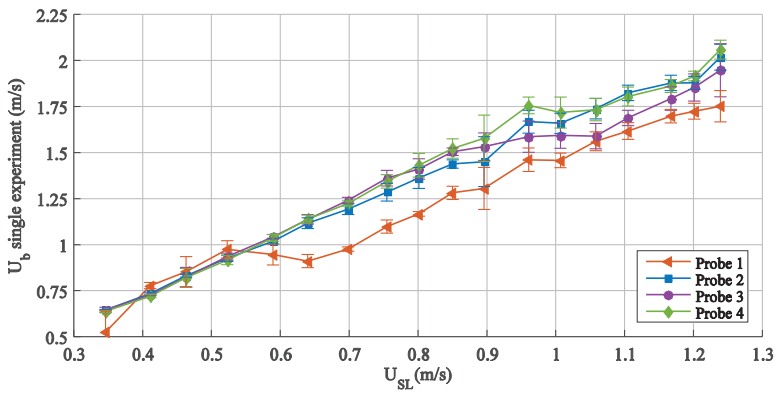
A bubble will expand as it propagates towards lower pressure in the pipe. The velocity might be affected by this expansion and also by the two U-bends of the pipe. All measurements (with capacitance) are shown in **Fig. 8**, each point is the average of 3 to 5 experiments. **Fig. 9** presents results for the Oil 4, which were measured only with the synchronized camera system.



a) Oil 1



b) Oil 2



c) Oil 3

Fig. 8 Bubble velocity in single bubble experiments. Oil 1 to Oil 3

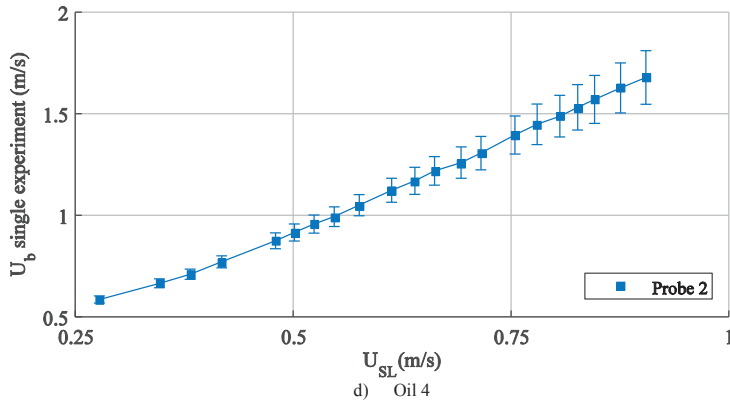


Fig. 9 Bubble velocity in single bubble experiments Oil 4

For the middle viscosity cases (Oil 2 and Oil3), the first probe shows lower values systematically, probably due to residual flow dynamics after the bubble injections. For the other measurements, the bubble velocity is quite similar at the different measuring stations. This is also seen for measurements in slug flow. **Fig. 10** gives an example of slug flow measurement, where the gas and liquid flow rate have been varied between typically 0.21 to 1.04 m/s and 0.15 to 0.69 m/s respectively. Slug flow experiments were performed with Oil 1, Oil 3 and Oil 4.

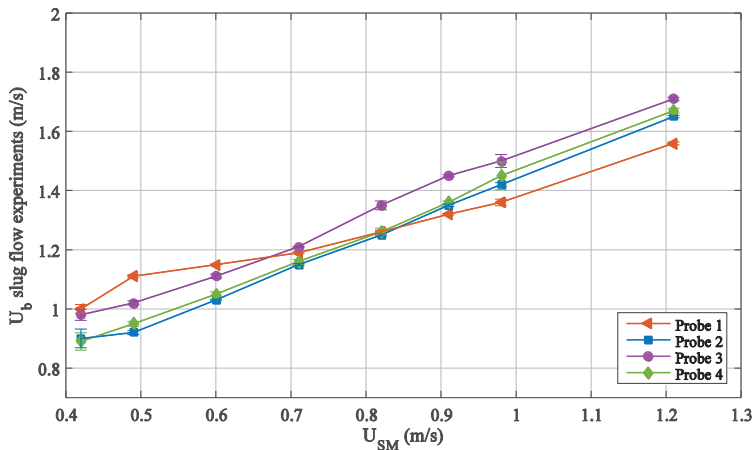


Fig. 10 Bubble velocity in slug flow experiments Oil 1

Fig. 11 presents a graphic comparison between the bubble translational velocity measured from the slug flow experiments and the ones obtained from the single bubble experiments. The plots in **Fig. 11** shows the linear fitting of the experimental data for the single bubble case on the abscissas, versus the linear fitting of the experimental data for the slug flow cases (on the ordinates). The result of the comparison shows a deviation between the two methods within the 20%, which indicates that, in terms of the development flow in the liquid slug region, the single bubble experiments can be used to describe the bubble propagation in continuous slug flow.

The bubble velocity U_b in slug experiments are based on the mixture velocity, which is equivalent to the superficial liquid velocity for the single bubble experiments.

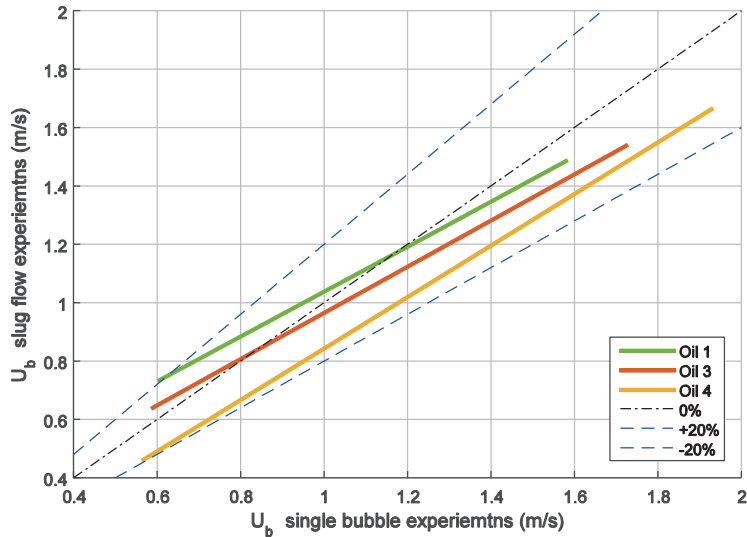


Fig. 11.- Comparison between continuous slug flow and single bubble experiments at probe 2.

Drift velocity. The Fig. 12 shows the correlation proposed by Jeyachandra et al. (2012) for the drift velocity, considering the viscous effect. The comparison of the experiment results with Oil-1 and Oil-4 indicate an excellent agreement with the correlation; therefore, from now on, the drift velocity will be taken from **Table 5** according to the cited correlation.

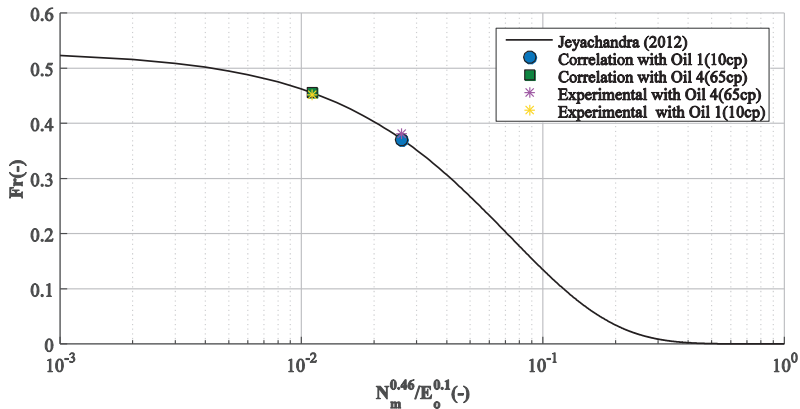


Fig. 12.- Drift Velocity. Comparison of experimental results against correlation of Jeyachandra et al. (2012)

Table 5 Drift velocities for ID 0.06m and different viscosities

	FrExp (-)	UbExp (m/s)	Fr Jeyachandra 2012 (-)	Ub Jeyachandra 2012 (m/s)
Oil 1	0.45	0.35	0.45	0.35
Oil 2	-	-	0.43	0.33
Oil 3	-	-	0.42	0.32
Oil 4	0.38	0.29	0.37	0.28

Distribution coefficient. The distribution parameter C_0 can tentatively be estimated using the vertical position of the bubble nose relative to the centerline of the pipe. **Fig. 13** shows images of the bubble front in the pipe at different superficial liquid velocities.

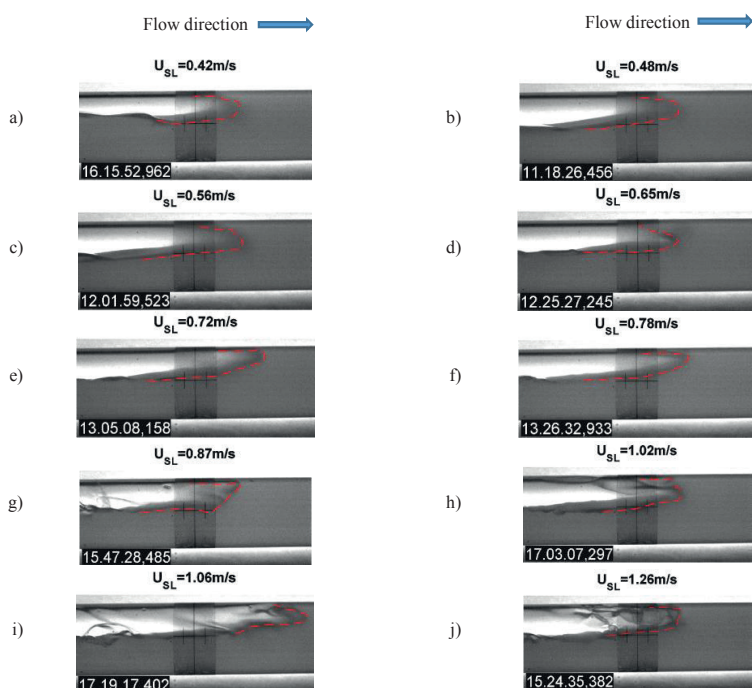


Fig. 13.- Bubble front in laminar flow (a), transitional region (b-d) and turbulent flow (e -j) for OIL 1. Pipe length recorded 22cm

Following the images sequence when the liquid velocity increases, a progressive change in the nose shape can be observed. At lower velocity and close to the laminar region, the front is narrow with a smooth interface, while at higher velocities and closer to the turbulent region, the fronts start to show a flatter shape followed by a wavy interface. The position of the bubble nose is estimated from the images and shown in **Fig. 14**.

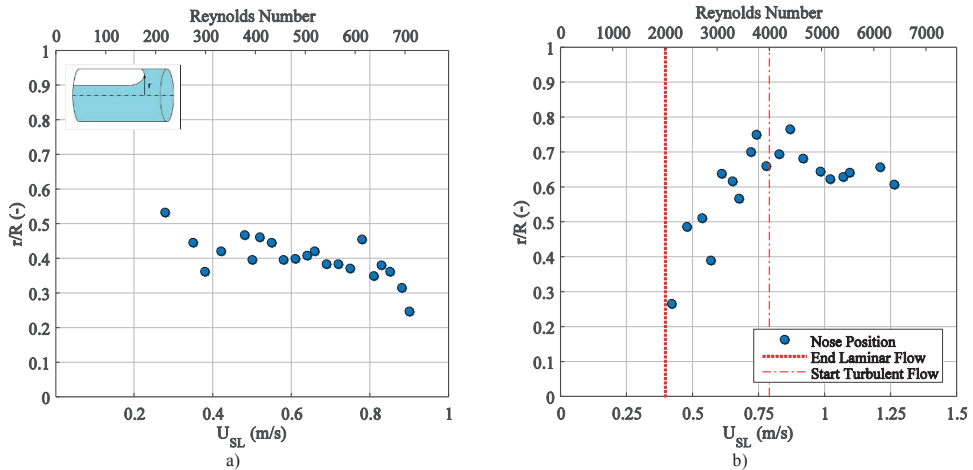


Fig. 14 Bubble front position change in term of the superficial liquid velocity. a) Oil 4 in laminar region, b) Oil 1 transition to turbulent region

In laminar and turbulent flow, the front position tends to move slightly from the top of the pipe toward the centerline; with a flow range region where the bubble tip stays at a relative constant distance from the centerline of the pipe (r). In the transitional region, on the contrary, the bubble nose moves away from the center, toward the top of the pipe and the bubble front shape was now fluctuating along the pipe as is shown in **Fig. 15**, which makes it more difficult to define the front position. It is worth noting that **Fig. 14** aims to show the movement tendency of the bubble tip rather than to have a precise measure of the distance to the pipe centerline.

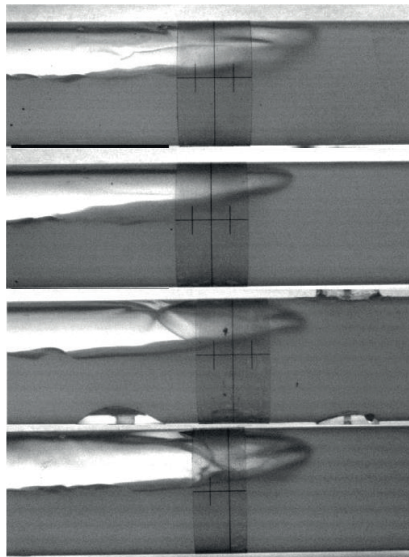


Fig. 15.- Transition region at different locations of the pipe with Oil 1 $U_{sl}=0.98\text{m/s}$ $U_b= 1.43\text{m/s}$

Translational bubble velocity. Fig. 17 shows the comparison of common theoretical correlations and the experimental data obtained for single bubble measurements and for slug flow. Bendiksen (1984) defined two velocity intervals with approximately constant C_o and U_o . The transition between both regions occurs for a critical velocity (U_{cr}) at which C_o will increase as the radial position of the bubble nose decreases, accompanied by a reduction in the drift velocity due to the change of the stagnation point. Bendiksen (1984) observed a change in the radial position over a narrow liquid velocity interval that produces an abrupt transition between both regions. Thereafter, Netto et al. (1999) proposed to define the U_{cr} as a function of the drift velocity and the C_o (Eq. 23). Both authors worked mainly on turbulent flow and defined the change in C_o in terms of that condition. The results in Fig. 16 to Fig. 17 suggest that a similar transition occurs in laminar flow with a change of C_o higher due to the laminar profile shape.

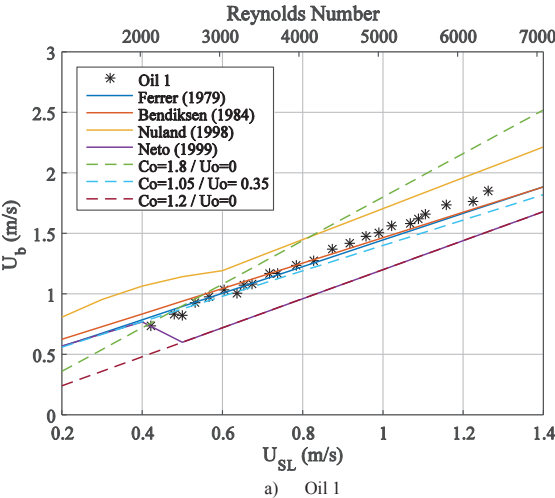


Fig. 16.- Comparison of experimental data against common theoretical correlations. a) OIL1 0.010Pa.s,

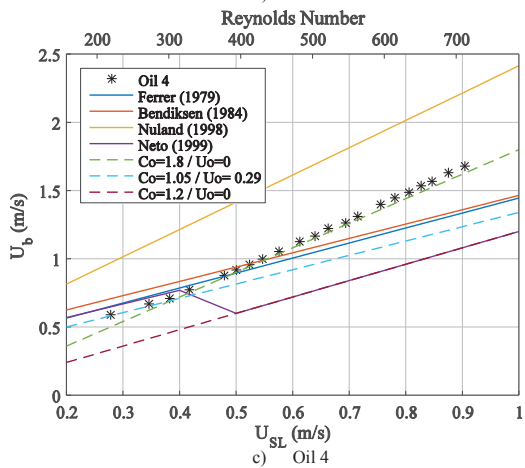
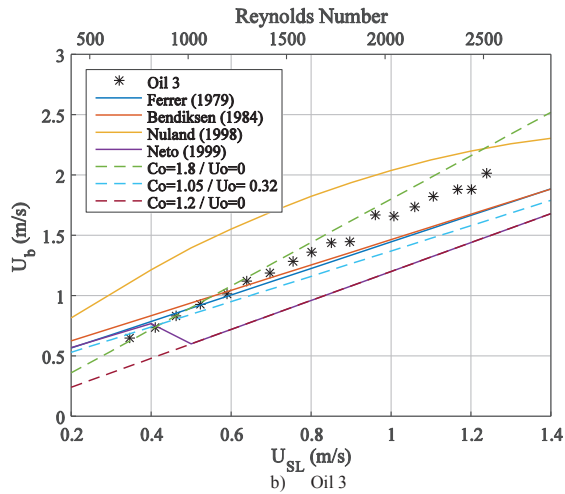
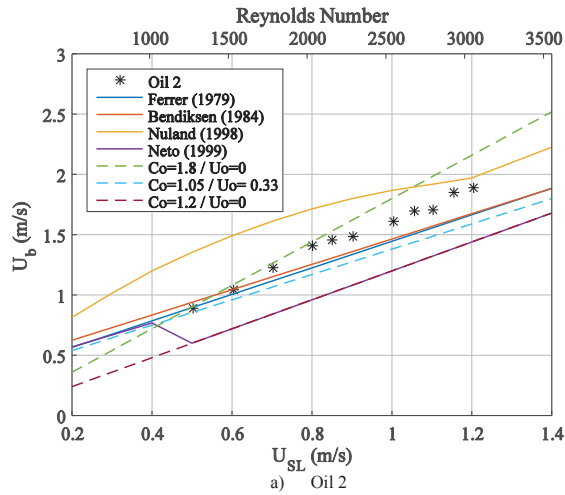


Fig. 17.- Comparison of experimental data against common theoretical correlations. a) OIL2 0.020Pa.s, b) OIL3 0.026Pa.s, c) OIL4 0.065Pa.s

Table 6 summarizes the transition criterion in terms of the Reynolds number, distribution coefficient C_o and the drift velocity U_o .

Table 6 Transition criteria for C_o and U_o in terms of the Reynolds number for horizontal flow				
		Criterion	C_o	U_o
Laminar: $Re < 2000$	$U_{crL} = \frac{U_o(\rho_l, \rho_g, D, \sigma, \mu)}{C_{o_{lam}}^2 - C_{o_{lam}}^1}$	$U_{sl} < U_{crL}$	$C_{o_{lam}}^1 \cong 1.05$	$U_o = U_o(\rho_l, \rho_g, D, \sigma, \mu)$
		$U_{sl} \geq U_{crL}$	$C_{o_{lam}}^2 \cong 1.8$	$U_o = 0$
Turbulent: $Re > 4200$	$U_{crT} = \frac{U_o(\rho_l, \rho_g, D, \sigma, \mu)}{C_{o_{turb}}^2 - C_{o_{turb}}^1}$	$U_{sl} < U_{crT}$	$C_{o_{turb}}^1 \cong 1.05$	$U_o = U_o(\rho_l, \rho_g, D, \sigma, \mu)$
		$U_{sl} \geq U_{crL}$	$C_{o_{turb}}^2 = 1.2$	$U_o = 0$

It is useful to define a third shift criterion for the transitional region since the bubble velocity should increase continuously, but moving from the conditions in laminar region to the ones in turbulent flow. A critical case in the transitional region would be when the liquid velocity value stays between the critical velocities defined for the laminar and turbulent region ($U_{crL} \leq U_{sl} < U_{crT}$). This means that the bubble velocity will change from a higher C_o without drift velocity, in the laminar flow, to a lower C_o with drift velocity corresponding to the turbulent flow. Therefore, in order to get a smooth transition between those two extreme cases, it is possible to take a weighted average in terms of the Reynolds number as suggested Nuland (1998), but on the bubble velocity directly, as it is expressed in **Eqs. 31** and **32**, instead of only on the C_o parameter.

$$U_b^{tr} = U_b^{turb} w + U_b^{lam} (1-w) \dots\dots\dots (31)$$

$$w = \frac{Re - Re_{tr}}{Re_{turb} - Re_{tr}} \dots\dots\dots (32)$$

Where U_b^{turb} and U_b^{lam} are calculated according to the relations in **Table 6**.

Fig. 18 shows the bubble velocity, following the above criteria for the analyzed experiments. The results of the single bubble experiments are well described for the criteria in **Table 6**.

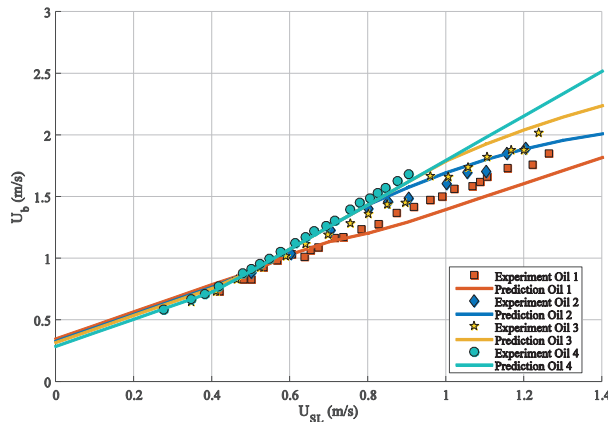


Fig. 18.- Bubble velocity U_b vs. U_{SL}

Likewise, the experimental points in the transitional region adjust well to the weighted average of the bubble velocity between the laminar and turbulent flow conditions.

Conclusions

The front propagation velocity of elongated bubbles was experimentally studied for different Reynolds numbers, covering laminar flow, transitional region and the beginning of the turbulent flow. Both distribution parameter and drift velocity parameters of the bubble velocity equation were determined. The results for the drift velocity agree well with the correlation suggested by Jeyachandra et al. (2012)) for the operational conditions used. The distribution parameter C_o adjusted well for current correlations in turbulent flow, but the results suggested more discrepancies in the laminar and transitional region. C_o in the laminar region was found to be less than 2 (around 1.8), in concordance with the bubble nose position over the centerline of the pipe. Furthermore, the bubble tends to move toward the center of the pipe as the liquid viscosity increase resulting in a higher C_o . A shift criterion in terms of the final bubble velocity is proposed instead of changes the individual parameters (C_o and U_o) for different Froude numbers. The bubble velocity in the transition region can be determined by a weighted average in terms of the Reynolds number in order to obtain a smooth change between the laminar and the turbulent region. The three shift criteria, for laminar flow, transition and turbulent flow fit fairly well with the experimental data presented here.

The bubble velocity was measured in both solitary bubbles and bubbles in continuous slug flow. The comparison between both methods suggests that for pipelines long enough, measurements in continuous slug flow agree reasonably well with an isolated bubble.

Acknowledgment

This work was supported by Petromaks project from the Research Council of Norway and Statoil.

Nomenclature

Ar	Archimedes number $Ar = \frac{gD^3\rho_l}{\mu_l^2}(\rho_l - \rho_g)$
C_o	Distribution parameter
C_o^l, C_{o1}	C_o for laminar flow
C_o^t, C_{o2}	C_o for turbulent flow
C_o^{tr}	C_o in transitional region
D	Pipe internal diameter
Eo	Eötvös number $E_o = \rho_l g D^2 / \sigma$
Fr	Froude number $Fr = U / \sqrt{gD}$
Fr_{crit}	Critical Froude number
g	Gravity acceleration
n	Coefficient of the power law for the velocity profile in turbulent flow
N_μ	Inverse of the square root of Ar

R	Inner pipe radius
Re	Reynolds number $Re = \rho_l UD / \mu$
Re_{tr}	Reynolds number limit for transition from laminar to turbulent flow
Re_{turb}	Reynold number limit for turbulent flow
\bar{U}	Mean flow velocity
U_b	Bubble front velocity
U_c	Maximum velocity of the liquid profile
U_o	Bubble drift velocity
U_m	Mixture velocity
U_{sl}	Liquid superficial velocity
f	Friction factor
w	weighted average in terms of the Reynolds
μ_l	Liquid dynamic viscosity
ρ_G	Gas density
ρ_L	Liquid density
Σ	Inverse Eötvös number $\Sigma = 1/E_o$
σ	Surface tension
θ	Pipe inclination

References

- BEN-MANSOUR, R., AL-SARKHI, A., SHARMA, A. K., JEYACHANDRA, B. C., SARICA, C. & GOKCAL, B. 2010. Effect of Pipe Diameter and High Oil Viscosity on Drift Velocity for Horizontal Pipes. BHR Group 2010 Multiphase 7.
- BENDIKSEN, K. H. 1984. An Experimental Investigation of the Motion of Long Bubbles in Inclined Tubes. *International Journal of Multiphase Flow*, 10, 467-483.
- BENDIKSEN, K. H. 1985. On the Motion of Long Bubbles in Vertical Tubes. *International Journal of Multiphase Flow*, 11, 797-812.
- ÇENGEL, Y. A. & CIMBALA, J. M. 2010. *Fluid Mechanics: Fundamentals and Applications*, McGraw-Hill Higher Education.
- COLLINS, R., DEMORAES, F. F., DAVIDSON, J. F. & HARRISON, D. 1978. Motion of a Large Gas Bubble Rising through Liquid Flowing in a Tube. *Journal of Fluid Mechanics*, 89, 497-514.
- FABRE, J. 1994. Advancements in Two-Phase Slug Flow Modeling. *Society of Petroleum Engineers Journal*.
- FABRE, J. & LINE, A. 1992. MODELING OF 2-PHASE SLUG FLOW. *Annual Review of Fluid Mechanics*, 24, 21-46.
- FERRE, D. 1979. Horizontal Slug Flow in Pipes. *Revue De L Institut Francais Du Petrole*, 34, 113-142.
- FOLETTI, C., FARISE, S., GRASSI, B., STRAZZA, D., LANCINI, M. & POESIO, P. 2011. Experimental investigation on two-phase air/high-viscosity-oil flow in a horizontal pipe. *Chemical Engineering Science*, 66, 5968-5975.
- FRECHOU, D. 1986. Etude expérimentale de l'écoulement gaz-liquide ascendant à deux et trois fluides en conduite verticale. *Oil & Gas Science and Technology - Rev. IFP*, 41, 115-129.
- HINZE, J. O. 1975. *Turbulence*, Hsieh-Cheng.
- JEYACHANDRA, B. C., GOKCAL, B., AL-SARKHI, A., SARICA, C. & SHARMA, A. K. 2012. Drift-Velocity Closure Relationships for Slug Two-Phase High-Viscosity Oil Flow in Pipes. *Spe Journal*, 17, 593-601.

- JOHANSEN, M. 2006. *An experimental study of the bubble propagation velocity in 3-phase slug flow*. PhD, NTNU.
- MUNSON, B. R., YOUNG, D. F. & OKIISHI, T. H. 2006. *Fundamentals of Fluid Mechanics*, John Wiley & Sons, Incorporated.
- NETTO, J. R. F., FABRE, J. & PERESSON, L. 1999. Shape of long bubbles in horizontal slug flow. *International Journal of Multiphase Flow*, 25, 1129-1160.
- NICKLIN, D. J., WILKES, J.O., DAVIDSON, J.F. 1962. Two phase flow in vertical tubes. *Trans. Inst. Chem. Engs.*, 61-68.
- NULAND, S. 1998. Bubble front velocity in horizontal slug flow with viscous Newtonian shear thinning and Bingham fluids. *Third International conference on multiphase flow*. Lyon, France.
- VAN HOUT, R., BARNEA, D. & SHEMER, L. 2002. Translational velocities of elongated bubbles in continuous slug flow. *International Journal of Multiphase Flow*, 28, 1333-1350.
- WEBER, M. E. 1981. Drift in Intermittent 2-Phase Flow in Horizontal Pipes. *Canadian Journal of Chemical Engineering*, 59, 398-399.
- ZUKOSKI, E. E. 1966. Influence of Viscosity Surface Tension and Inclination Angle on Motion of Long Bubbles in Closed Tubes. *Journal of Fluid Mechanics*, 25, 821-&.

Appendix A

Fig. 19 Shows the fitting curve of the Power Law velocity profile for turbulent flow presented by Munson et al. (2006). The coefficient n is taken from the equation of the fitting curve

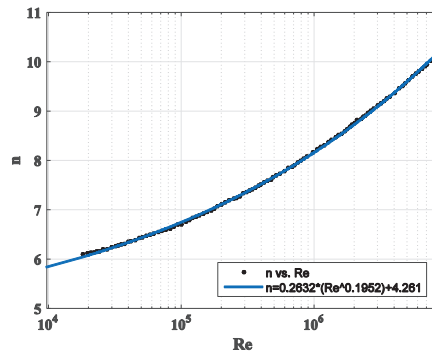


Fig. 19 Adaptation of Exponent n for the Power Law velocity profile by Munson et al. (2006)

PAPER V

Inlet Effects on Gas-Liquid Flow Regimes in Downwards Inclined Pipes

Is not included due to copyright

PAPER VI

Wake Effect on the Slug Bubble Velocity: Experiments in Laminar Flow

Wake Effect on the Slug Bubble Velocity: Experiments in Laminar Flow

Mariana J.C. Díaz and Ole J. Nydal.

Department of Energy and Process Engineering
Norwegian University of Science and Technology (NTNU)

Abstract

A bubble interaction phenomenon is studied experimentally for laminar two-phase slug flow in horizontal pipes of 60mm inner diameter. Two air bubbles injected into a liquid stream are tracked simultaneously along a measurement section of 2m long and at 23m from the air inlet. The first bubble (leading bubble) moves behind a very long liquid slug with a fully developed velocity profile. The second bubble (trailing bubble) travels behind the leading bubble separated by a liquid slug of a known and controlled length. The data set covers a range of different slug sizes (1-60 number of diameters) and different liquid velocities (0.4 to 0.9 m/s). As for the turbulent case, the experiments in laminar flow show that the trailing bubble front increases its velocity when the separation to the leading bubble decreases. Thus, short slugs tend to die by bubbles overtaking and merging. The simultaneous observation of a couple of bubbles gives the behavior and shape of each bubble within the interaction region both quantitatively and qualitatively.

Keywords: wake effect, laminar flow, slug flow, two-phase flow.

1 Introduction

Slug flow is a common flow pattern in multiphase pipe flow systems. It is an intermittent and irregular flow, where liquid slugs travel along the pipeline separated by elongated air bubbles. This type of flow exhibits velocity, pressure, and phase fraction fluctuations. There are mainly two strategies to modeling slug flow: by averaging the slug flow based on a defined unit-cell structure, and by resolving dynamically the evolution of individual slugs. A dynamic flow model intends to predict the slug formation, their evolution or decay, and their characteristics such as frequency, slug length, liquid fractions, and velocities.

For unit cell models the bubble velocity relation is based on developed flow conditions. For slug tracking models, the wake effect can be included, where the bubble velocity is influenced by the wake of the bubble ahead of the slug. This gives a mechanism of bubble

overtaking and merging of short slugs in the entrance regions. Shemer and Barnea (1987) note that the short slugs are commonly generated at the entrance of the pipe, where the liquid slugs are not long enough to be fully developed. The velocity fluctuations in the slug liquid body decay with the distance from the slug front, and so does the maximum liquid velocity in the slug. Since the bubble velocity is related to the velocity profile of the liquid ahead of it, the bubble nose behind a shorter slug will move faster than the bubble behind a longer slug, and eventually, will overtake and merge with the preceding bubble. This overtaking and merging process takes place until the slug becomes greater than the length needed to approach a fully developed velocity profile at the tail of the slug. Once the slugs are sufficiently developed, the bubbles propagate at a constant averaged velocity proposed by Nicklin (1962):

$$U_b = C_0 U_m + U_0 \quad (1)$$

Where U_b is the front bubble propagation velocity, C_0 the distribution parameter, U_m the average mixture superficial velocity, and U_0 the drift velocity.

Some studies have been made regarding the bubble-bubble interaction mechanism in order to supply a relation between the bubble front velocity and the slug length ahead of it. Moissis and Griffith (1962) were probably one of the first ones to propose a relation of the increasing velocity in terms of the separation distance from the preceding bubble. Others have made detailed measurements to improve the Moissis and Griffith (1962) correlation and extend it to different geometries or flow conditions (see **Table 1**).

Campos and Decarvalho (1988) defined two regions within the liquid slug: a wake region generated by the bubble just in front of it, and a region where the liquid profile recovers towards its stable shape condition. They focused on the “wake region” of rising bubbles in stagnant flow in vertical pipes and defined three possible patterns in the wake region as a function of the pipe inner diameter and the liquid properties according to the dimensionless number $N_f = \sqrt{gD^3}/\nu$. Where g is the acceleration due to gravity, D the pipe inner diameter, and ν the liquid kinematic viscosity. Their results indicated that the wake region of bubble rising in a vertical pipe might be classified as laminar ($N_f < 500$), transition flow ($500 < N_f < 1500$) and turbulent flow ($N_f > 1500$).

Pinto and Campos (1996) continued the research of Campos and Decarvalho (1988), also for two consecutive bubbles rising in a vertical column of stagnant liquid. In this experimental study, they reported that for the turbulent wake region the acceleration of the trailing bubble is independent of N_f , while in the case of laminar and transition wake region, the acceleration increases with the value of N_f for at given slug length. Pinto et al. (1998) extended the previous work to co-current flowing liquid instead of stagnant flow. They defined a pattern classification

of the wake region in terms of only the Reynolds number calculated from the mean relative velocity of the liquid flowing undisturbed ahead of the slug front, Re_{vl} :

$$Re_{vl} = \frac{V_L D \rho_L}{\mu_L} \quad (2)$$

$$V_L = U_b - U_L \quad (3)$$

Where V_L is the liquid mean relative velocity, U_b the bubble front propagation velocity, U_L the mean actual liquid velocity, D the pipe inner diameter, and ρ_L and μ_L the density and dynamic viscosity of the liquid respectively.

Based on this Reynolds number (**Eq. 2**) the authors classify the wake region as laminar for $Re_{vl} < 175$, as transition flow in the range of $175 < Re_{vl} < 525$ and as turbulent for $Re_{vl} > 525$. They carried out an experimental study over a large range of liquid Reynolds numbers to cover from laminar to turbulent flow in the liquid slug zone, but limited the study to turbulent pattern at the wake region. They found that for turbulent co-current flowing liquid, the minimum distance for interaction of slugs is about $5D$ regardless of the gas-liquid flow condition, and slugs shorter than this value will induce a strong velocity change of the trailing bubble front. For the laminar liquid flow, the minimum slug length was around $10D$, and the trailing bubble might accelerate substantially for $Ls < 5D$ and collapse with the leading bubble. However, they also reported that under particular conditions within laminar flow the separation distance between bubbles might even increase and, the bubbles never collapse. Mayor et al. (2007) also carried out an experimental study for vertical pipe with laminar flow. They reported a considerable difference of the bubble-bubble interaction curves for laminar and turbulent regime. They found the higher bubble acceleration in turbulent flow for slugs around $8-10D$, with most of the coalescence in the entrance of the test section. While for laminar regime, the coalescence was observed along the whole test section and the higher bubble velocity was register mainly for slugs shorter than $2D$, with a strong acceleration for slugs shorter than $1D$ where the trailing bubbled velocity reach up to twice the velocity of the leading bubble.

The mentioned studies have evaluated the bubble-bubble interaction for different flow conditions, either laminar, transition or turbulent flow, but only for vertical pipe. Barnea and Taitel (1993) Cook and Behnia (2000a), Fagundes Netto et al. (2001), Ujang et al. (2006), Wang et al. (2007) made experiments in horizontal flow, but mainly at turbulent flow conditions.

Cook and Behnia (2000a) performed an experimental study on the slug length decay in gas-liquid intermittent flow in near horizontal pipes. They suggested that the velocity ratio (bubble velocity /front Velocity) is much less in the co-current flow case than for the stagnant liquid, but for both cases, the correlation found was independent of the mixture velocity. Furthermore, they reported a minimum stable slug length close to $10D$. Fagundes Netto et al.

(2001) studied, in horizontal flow, the effect of the distance between two consecutive bubbles on the velocity propagation of the trailing bubble. They reported an increasing velocity of the trailing bubbles behind slugs shorter than a critical value, but they observed the opposite behavior for slugs larger than the critical value where the trailing bubble moves slower than the leading one.

Table 1 Correlation for the bubble front velocity as a function of the slug length.

Author	Pipe geometry	Correlation
Moissis and Griffith (1962)	Vertical	$\frac{U_b}{U_\infty} = 1.0 + 8 \exp\left(-1.06 \frac{L_S}{D}\right)$
Barnea and Taitel (1993)	Horizontal	$\frac{U_b}{U_\infty} = 1.0 + 5.5 \exp\left(-0.6 \frac{L_S}{L_{stab}}\right)$
Cook and Behnia (2000a)	Horizontal stagnant flow	$\frac{U_b}{U_\infty} = 1.0 + 1.14 \exp\left(-0.48 \frac{L_S}{D}\right)$
	Horizontal co-current flow	$\frac{U_b}{U_\infty} = 1.0 + 0.56 \exp\left(-0.46 \frac{L_S}{D}\right)$
Fagundes Netto et al. (2001)	Horizontal	$v = 0.22 \left(1 - \frac{L_S}{6.3}\right) \exp\left(-0.16 \frac{L_S}{D}\right)$
Shemer (2003)	Inclined	$\frac{U_b}{U_\infty} = 0.95 + 0.27 \exp\left(-0.51 \frac{L_S}{D}\right) + \frac{1}{(L_S/D)^{1/4}}$
Mayor et al. (2007)	Vertical Re _{v1} : laminar R _{u1} : laminar	$\frac{U_{b,i}^{tail}}{U_\infty} = -3.85 + 0.82 \exp\left(-\frac{(h_{s,i-1} - 0.3)}{0.48}\right) + 4.91 \exp\left(-\frac{(h_{s,i-1} - 0.3)}{1002.48}\right)$
Mayor et al. (2008)	Vertical Re _{v1} : turbulent R _{u1} : laminar	$\frac{U_{b,i}^{tail}}{U_\infty} = 1 + 0.91 \exp\left(-\frac{(h_{s,i-1} - 0.811)}{0.775}\right) + 0.02 \exp\left(-\frac{(h_{s,i-1} - 0.811)}{14.574}\right)$

In Table 1, U_b and $U_{b,i}^{tail}$ are the bubble front velocity of a trailing bubble, U_∞ is the bubble front velocity of a bubble behind a very long slug (typically $>100D$), v is the bubble velocity ratio defined as $v = (U_b - U_\infty)/U_\infty$, L_S and $h_{s,i-1}$ are the slug length in front of the bubble measured in pipe diameters, and D is the pipe inner diameter.

Multiphase oil and gas pipelines with high viscous liquids commonly imply operating range within the laminar flow regime. Most of the researcher have focused on the turbulent region, and little information is available for laminar and transition flows. The present investigation aims at measuring the wake effect in laminar slug flow in horizontal pipes and

extending the range of the bubble propagation relation, which can be applied in slug flow models.

2 Experimental Setup

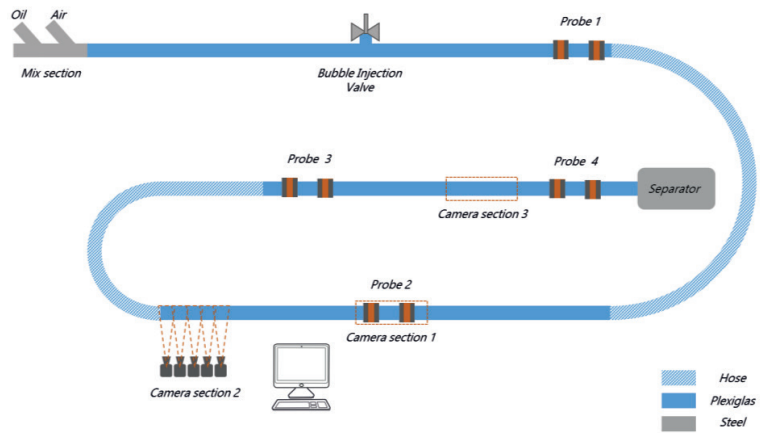
The experiments with two consecutive bubbles injected into a liquid pipe flows were carried out at the Multiphase Flow Laboratory at NTNU. The test section of 50m length consists of three 16m straight sections of acrylic pipes of 60mm inner diameter, together with two bend sections of radius 1.42m and 0.92m respectively as showed in **Fig. 1**. The flow loop is operated with oil and air at atmospheric pressure and room temperature of around 21°C. Flow rates are remotely controlled by valves and pumps through a dedicated program for data acquisition and control (sample rate 100ms). **Table 2** summarizes the fluid properties

Table 2 Fluid Properties

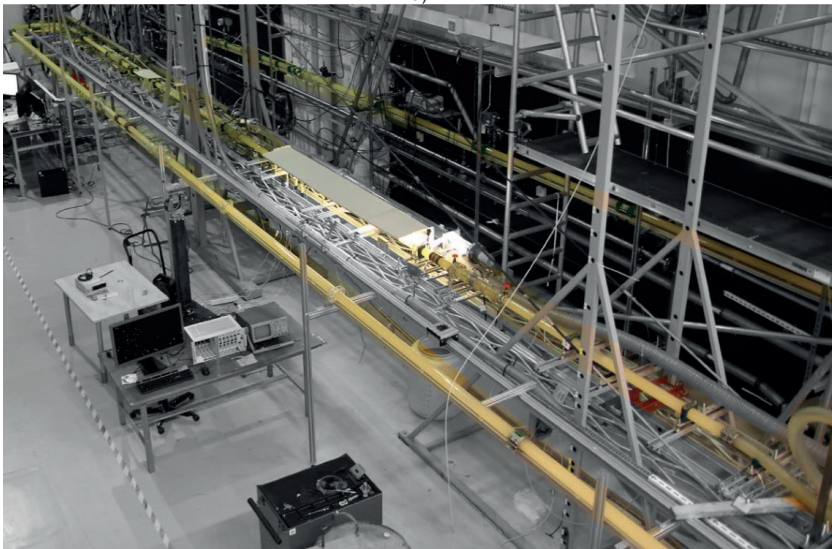
Parameter	Oil	Air
Viscosity (Pa s)	0.065	1.84e-5
Density (kg/m ³)	831	1.2
Surface tension (N/m)	≈0.0263	-

For these experiments, only oil is fed into the test section at a given flow rate while a pair of air bubbles are injected into the liquid stream by mean of a fast-acting magnetic valve (Bosch Rexroth Series 560, 15/30 ms opening/closing time Johansen (2006)). The valve, placed at 110 diameters from the inlet, is remote controlled and bubbles are created by setting the valve opening time, the number of injections (two in these experiments) and the time interval between consecutive injections. The bubble dimensions depend on the air pressure, opening time and liquid velocity in the test section. Consequently, the two first parameters should be adjusted for the different liquid flow rates in order to generate coherent bubbles. The air pressure is kept between 100 and 150 kPa.

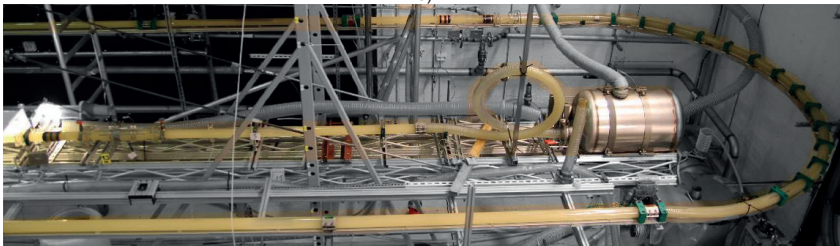
The bubbles propagation velocity is measured by means of videos recording at 23m from the air inlet (**Fig. 1**). The video system is shown in **Fig. 2**, and this include up to five GigE cameras model Basler acA640-120fps, a computer Intel ® core™ i7 and a GigE Vision frame grabber of National Instrument model PCIe-8233. The video synchronization was done by means of a dedicated program written in LabVIEW2012®, which allowed starting/stopping the video record at the same time for all the cameras, and stamping the capturing time on each frame with a precision of 0.008s.



a)



b)



c)

Fig. 1.- a) Sketch of the experimental set-up; b) and c) picture of the facility at Multiphase Flow Laboratory

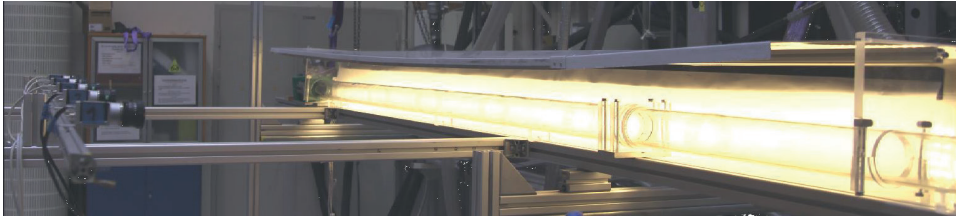


Fig. 2 Visualization system

Special care is taken regarding the surrounding illumination in order to have a uniform color distribution in the image and to avoid reflection from external lights that might disturb the image. The idea is to keep a relatively static image in the videos, so the only mobile “object” is the bubble traveling inside the pipe. In this way, it is possible to track the bubble motion and get a close view of the interaction between consecutive bubbles.

The image processing was done with a dedicated code written in Matlab2014®. The routine loads the videos, extracts each frame and reads the time stamped and the RGB valued of the pixels over a straight line given as an input, and finally gives a matrix with time and the pixel information as an output. The RGB value of a certain pixel in the image will change from low intensity (dark color) to high intensity (light color) according to the passing of the bubble through that specific point.

The output of the image processing is converted to coordinates of time and axial position after a careful process of calibration, where it is taken into consideration the image deformation (due to the camera lens), the image superposition of consecutive cameras, and the relation between pixels and the real distance. After the calibration process, it is then possible to track the horizontal profile evolution and to pinpoint the front and tail of the bubbles simultaneously.

Fig. 3 shows an example of the bubble movement in time and space.

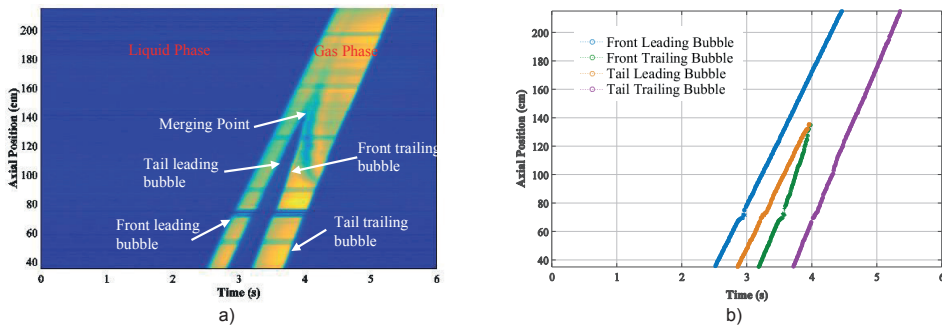


Fig. 3 Bubbles movement a) Horizontal profile of every frame b) Position and time coordinate of the front and tail of each bubble

When the two bubbles travel separately, the front velocity is calculated by a linear regression of the temporal and spatial coordinates. The slug length is calculated from the velocity of the first tail and the time interval between the tail of the leading bubble and the front

of the second bubble at a given position. When a collapse event occurs, the velocity and slug length are calculated directly from the discrete points in order to get the actual change in the slug length and the front velocity. This last method produces more scattered results than the linear regression. Therefore, it is reported the mean value of intervals of one pipe diameter.

The results analysis consists of 402 experimental points, which include seven different liquid superficial velocities, in a Reynolds number range from 298 to 690.

3 Results and Discussion

Fig. 4 to **Fig. 7** show the interaction of two consecutive and insulated bubbles at different stages at $U_{SL} = 0.53\text{m/s}$. When the slug length between the two bubble is large enough (**Fig. 4**), each bubble keeps a defined shape with the tip close to the top of the pipe and the trailing bubble travel slightly faster than the leading one. As the trailing bubble closes the distance, its nose turns sharper, and the bubble seems to stretch and increase in length at the time it approaches the leading bubble (**Fig. 5**). During the merging process in **Fig. 6**, the front of the leading bubble seems unaffected by the union of both bubbles while the nose of the trailing bubble is no longer visible. Instead, there is a sort of hydraulic jump in the union between bubbles, which eventually disappears when the tail of the second bubble reaches the union, and now a single and longer bubble moves at the velocity of the original leading-bubble (**Fig. 7**).

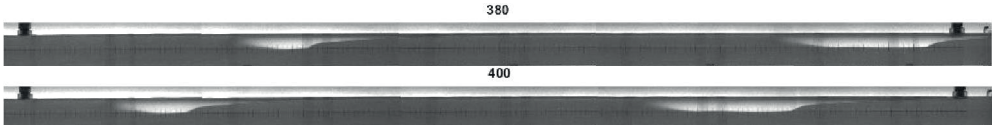


Fig. 4 Bubbles interaction long before collapse (initial slug length 13.3D)

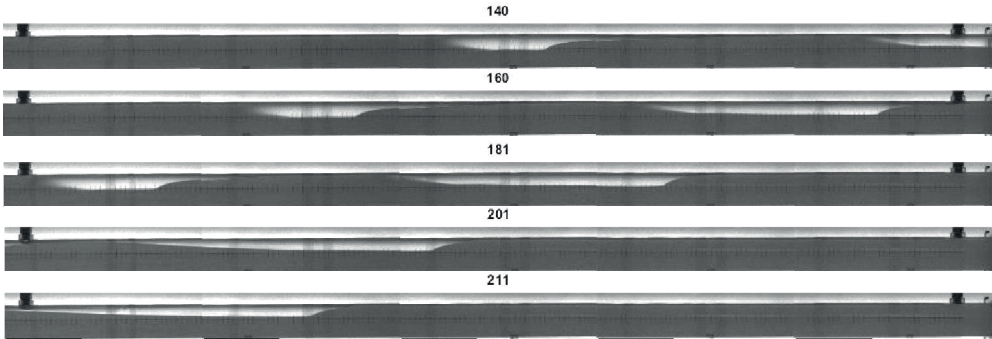


Fig. 5 Bubbles just before collapse (initial slug length 7.6D)

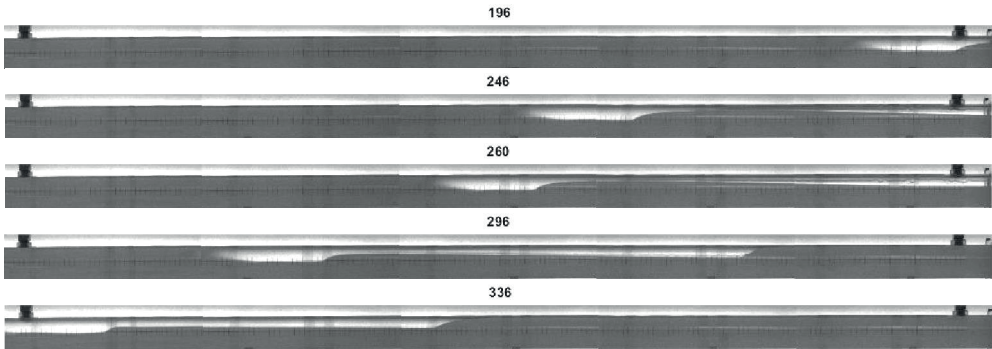


Fig. 6 Bubbles collapsing (initial slug length 5D)

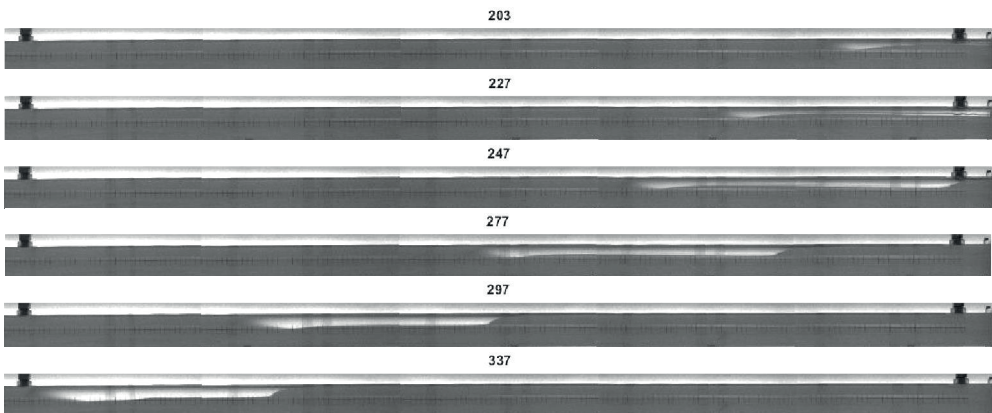


Fig. 7 Bubble after collapse

The “leading” bubble travels behind a slug of “infinite” length, which means that the liquid profile just in front of the bubble nose should be fully developed. Under this consideration, the front velocity of the leading bubble can be expected to correspond with the bubble velocity relation of Nicklin (1962) of **Eq. 1**. This relation is shown in **Fig. 8**, where the leading front velocity is plotted against the superficial liquid velocity. The experimental data compares well with the results reported for single bubble experiments in Mariana J.C. Diaz (2016), where it was obtained a value of $Co=1.8$ and negligible drift velocity for horizontal pipes in laminar flow with liquid velocities higher than a critical value.

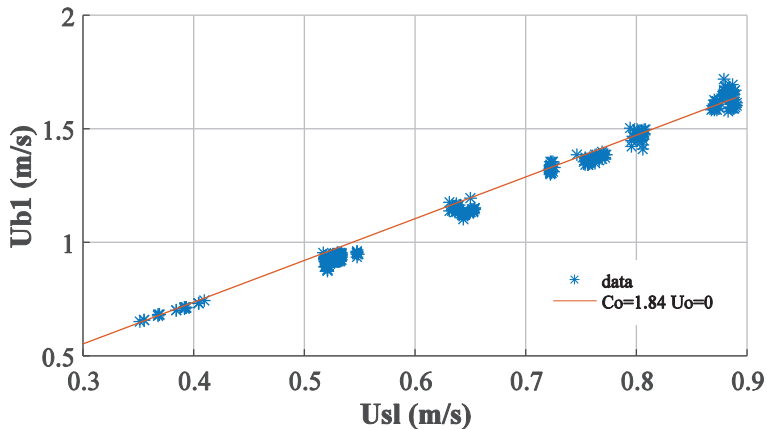


Fig. 8 Bubble front velocity of leading bubble.

For the leading bubble, the tail and front move at the same velocities. **Fig. 9** shows the comparison of the experimental measurements for the tail and front velocity of the leading bubble. The difference is less than 10% with higher dispersion for the lower liquid velocity tested. The measurements suggest that the leading bubble is independent of the merging phenomenon, and the expansion effect in the experiments is small.

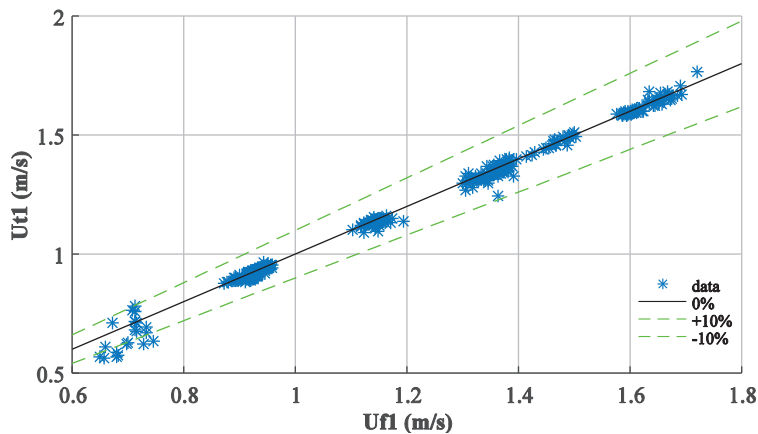


Fig. 9 Comparison of front (Uf1) vs. tail velocity (Ut1) of the leading bubble

When comparing the movement of both bubbles in **Fig. 10**, the trailing bubble tends to increase the front velocity in comparison with the leading one; presenting a velocity increment between 10% and 30% for cases with a merging event. Looking only into the trailing bubble behavior in **Fig. 11**, the comparison between the tail and front velocity is more dispersed than in the leading case. In general, the tail moves coupled with the front, but present larger differences when the bubbles are about to merge.

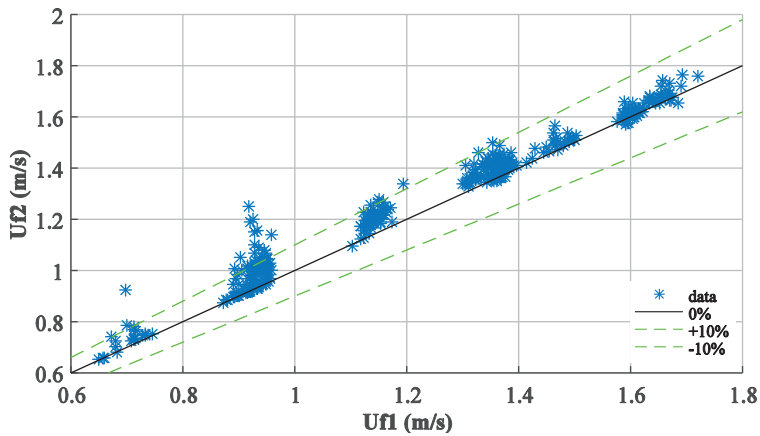


Fig. 10 Comparison between leading (U_{f1}) and trailing bubble (U_{f2})

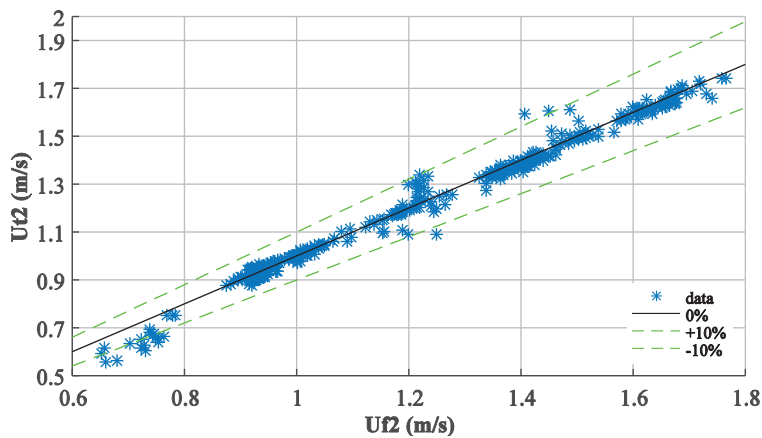


Fig. 11 Comparison of front (U_{f2}) vs. tail velocity (U_{t2}) of the trailing bubble.

The relation between the separation distance between the bubbles and the velocity change of the trailing bubble is shown in Fig. 12. The velocity changes are given in terms of the front velocity ratios of the two bubbles, the trailing bubble (U_{b2}) and the leading one (U_{b1}). The figures plotted correspond to the mean values of the measurements within intervals of 1D of slug length. The error bars reported in Fig. 12 were calculated based on the standard deviation of the velocity at the given interval and the number of cases observed within this range. Therefore, the uncertainty increases as the number of cases evaluated in the range decrease. The shortest slug measured was around 1D.

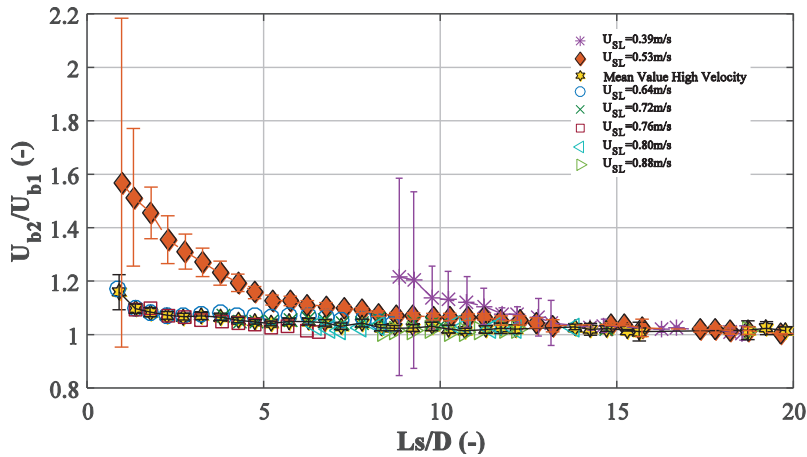


Fig. 12 Ratio of bubble front velocity vs. slug length

The experimental data suggests a dependence of the trailing bubble acceleration with the liquid velocity of the stream, in contradiction with the correlation for turbulent flow reported in the literature. As the liquid velocity decreases, the acceleration is higher and the minimum distance for the bubbles to start to interact increases. Thus, for the lower liquid velocity (0.39m/s), the bubble interaction started around 13D. While for the higher liquid velocity (0.88m/s), there were not detected slugs shorter than 8D with a slight velocity increment.

For the lower velocity of 0.39m/s, it was difficult to achieve a coherent bubble shape, and most of the collisions took place before the measurement section and closer to the injection point, where the incidence of shorter slugs was higher. Nevertheless, with the few data available on this flow range, it was possible to observe a bubble interaction effect after 13D of separation distance and a sharper acceleration of the trailing bubble after 10D. As the liquid velocity increases, (until a certain level), the acceleration of the trailing bubble decreases for the same slug length range. However, for cases with liquid velocities higher than 0.64m/s, the bubble interaction effect (although very weak) seems to be independent of the liquid velocity.

This effect of liquid velocity on the trailing bubble acceleration might be related to the shape of the tail of the trailing bubble, which should influence directly on the liquid velocity profile ahead of the trailing bubble. **Fig. 13** shows the tail shape of the trailing bubble at different superficial liquid velocities. By simple observation of the pictures of the bubble tail, at low liquid velocity, a sort of hydraulic jump is generated at the beginning of the bubble tail followed by a long and thin tail. As the liquid velocity increases, the tail length after the hydraulic jump decreases until the thin tail almost disappear and the hydraulic jump may reach the top of the pipe ($U_{sl}=0.88\text{m/s}$).

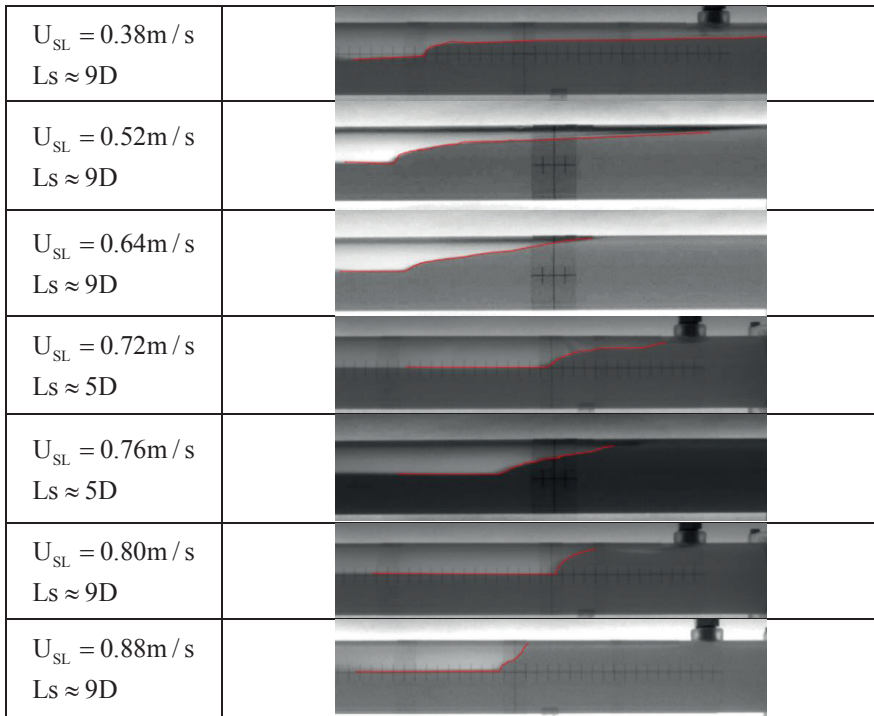


Fig. 13 Leading tie shape at different liquid velocity

Fig. 14 presents the comparison of the experimental data against different models found in the literature (Table 1) for both turbulent (different inclinations) and laminar (vertical pipes) conditions. It seems that the bubble interaction phenomenon within the laminar flow region in horizontal pipes are less pronounced than described by the models originated under turbulent flow conditions.

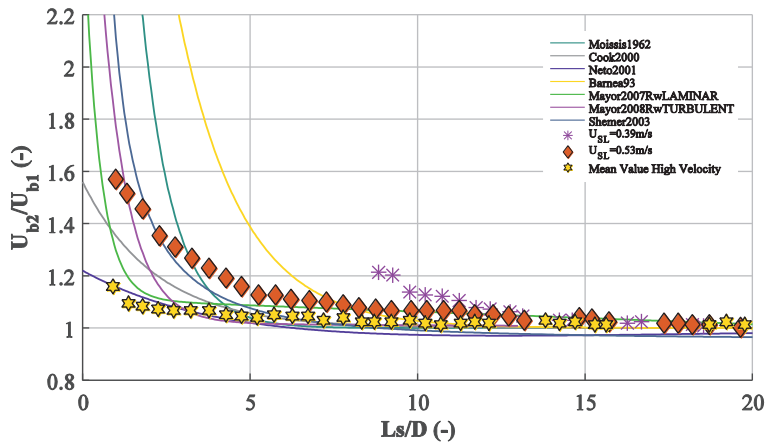


Fig. 14 Theoretical comparison

All the experimental data come closer to the correlation proposed by Mayor et al. (2007) for full laminar flow (in both wake and liquid region). However, if the experimental data is separated by the liquid velocity, only the higher flow rates is still predicted for Mayor et al. (2007), but the lower rates seem to follow best the correlation of Cook and Behnia (2000b) with an adjustment of the coefficients.

4 Conclusions

The bubble interaction phenomenon was studied experimentally for two-phase flow within the laminar region in horizontal pipes. Two air bubbles in a liquid stream were tracked simultaneously by means of video cameras and image processing. The border velocity of each bubble (front and tail) was measured for different liquid velocities and different slug lengths between bubbles. The simultaneous capturing of a couple of bubbles allows for observation of the behavior and shape of each bubble within the interaction region both qualitatively and quantitatively. The leading bubble seems to travel unaffected by the presence of the trailing bubble, the shape of the bubble does not change, and the border velocity remains constant for all liquid velocities. The trailing bubble front, on the other hand, accelerates as it approaches the tail of the leading one; its nose turns sharper, and the bubble shape seems to stretch and increase in length just before to collapse with the leading one. The experiment results showed an increment up to 30% of the front velocity of the trailing bubble relation to the leading one.

In contrast with results reported in the literature, the experiments suggest some influence of the liquid velocity on the relation curve of the slug length and the velocity change of the trailing bubble. The results may be divided in two cases: high-velocity and low-velocity range. In the former case, the trailing bubble velocity can be up to 1.2 times the theoretical value and the bubbles start to interact at shorter separation distance in comparison with the case of lower velocity. For this last case, the velocity change is higher (up to 1.6 times the leading bubble velocity) and starts around 10D of slug length. For a given slug-length, the difference on the velocity change is up to 38% higher for the low-velocity case respect the value reported for the higher velocity. Thus, for those low liquid flow rates ($U_{sl} < 0.64$) where the liquid velocity approaches the values for the drift velocity, the slug front decays to a hydraulic jump, with a free surface extending into the slug and affecting the trailing bubble for quite long slug lengths. For the high velocity cases ($U_{sl} \geq 0.64$), the wake effect seems to be unaffected by the liquid velocity change and, therefore, an average value of the full data above this liquid velocity may be considered.

When comparing the experimental data with the available correlations, the experiments describe well the physical phenomenon in a consistent manner. Most relations overestimate the wake effect. The overall tendency of the high velocity cases is well represented by the correlation proposed by Mayor et al. (2007) for fully laminar flow in vertical pipes, while Cook and Behnia (2000b) may adjust better for the lower velocity cases.

5 Acknowledgments

This work was supported by Petromaks project from the Research Council of Norway and Statoil.

6 References

- BARNEA, D. & TAITEL, Y. 1993. A Model for Slug Length Distribution in Gas-Liquid Slug Flow. *International Journal of Multiphase Flow*, 19, 829-838.
- CAMPOS, J. B. L. M. & DECARVALHO, J. R. F. G. 1988. An Experimental-Study of the Wake of Gas Slugs Rising in Liquids. *Journal of Fluid Mechanics*, 196, 27-37.
- COOK, M. & BEHNIA, M. 2000a. Slug length prediction in near horizontal gas-liquid intermittent flow. *Chemical Engineering Science*, 55, 2009-2018.
- COOK, M. & BEHNIA, M. 2000b. Slug length prediction in near horizontal gas-liquid intermittent flow. *Chemical Engineering Science*, 55, 2009-2018.
- FAGUNDES NETTO, J. R., FABRE, J. & PÉRESSON, L. 2001. Bubble-Bubble Interaction in Horizontal Two-Phase Slug Flow. *Journal of the Brazilian Society of Mechanical Sciences*, 23, 463-470.
- JOHANSEN, M. 2006. *An experimental study of the bubble propagation velocity in 3-phase slug flow*. PhD, NTNU.
- MARIANA J.C. DIAZ, O. J. N. Bubble Translational Velocity in Horizontal Slug Flow with Medium Liquid Viscosity. *Submitted to IJMF*.
- MAYOR, T. S., FERREIRA, V., PINTO, A. M. F. R. & CAMPOS, J. B. L. M. 2008. Hydrodynamics of gas-liquid slug flow along vertical pipes in turbulent regime - An experimental study. *International Journal of Heat and Fluid Flow*, 29, 1039-1053.
- MAYOR, T. S., PINTO, A. M. F. R. & CAMPOS, J. B. L. M. 2007. Hydrodynamics of gas-liquid slug flow along vertical pipes in the laminar regime - Experimental and simulation study. *Industrial & Engineering Chemistry Research*, 46, 3794-3809.
- MOISSIS, R. & GRIFFITH, P. 1962. Entrance Effects in a Two-Phase Slug Flow. *Journal of Heat Transfer*, 84, 29-38.
- NICKLIN, D. J., WILKES, J.O., DAVIDSON, J.F. 1962. Two phase flow in vertical tubes. *Trans. Inst. Chem. Engs.*, 61-68.
- PINTO, A. M. F. R. & CAMPOS, J. B. L. M. 1996. Coalescence of two gas slugs rising in a vertical column of liquid. *Chemical Engineering Science*, 51, 45-54.
- PINTO, A. M. F. R., PINHEIRO, M. N. C. & CAMPOS, J. B. L. M. 1998. Coalescence of two gas slugs rising in a co-current flowing liquid in vertical tubes. *Chemical Engineering Science*, 53, 2973-2983.
- SHEMER, L. 2003. Hydrodynamic and statistical parameters of slug flow. *International Journal of Heat and Fluid Flow*, 24, 334-344.
- SHEMER, L. & BARNEA, D. 1987. Visualization of the Instantaneous Velocity Profiles in Gas-Liquid Slug Flow. *Physicochemical Hydrodynamics*, 8, 243-253.

- UJANG, P. M., LAWRENCE, C. J., HALE, C. P. & HEWITT, G. F. 2006. Slug initiation and evolution in two-phase horizontal flow. *International Journal of Multiphase Flow*, 32, 527-552.
- WANG, X., GUO, L. J. & ZHANG, X. M. 2007. An experimental study of the statistical parameters of gas-liquid two-phase slug flow in horizontal pipeline. *International Journal of Heat and Mass Transfer*, 50, 2439-2443.